

ABSTRACT

Title of Thesis: A REDESIGN OF THE EXHAUST AND GAS
SAMPLING SYSTEM OF THE FIRE
PROPAGATION APPARATUS

Shuvam Roy, Master of Science, 2022

Thesis Directed By: Professor Stanislav Stoliarov, Fire Protection
Engineering

Standard bench scale fire apparatuses are useful tools to perform repeatable and reproducible fire tests that acquire key fire properties, such as heat release rate and time to ignition, for materials in a cost-effective manner. The Fire Propagation Apparatus (FPA) is one of the only standard bench scale apparatuses that has the ability to acquire these key fire properties in a controlled environment setting. However, the design of the apparatus is quite complex. In this work, the exhaust and gas sampling system designs were redesigned and constructed to increase modularity and manufacturability, adapt to the University of Maryland's Department of Fire Protection Engineering laboratory settings, and provide greater ease for the end user operations. After the construction of the FPA systems, tests were conducted to verify the accuracy of the measurement devices. Equations for the calculation of heat release rate from FPA sensor data were derived and used for a series of combustion experiments. These equations were compared to the ones provided in the standard to gain insight on their systematic differences.

A REDESIGN OF THE EXHAUST AND GAS SAMPLING SYSTEM OF THE
FIRE PROPAGATION APPARATUS

by

Shuvam Roy

Thesis submitted to the Faculty of the Graduate School of the
University of Maryland, College Park, in partial fulfillment
of the requirements for the degree of
Masters of Science
2022

Advisory Committee:

Professor Stanislav Stoliarov, Chair

Assistant Professor Fernando Raffan-Montoya

Professor James Milke

© Copyright by
Shuvam Roy
2022

Acknowledgements

First, I would like to thank my mother, father, my brother, and my extended family for the love and support towards throughout my whole life. I would not be able to reach for the clouds without the strong and tall foundation you have made for me, and for that I am forever grateful.

Next, I would like to thank my advisor, Dr. Stanislav Stoliarov, for, first, giving me the opportunity to work on this project, and second, for all the priceless time and effort you have given me to help me do my very best for this project. There were countless times I felt stuck and unsure of what direction to go, but you could always find a solution or next steps that I could use to keep moving forward.

I would like to also thank Dr. Fernando Raffan-Montoya. Just like with Dr. Stoliarov, I am so appreciative of all the time and effort you put in throughout this journey. You would teach me something new almost every day, and I have grown so much because of it.

Next, I would like to thank all of the students in Dr. Stoliarov and Dr. Raffan-Montoya's research groups. You all have helped me so much throughout this whole process, whether that be giving me invaluable research and life advice or giving me a helping hand for my project, and I genuinely could not have finished without your support.

I would like to thank FM Global for their sponsorship and patience for this project. Without them, this project would not even be possible.

Lastly, I would like to thank Dr. James Milke for taking the time to be on my committee and reading over my work.

Table of Contents

Acknowledgements.....	ii
Table of Contents.....	iv
List of Tables.....	vi
List of Figures.....	vii
List of Variables.....	x
Chapter 1: Introduction.....	1
1.1 Motivation.....	1
1.2 Flammability Testing Background.....	2
1.2.1 Cone Calorimeter.....	2
1.2.2 Controlled Atmospheric Pyrolysis Apparatus II (CAPA II).....	4
1.2.3 Fire propagation apparatus (FPA).....	5
1.3 Project Scope.....	14
Chapter 2: Apparatus Design Changes.....	15
2.1 FPA Lamp Stand Design Overview.....	15
2.2 Exhaust system.....	18
2.2.1 Exhaust System Structure.....	18
2.2.2 Intake funnel.....	23
2.2.3 Testing section.....	25
2.2.4 Thermocouples.....	27
2.2.5 Pitot Tube.....	28
2.2.6 Gas sampling probe.....	29
2.3 Gas sampling system.....	32
2.3.1 Sampling System Shelf.....	34
2.3.2 Soot filter.....	35
2.3.3 Chiller.....	36
2.3.4 Pump.....	37
2.3.5 Drierite.....	39
2.3.6 Mass flow controllers.....	39
2.4 Analyzing and Data Acquisition Equipment.....	39
2.4.1 CO/CO ₂ /O ₂ analyzer.....	42
2.4.2 Hydrocarbon Analyzer.....	44
2.4.3 Surge Protector.....	46
2.4.4 Atmospheric Pressure/Humidity/Temperature Probe.....	46
2.5 Calibration system.....	47
Chapter 3: Apparatus Characterization.....	48

3.1 Mass flow check	48
3.1.1 Pressure Transducer Calibration	48
3.1.2 Pitot Tube Flow Calculation	49
3.1.3 Anemometer flow calculation.....	53
3.2 Sample Flow Concentration Check	57
3.2.1 Calculating concentration of species in the duct flow	58
3.2.2 Characterizing CO/CO ₂ /O ₂ analyzer outputs.....	60
3.2.3 CO ₂ concentration check test.....	61
3.2.4 O ₂ concentration check test.....	64
3.2.5 Delay and Response time calculations.....	66
Chapter 4: Heat Release Rate Measurement Methodology	72
4.1 Carbon Oxide Generation Heat Release Rate Calculation	72
4.2 Oxygen Consumption Heat Release Rate Calculations	78
4.3 PMMA burn tests for heat release rate formula comparisons.....	81
Chapter 5: Summary and Future Work.....	90
Appendices.....	92
A : Standard Procedures.....	92
B : Mechanical Drawings.....	100
C : CO ₂ and CO calculations	102
D : MATLAB Script	104
E : Parts List.....	108
Bibliography	110

List of Tables

Table 3-1. Example of Anemometer flow calculation at a single flow condition.	56
Table 3-2. Comparison between concentration of CO ₂ being sampled to the analyzer and the concentration of CO ₂ measured by the analyzer.	64
Table 3-3. Comparison between concentration of O ₂ being sampled to the analyzer and the concentration of O ₂ measured by the analyzer.	66
Table 3-4. Delay times for standard signal outputs for an inlet air flowrate of 200 slpm	71
Table 4-1. Heat of combustion of PMMA calculated from experimental measurements and calculated from the stoichiometric equation.	86
Table 4-2. Mass of carbon products generated for each combustion test.	87

List of Figures

Figure 1-1. Experimental setup of the cone calorimeter [6].	3
Figure 1-2. Experimental setup of CAPA II [4].	5
Figure 1-3. Dimensioned diagram of the ASTM standard FPA design [5].	6
Figure 1-4. Location of FPA sample ignitor [8].	7
Figure 1-5. Picture of entire exhaust system designed by ASTM E2058 which includes the 260 mm long intake funnel, 914 mm long mixing duct, 457 mm long test section, and 279 mm long blast gate section [5].	9
Figure 1-6. Exploded view of the ASTM E2058 standard intake funnel [5].	10
Figure 1-7. ASTM standard gas sampling flow diagram [5].	11
Figure 2-1. Picture of FPA Lamp Stand with 4 IR heaters.	16
Figure 2-2. Picture of FPA combustion air distribution system.	17
Figure 2-3. Section view of UMD FPA Design with dimensions.	19
Figure 2-4. 3-D view of the FPA setup. Items highlighted in red are new additions while items in black are existing structures.	20
Figure 2-5. Picture of V-clamps for connecting FPA duct sections.	21
Figure 2-6. Picture of steel plates clamping the duct fixture in place.	22
Figure 2-7. Picture of mixing section and test section installed.	22
Figure 2-8. View looking up from the bottom of the duct system. At the transition of the intake funnel, an orifice plate with an internal diameter of 140 mm is mounted.	24
Figure 2-9. Diagram of testing section.	26
Figure 2-10, Picture of Thermocouple port	28

Figure 2-11. Picture of inside of testing section with the pitot tube installed.	29
Figure 2-12. Diagram of FPA sampling flowchart.	33
Figure 2-13. Dimensioned diagram of sampling system shelf.	34
Figure 2-14. Picture of FPA soot filter.	35
Figure 2-15. Picture of FPA chiller.....	36
Figure 2-16. Picture of sample pump for FPA.....	37
Figure 2-17. Front view of the FPA sampling system shelf.	38
Figure 2-18. FPA electrical diagram.....	41
Figure 2-19. Picture of CO/CO ₂ /O ₂ analyzer.....	44
Figure 2-20. Picture of Hydrocarbon Analyzer.	45
Figure 2-21. Picture of barometric pressure/absolute temperature/absolute humidity probe.	46
Figure 2-22. Picture of calibration panel.	47
Figure 3-1. Calibration curve for FPA Pressure Transducer.	49
Figure 3-2. Comparison between Bernoulli flow calculations and Veris flow calculations for case with T = 16 °C and P _a = 101325 Pa.	52
Figure 3-3. Comparison between Bernoulli flow calculations and Veris flow calculation for case with T = 38 °C and P _a = 99000 Pa.	53
Figure 3-4. Setup for Anemometer flow calculations.....	54
Figure 3-5. Diagram showing the anemometer probe locations and corresponding sectional areas..	55
Figure 3-6. Comparison between Anemometer and Pitot readings for different flow scenarios.....	57

Figure 3-7. Setup for the CO₂ concentration check tests. 62

Figure 3-8. CO₂ concentration measured by gas analyzer over time for CO₂ gas flow test
5..... 68

Figure 3-9. O₂ concentration measured by gas analyzer over time for N₂ gas flow test 3.
..... 69

Figure 4-1. Picture of PMMA sample used in FPA burn test..... 82

Figure 4-2. Concentrations measured by the analyzer for one of PMMA burn tests.. 83

Figure 4-3. Temperature and differential pressure measured for one of PMMA burn tests..
..... 83

Figure 4-4. Heat release rates calculated using measurements from one FPA burn test.. 84

Figure A-1. Ball valves on calibration panel in correct orientation for zero calibration. . 93

Figure A-2. Picture of analyzer screen after Step 5. 94

Figure A-3. Picture of analyzer screen after Step 6. 95

Figure A-4. Ball valves on calibration panel in correct orientation for span calibration.. 96

Figure A-5. Picture of analyzer screen after Step 11. 97

Figure A-6. Picture of analyzer screen after Step 12. 98

Figure B-1. Drawing of test section without the insertion of testing instruments. The
flanged ends of the section are not shown. 100

Figure B-2. Drawing of Gas Sampling Probe used in University of Maryland FPA. 101

List of Variables

μ = dynamic viscosity of air at 20 °C

L = length from center of gas sampling probe to edge of wall duct

\dot{V}_{probe} = volumetric flowrate drawn from one end of gas sampling probe

R = inside radius of sampling probe

ΔP_{probe} = pressure drop from gas sampling probe

\dot{V}_{hole} = volumetric flowrate being drawn from each orifice

A_{hole} = cross-sectional area of the orifice

ρ = density of air

P = pressure of fluid in Bernoulli

γ = specific weight

h = height in Bernoulli

u = velocity

P_a = static pressure at the point of measurement

MW = molecular weight of air

R = universal gas constant

T = temperature of the duct flow

P_{room} = ambient pressure in the room

ΔP = differential pressure measured by the pitot tube

\dot{V} = volumetric flow in the duct

D = inside diameter of duct

K = pitot tube flow coefficient

Y_v = expansion factor

F_a = the thermal expansion factor of the gas

h_w = differential pressure measured in inches of water column

Z_f = the flowing compressibility of the gas

A = cross sectional area of the duct

\dot{m}_{duct} = mass flow inside the duct

$X_{i,calculated}$ = molar fraction of species i calculated in the sample flow

\dot{N}_i = molar flow of species i inside the duct

$\dot{N}_{total,dry}$ = total molar flow of all species in the duct minus water vapor

\dot{N}_{air}^t = total molar flow of the room air entering the duct at time step t

$X_{H_2O}^0$ = the moisture content in the room air

\dot{N}_{bottle} = molar flow of the gas produced by gas cylinder

\dot{V}_{bottle} = standard volumetric flow of the mixture from the gas cylinder

RH = relative humidity measured by the Omega iBTHX-W probe

P_{sat} = saturated vapor pressure at the room's temperature

T_a = ambient temperature measured by the Omega iBTHX-W probe

\dot{N}_{total}^t = total molar flow entering the duct at time step t

$X_{i,bottle}$ = concentration of species i in the gas cylinder

$X_{i,dry air}$ = concentration of species i in the room air without moisture

$X_{i,measured}$ = concentration measured by the analyzer for species i.

$V_{output,i}$ = the voltage output produced by the analyzer for species i

$X_{max,analyzer,i}$ = maximum concentration range for analyzer for species i

$error_{CO_2}$ = error between calculated and measured CO₂ concentrations

$error_{O_2}$ = error between calculated and measured O₂ concentrations

X_m = the measurement value from the instrument

X_0 = the value of the property being measured before the step change

X_1 = the value of the property being measured after the step change

t = time

τ = the time constant

$t_{delay,i}$ = time delay of measurement signal i

\dot{V}_{inlet} = volumetric flowrate of the inlet air flow

$t_{sampling}$ = time for sample gas to travel from the sampling probe to the analyzer

\dot{Q} = heat release rate

$\dot{m}_{CO_2,generated}$ = mass generation rate of CO₂

$\dot{m}_{CO,generated}$ = mass generation rate of CO

ΔH_{CO_2} = net heat of combustion per unit mass of CO₂ generated

ΔH_{CO} = net heat of combustion per unit mass of CO generated

$Y_{CO_2}^t$ = mass fraction of CO₂ in the duct flow at time t

$Y_{CO_2}^0$ = mass fraction of CO₂ in the duct before the ignition of the sample

MW_i = molecular weight of species i

MW_{duct}^t = molecular weight of the gaseous mixture in the duct flow at time t

MW_{duct}^0 = average molecular weight of the gaseous mixture in the duct before ignition

X_i^0 = average molar fraction of species i in the duct before ignition

X_i^t = molar fraction of species i in the duct at time t

$n_{total-H_2O}^t$ = total number of moles in the duct minus the moles of water at time t
 n_i^t = number of moles of species i in the duct at time t
 n_{total}^t = total number of moles in the duct at time t
 $n_{i,comb}^t$ = number of moles of species i produced in the combustion process at time t
 n_i^0 = average number of moles of species i in the duct before ignition
 $X_{i,measured}^0$ = average concentration of species i measured by the analyzer before ignition
 H_{atoms} = number of hydrogen atoms in the fuel
 C_{atoms} = number of carbon atoms in the fuel
 $n_{total-H_2O}^0$ = average number of moles in the duct minus water vapor before ignition
 $\dot{Q}_{standard}$ = heat release rate formula given by ASTM standard
 \dot{G}_{CO_2} = mass generation rate of CO₂ for ASTM standard formula
 \dot{G}_{CO} = mass generation rate of CO for ASTM standard formula
 $Q_{standard}$ = total heat released calculated from the standard heat release rate equation
 $Q_{derived}$ = total heat released calculated from the heat release rate equation derived (Q)
 $error_{heat}$ = error between heat released calculated from derived and standard equation
 \dot{Q}_{O_2} = heat release rate calculated from oxygen consumption calorimetry principles
 $\dot{m}_{O_2,consumed}$ = mass consumption rate of O₂ during the combustion process
 ΔH_{O_2} = heat of combustion per unit mass of oxygen consumed provided by ASTM
 $Y_{O_2}^0$ = average mass fraction of oxygen in the duct flow before ignition
 $Y_{O_2}^t$ = the mass fraction of oxygen in the duct flow at time t
 $\dot{Q}_{standard,O_2}$ = heat release rate formula using oxygen consumption given by ASTM
 \dot{D}_{O_2} = consumption rate of O₂ for ASTM standard equation

Chapter 1: Introduction

1.1 Motivation

Because of their inexpensive nature, mechanical properties, and abundance, polymeric materials have been increasing in popularity, especially in building construction. The \$102.23 billion global building and construction plastics market size in 2017 is expected to grow 7.3% by 2025 [1].

This increase in polymer use poses risk of catastrophic fires because of the flammability of these materials, as evident of the Grenfell Tower fire in 2017 [2]. To prevent such catastrophes, the material and flammable properties of polymers need to be carefully evaluated through fire tests. Bench scale fire tests provide an advantage to large scale fire tests because the equipment is small enough in scale to be placed in a typical laboratory setting and the reproducibility and replicability of standardized bench scale tests are higher than that of large-scale tests. Bench scale tests measure key fire properties of materials, such as ignitability and heat release rate to assess their fire risk. Some bench scale tests that measure these properties are the Cone Calorimeter [3], Controlled Atmosphere Pyrolysis Apparatus II (CAPA II) [4], and the Fire Propagation Apparatus (FPA) [5]. Although all these tests measure a material's fire properties at a bench scale, a thorough description of each test's setup and conditions need to be explored to understand each test's advantages and limitations.

1.2 Flammability Testing Background

1.2.1 Cone Calorimeter

The cone calorimeter, developed by NIST in 1980 and standardized through ASTM E1354 in 1990 [3], is the most widely used bench scale fire test. It makes the use of oxygen consumption calorimetry to determine the heat release rate. As can be seen from Figure 1-1, the sample is placed on a load cell in an open environment directly below a hood and a conical heater comprised of electrical coils. The electrical coils provide a radiative heat flux to the surface of the material of up to 100 kW/m^2 [3]. Once the surface of the material reaches the pyrolysis temperature, a spark plug placed above the sample ignites the pyrolyzed vapors to establish a diffusion flame. The time to ignition, used to characterize the ignitability property of a material, is recorded at this time. The products of combustion enter the hood and travel through the duct where a gas sampling ring takes a portion of this flow and redirects it to an oxygen analyzer to measure the concentration of O_2 at the sampling location. A thermocouple is also inserted in the exhaust flow to measure the temperature. The differential pressure is measured across an orifice plate located 350 mm downstream of the fan blower. The oxygen concentration, temperature reading, and differential pressure reading is used to calculate the heat release rate of the material using O_2 consumption calorimetry principles. The mass loss rate of the sample is measured by the load cell.

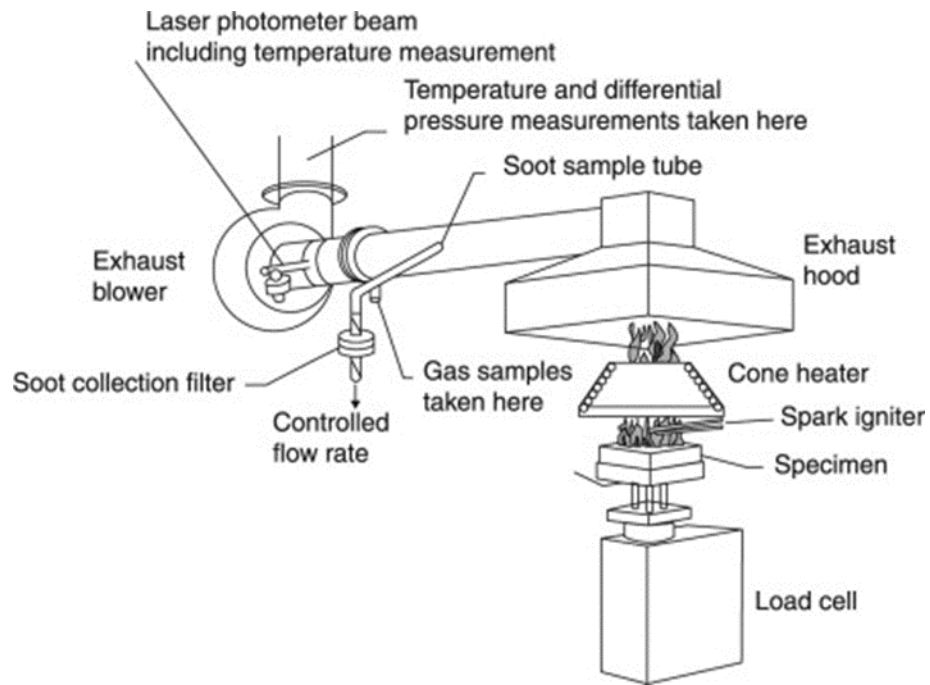


Figure 1-1. Experimental setup of the cone calorimeter [6].

Although the cone calorimeter is the most manufactured and reproduced bench scale fire test, the apparatus has its limitations. Because the sample is placed in an open environment, there is no option to control the ventilation conditions for the sample. Thus, the global equivalence ratio for the sample fire cannot be altered, giving no insight on the material fire behavior in under ventilated or inert atmospheric scenarios. Studying the fire behaviors of an under ventilated fire is critical in fire toxicity analysis due to species produced in incomplete combustion, such as carbon monoxide. Inert atmospheric gasification experiments are critical in isolating material pyrolysis from surface oxidation and gas-phase combustion [4].

There is a version of the cone calorimeter that provides the ability to control the global equivalence ratio for the sample fire, named the controlled atmosphere cone calorimeter [7]. For the controlled atmosphere cone calorimeter, the sample holder and

conical heater are placed in a sealed chamber instead of an open environment. The inlet air flow enters through pipes at the bottom of the sealed chamber. Velocity equilibrium for this inlet flow is supported by a glass bead bed placed on the bottom of the sealed chamber. Because of the sealed chamber, a N₂/air mixture can be injected from the bottom to manipulate the gaseous environment surrounding the sample.

1.2.2 Controlled Atmospheric Pyrolysis Apparatus II (CAPA II)

The Controlled Atmosphere Pyrolysis Apparatus II (CAPA II) has the option to provide an anaerobic environment, which the traditional cone calorimeter lacks. The CAPA II setup, as seen from Figure 1-2, consists of an open to atmosphere gasification chamber which holds the sample holder, a mass balance to measure the mass loss rate of the sample, and a conical heater that can provide a radiative heat flux of up to 100 kW/m² [4]. The conical heater is positioned on a moving track for fast placement and removal above the sample. The gasification chamber consists of two concentric aluminum tubes. A continuous flow of gas is introduced in the channel between the two aluminum tubes, which allows the apparatus to control the environment around the sample, making it oxygen limited or completely inert. The chamber is cooled by running water through copper tubes that are wrapped around the walls of the aluminum tubes. An infrared camera is used to measure the backside temperature of the sample.

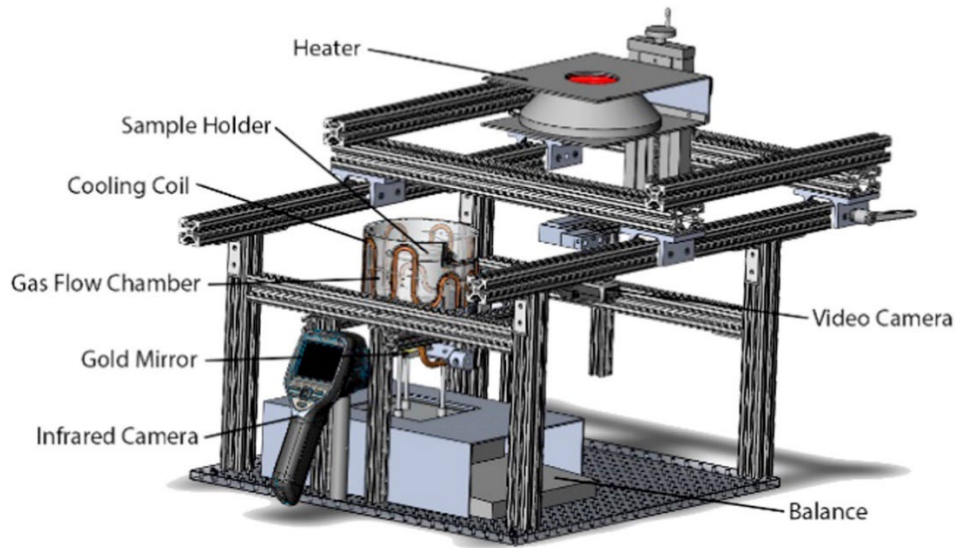


Figure 1-2. Experimental setup of CAPA II [4].

Unlike the cone calorimeter, the CAPA II is only used for non-flaming combustion tests and does not have the option to collect and analyze products of combustion. However, due to the prescribed gas flow from the gasification chamber, the CAPA II is able to provide a controlled gaseous environment, which is beyond the scope of the traditional cone calorimeter.

1.2.3 Fire propagation apparatus (FPA)

The Fire Propagation Apparatus (FPA) is a bench scale testing apparatus that was developed by FM Global in the 1970s and standardized through ASTM E2058 [5]. Fire properties that are measured using the fire propagation apparatus are the time to ignition, chemical and convective heat release rate, mass loss rate, and effective heat of combustion [5]. The apparatus, as seen from Figure 1-3, consists of an infrared heating system, a load cell, a combustion air distribution system, a water-cooled shield, and an exhaust system that collects and analyzes the exhaust flow.

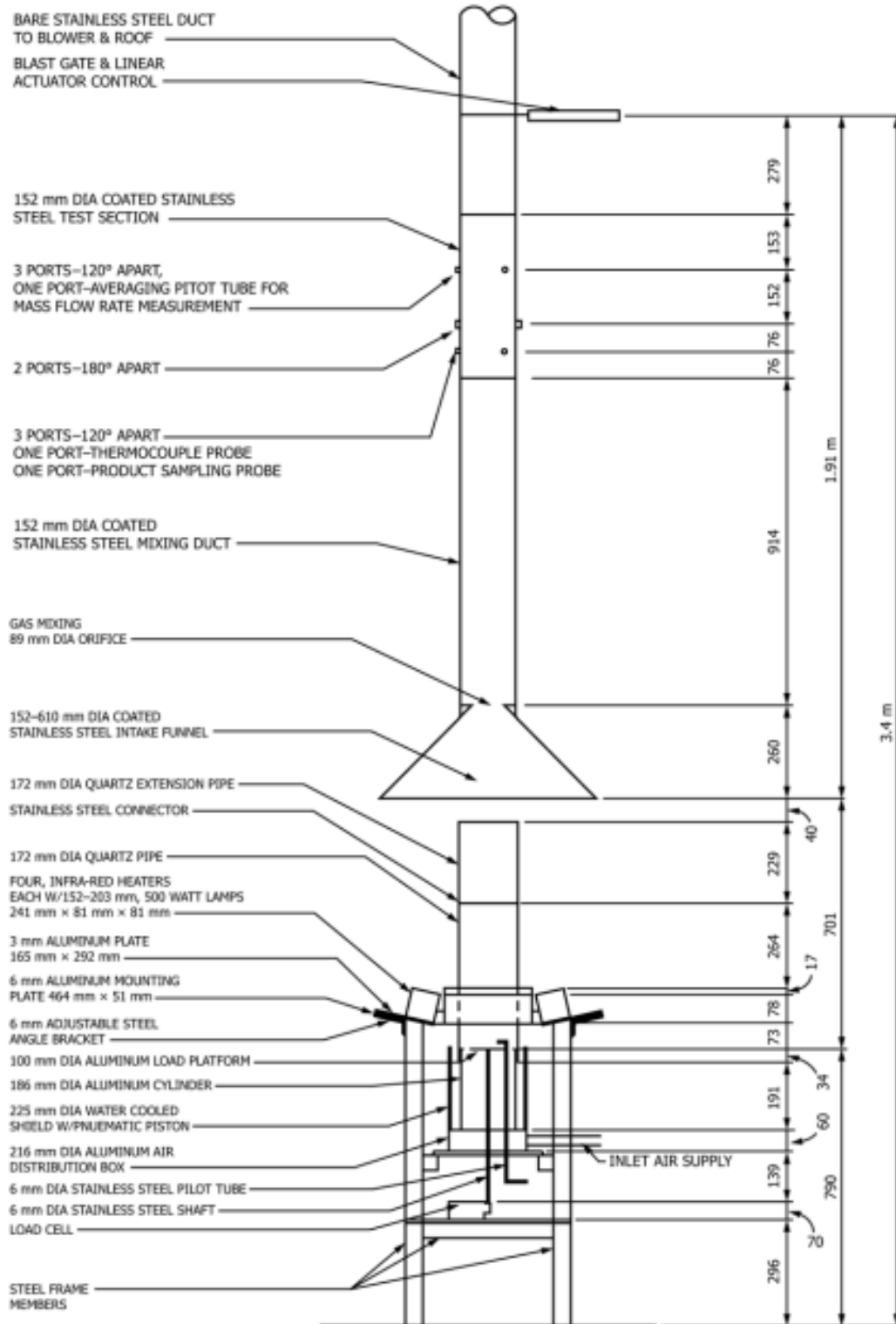


Figure 1-3. Dimensioned diagram of the ASTM standard FPA design [5].

Unlike the cone calorimeter and CAPA II, the sample is heated up through four IR heaters consisting of tungsten quartz lamps enclosed in a compact reflector body. The lamps provide a radiative heat flux to the sample of up to 110 kW/m^2 . To achieve this radiative flux, the lamps produce up to 510 kW/m^2 of radiant flux in front of the quartz window that covers the lamps and operate at approximately $2205 \text{ }^\circ\text{C}$. The lamp bodies are water cooled and the lamp chambers are air cooled so that the lamps do not overheat.

Unlike the cone calorimeter, the sample is ignited through a pilot flame with stoichiometric ethylene/air mixture placed 10 mm above the sample surface and 10 mm radially inward from the sample surface edge. The ignitor placement can be seen in Figure 1-4.



Figure 1-4. Location of FPA sample ignitor [8].

The sample sits on a sample holder that is placed within the combustion air distribution system. The sample holder consists of a platform to hold the 100 mm diameter samples and a 6.35 mm diameter stainless steel shaft that goes through an orifice at the

bottom of the combustion air distribution system. The bottom of the steel shaft is placed on a load cell beneath the combustion air distribution system that tracks the sample mass.

The combustion air distribution system provides well-controlled gaseous flow to the sample. It is constructed using an aluminum chamber that contain eight aluminum discharge tubes arranged in a circle with an inner diameter of 165 mm. Each discharge tube is equally distributed along the circle and provide inlet gasses at a uniform flowrate. The flow of all the discharge tubes add up to a total flow of 200 lpm in the combustion air distribution chamber. 172 mm diameter quartz tubes sit on top of the aluminum chamber and extend the air distribution chamber to 40 mm below the collection hood. The quartz tubes maintain the controlled gaseous flow to the fire above the sample while also allowing the IR radiative heating to reach the sample surface.

The water-cooled outer shield prevents the sample from being exposed to the IR heaters during the heater stabilization period, and it is manufactured through two aluminum cylinders welded together with an inlet and outlet for water circulation [5]. It is raised during the lamp stabilization process to shield the sample from the IR heaters and lowered through the use of a pneumatic cylinder when the lamps have stabilized to expose the sample to the radiant heat.

The exhaust system is a vertical duct system that consists of four stainless steel sections: the intake funnel, the mixing section, the testing section, and the blast gate section. The intake funnel, as seen from Figures 1-5 and 1-6, has an opening diameter of 610 mm that reduces to an 89 mm diameter orifice when flanged to the mixing section from the inside. This reduction in diameter is made along a length of 260 mm. The mixing section has a constant diameter of 152 mm and has a length of 914 mm. The mixing section

flanges to the test section that has a diameter of 152 mm and a total length of 457 mm. The testing section connects to the blast gate section which has a diameter of 152 mm and a length of 279 mm. The blast gate section includes a blast gate that controls the exhaust flow. The exhaust flow should be controlled between 0.1 and 0.3 m³/s and should be capable of a flowrate of 0.25 m³/s during a test, which is more than ten times the exhaust flowrate required of the cone calorimeter (0.024 m³/s).

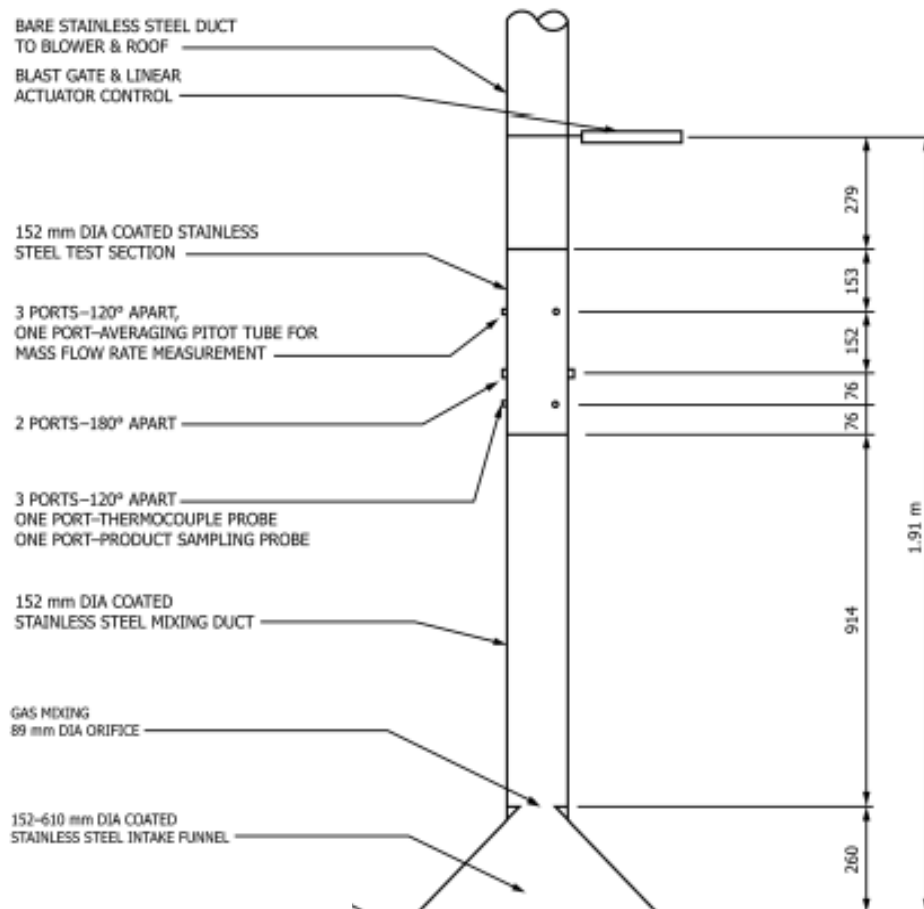


Figure 1-5. Picture of entire exhaust system designed by ASTM E2058 which includes the 260 mm long intake funnel, 914 mm long mixing duct, 457 mm long test section, and 279 mm long blast gate section [5].

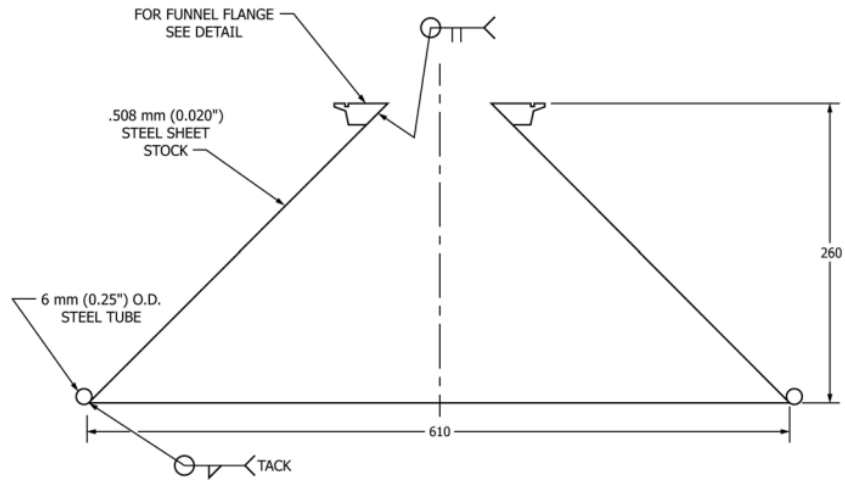


Figure 1-6. Exploded view of the ASTM E2058 standard intake funnel [5].

The test section consists of a thermocouple port to take temperature measurements, a pitot tube port to take differential pressure measurements, and a sampling port to take gas concentration measurements. The flow diagram for the gas sampling system is provided by the ASTM standard and is shown in Figure 1-7. The sampling line consists of a filter with a 5-micron pore size, a condenser operating at temperatures in the range -5 to 0 °C, a Drierite tube, a second filter before the analyzer, a sampling pump, a system flowmeter, and manifolds to direct flow to multiple analyzers (CO₂, CO, O₂, and hydrocarbon). The carbon monoxide and carbon dioxide analyzers, which are used for the heat release rate calculation, should be able to read measurements within the range of 0-500 ppm and 0-15000 ppm respectively.

A notable advantage of the FPA when compared to the traditional cone calorimeter is that the FPA has the ability to control the gaseous environment around the sample through its combustion air distribution system, allowing the user to run tests in a variety of ventilation cases. Although the CAPA II can also control the gaseous environment around the sample, it does not have the capability to capture and analyze products of combustion like the FPA and cone calorimeter. In this sense, the FPA combines the features of both the CAPA II and the traditional cone calorimeter in one bench scale test.

The controlled atmosphere cone calorimeter provides a somewhat controlled gaseous environment as well. However, although a leak-free chamber is strived for in this apparatus, a truly hermetic seal cannot be produced due to practical reasons [7]. An overpressure of the chamber, due to the injection of controlled gaseous flow, or a negative pressure of the chamber, due to the exhaust blower, can cause unwanted leaks. Because of this, the controlled atmosphere cone calorimeter does not provide as controlled of a gaseous environment as the FPA does. Furthermore, because the sample and heater are located inside a chamber in the controlled atmosphere cone calorimeter, prolonged heater operation causes the chamber to become warmer than the ambient air [7]. Due to this, the FPA provides a more temperature controlled burning condition.

It is worthy to note that, although the cone calorimeter and FPA both utilize calorimetry to measure heat release rate, the cone calorimeter utilizes oxygen consumption calorimetry while the FPA primarily utilizes carbon oxide generation calorimetry. Oxygen consumption calorimetry uses the effective heat of combustion of oxygen in its heat release rate equation, which is relatively constant for all polymeric fuels as 13.1 ± 0.7 kJ/g [9]. This makes oxygen consumption calorimetry very versatile as, except for a few exceptions,

the fuel composition does not matter when calculating the heat release rate. Carbon oxide generation calorimetry uses the effective heat of combustion per gram of CO and CO₂ generated, which remain approximately constant within each generic group of fuel [9][10]. However, the uncertainty is greater if the fuel that is being tested is unknown or a composite of multiple materials. Using the average of fuels listed in Table A.38 of the SFPE Handbook, the net heat of combustion per unit mass of CO₂ generated is 13.3 kJ/g ± 1.5 kJ/g and the net heat of combustion per unit mass of CO generated is 11.1 ± 2 kJ/g [11]. This shows that, when the fuel is unknown, the uncertainty of the heat of combustion term in the heat release rate equation is approximately doubled when using carbon oxide generation rather than oxygen consumption. Carbon oxide generation analysis can be more desired in under-ventilated fires as the CO term in its calculation corrects for the increased CO generation in under-ventilated fires, which the oxygen consumption method fails to do [12]. Because the FPA can be run in under-ventilated scenarios, carbon oxide calorimetry is used to correct for sootier fires that have increased CO generation. Furthermore, the larger flowrate in the FPA exhaust results in considerable dilution of the combustion products such that the oxygen concentration change measured by the gas analyzer is significantly less than that measured in the cone calorimeter. However, without specifying the fuel composition of the fuel, there is no guarantee that the carbon oxide generation calorimetry is more accurate than oxygen consumption calorimetry. The oxygen consumption method is still recognized as the most accurate and practical technique for measuring heat release rates from experimental fires in the fire community [12].

Carbon oxide generation calorimetry corrects for the additional CO generation that occurs in under-ventilated scenarios. This equation can be corrected even further for fires

with prevalent incomplete combustion by including a term for the formation of hydrocarbons [12]. To make this correction, a hydrocarbon analyzer can be used to measure the concentration of hydrocarbons in the sample flow.

Even with the proficiency of the FPA, there are drawbacks in the complexity of its design. There are many components to the FPA for it to function correctly. Furthermore, because of the age of the ASTM standard, it lacks detail in certain areas, adding the challenge of manufacturing parts and constructing a streamlined version in today's age.

1.3 Project Scope

Recently, the Department of Fire Protection Engineering started the construction of an FPA in the Koffel Associates Fire Standards Laboratory at the University of Maryland for use in the department's research and instructional labs. In doing so, the standard design was revised to improve its manufacturability, maintenance, and operability. The bottom half of the FPA, which includes the infrared heating system, load cell, combustion air distribution system, and water-cooled shield, was already redesigned and constructed by Chaffer [8]. The redesign's purpose was to make it easier to manufacture, make it more modular, and make it easier for the end user operations. These same ideas are echoed in the redesign of the exhaust and gas sampling system that was carried out in this work. At the end, the project's goal was to deliver a working FPA that can accurately collect and analyze products of combustion.

Chapter 2: Apparatus Design Changes

2.1 FPA Lamp Stand Design Overview

Although the bottom half of the FPA, which includes the IR lamps, lamp frame structure, water cooled outer shield, quartz tubes, load cell, and combustion air distribution system, was not included in the scope of this project, it is important to familiarize with the general design to understand the reason for the design changes to the exhaust and gas sampling/analyzing system. A more in-depth description of the bottom half design can be found in Chaffer's thesis [8].

The lamp frame structure was constructed using t-slot aluminum framing instead of steel, as seen from Figure 2-1. The t-slot aluminum requires no welding, making the assembly process, and disassembly process if maintenance is required, much more manageable. The modularity of the t-slot framing also allows for expansions to the structure in the future. Furthermore, the t-slot aluminum and its corresponding hardware are mass manufactured, so replacement parts are not difficult to obtain.

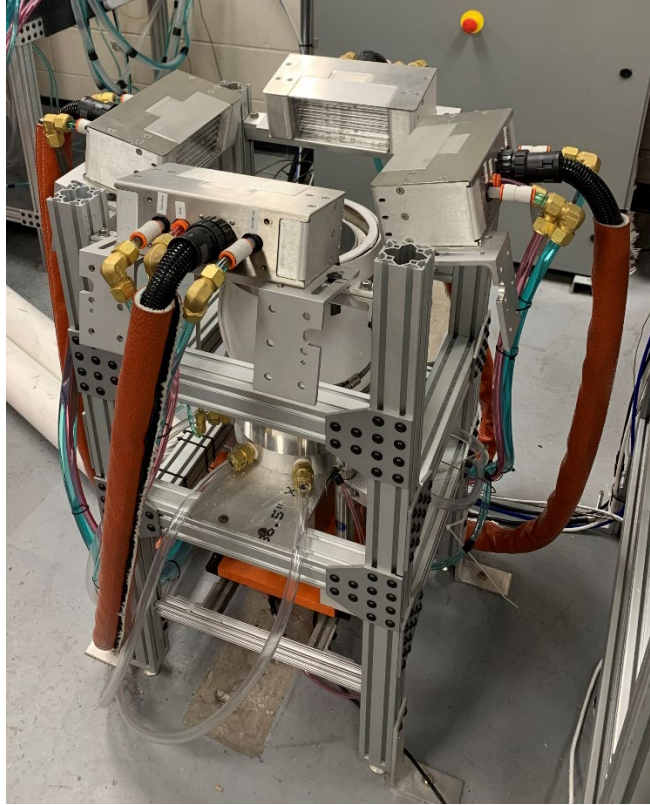


Figure 2-1. Picture of FPA Lamp Stand with 4 IR heaters.

Similarly, welding was avoided for the combustion air distribution system and mass-produced fittings were used for the inlet tubes. The installation of the combustion air distribution system can be seen in Figure 2-2.

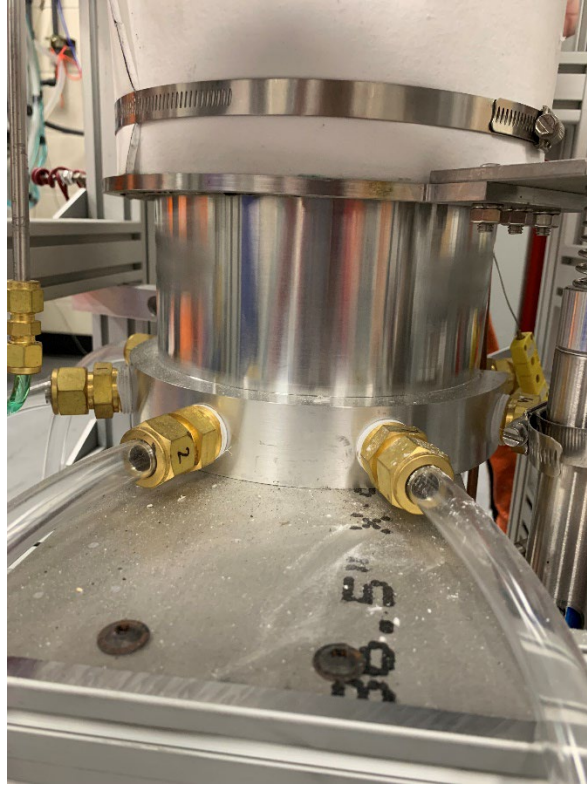


Figure 2-2. Picture of FPA combustion air distribution system.

Two quartz tubes, per the standard, extend from the top of the aluminum cylinder that makes up the combustion air distribution system. The quartz tubes are connected to each other through an aluminum adapter with ceramic paper insulation on the inside to provide a gasket. With the quartz tubes installed, the FPA stand extends to a height of 1.45 m.

The water-cooled outer shield was made of stainless steel and was wrapped in ceramic paper insulation in order to provide increased heat control at higher fluxes. The water-cooled outer shield is raised and lowered with the use of pneumatic cylinders that are actuated with an electrical switch.

The load cell was mounted to the FPA frame below the combustion air distribution chamber through a steel plate and four Neoprene rubber blocks. The rubber blocks isolate the load cell from the frame to reduce vibration effects to the load cell signals. The sample holder sits on top of the load cell and enters the combustion air distribution chamber through an orifice at the bottom of the chamber. The sample is placed in a stainless steel horizontal sample dish, which is placed on top of the sample holder prior to burn tests.

For the exhaust system and gas analyzing system design, the design changes strongly emulate that of the bottom half construction. Welding was avoided, and whenever possible, mass-manufactured parts were used for ease of construction and repair. T-slot aluminum profiles were used for frame structures for increased modularity and design consistency.

2.2 Exhaust system

2.2.1 Exhaust System Structure

The design for the exhaust system incorporated the same four sections as the standard (intake funnel, mixing section, test section, and blast gate section). However, as shown in Figure 1-3, the total height of the FPA system is designed to be 3.4 m, which was not feasible for the University of Maryland laboratory. Since the bottom half construction was already fixed in place, the height of the exhaust system needed to be reduced to accommodate for the ceiling height. For this reason, the design was altered to have a tee upstream of the exhaust blower to split the main duct into two. The design of the University of Maryland FPA exhaust system is shown in Figure 2-3 and 2-4. The 0.152 m diameter duct, which in this paper will be called the main exhaust, collects the combustion particles

of the FPA. It consists of the intake funnel, mixing section, and test section. The end of the intake funnel is centered with the center of the FPA quartz tubes and is directly 40 mm above the top of the quartz tube. The 0.203 m diameter duct, which will be named the accessory exhaust, is mounted to the wall and contains a blast gate at the end at a height of 1.83 m. This allowed the height of the blast gate section to be subtracted from the overall height of the main exhaust, while also making the blast gate much more accessible to the end user.

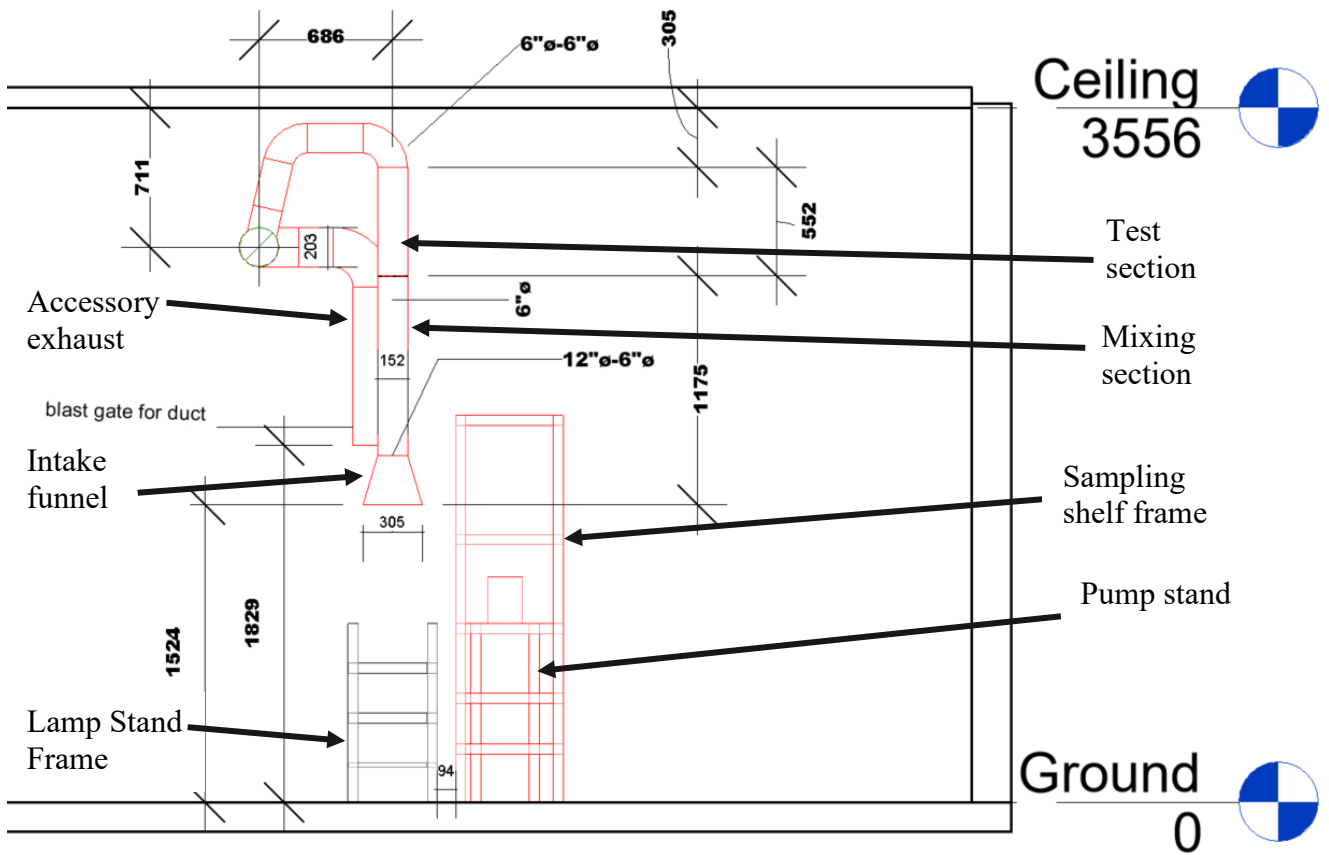


Figure 2-3. Section view of UMD FPA Design with dimensions. Dimensions are in mm unless stated otherwise. Items highlighted in red are new additions while items in black are existing structures.

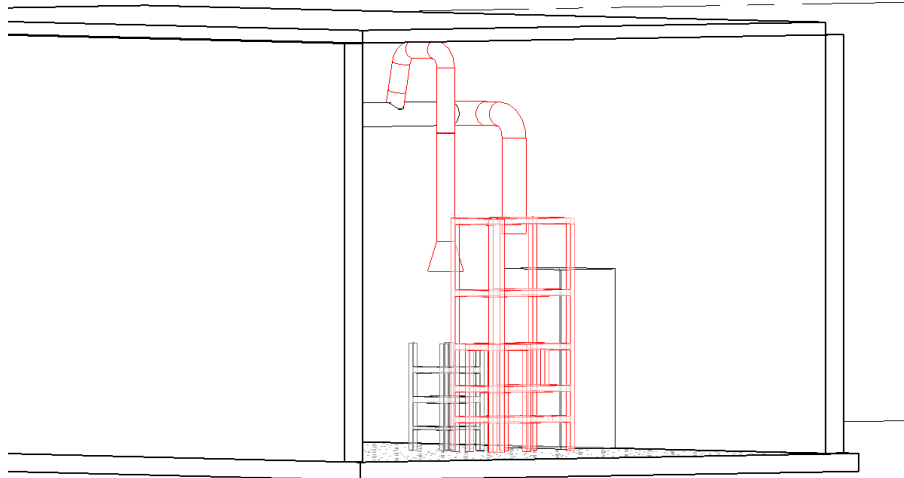


Figure 2-4. 3-D view of the FPA setup. Items highlighted in red are new additions while items in black are existing structures.

The main exhaust sections were each custom machined and manufactured by MetalFab from 0.9525 mm thick (20-gauge) 304 stainless steel. The standard calls for 1.575 mm thickness for the duct wall, but this is reduced in the current design because it allowed the duct sections to be easily flanged together but still retain their structural and mechanical integrity. Unlike the standard, these sections were flanged together using V-clamps, such as the one shown in Figure 2-5. These clamp the end of the duct sections together by placing the clamp around the section flanges so that both the section ends fit within the cavity of the clamp. Then, the 3/8" bolts are used to tighten the V-clamp around the section flanges to connect the two sections together tightly and securely. These V-clamps are used to connect the intake funnel to the mixing section, connect the mixing section to the test section, and the test section to the 0.152 m stainless steel spiral duct that extrudes from the main duct tee. These V-clamps were used instead of the flange design shown in the standard for their simplistic design and ease of installation/uninstallation. The flanges in the standard needed to be welded to the duct sections and welding wanted to be avoided whenever possible. Furthermore, the design was very intricate with tiny grooves

that could have been a challenge to manufacture. Lastly, it was not clear in the standard how to connect the duct sections using the flanges suggested in the standard.

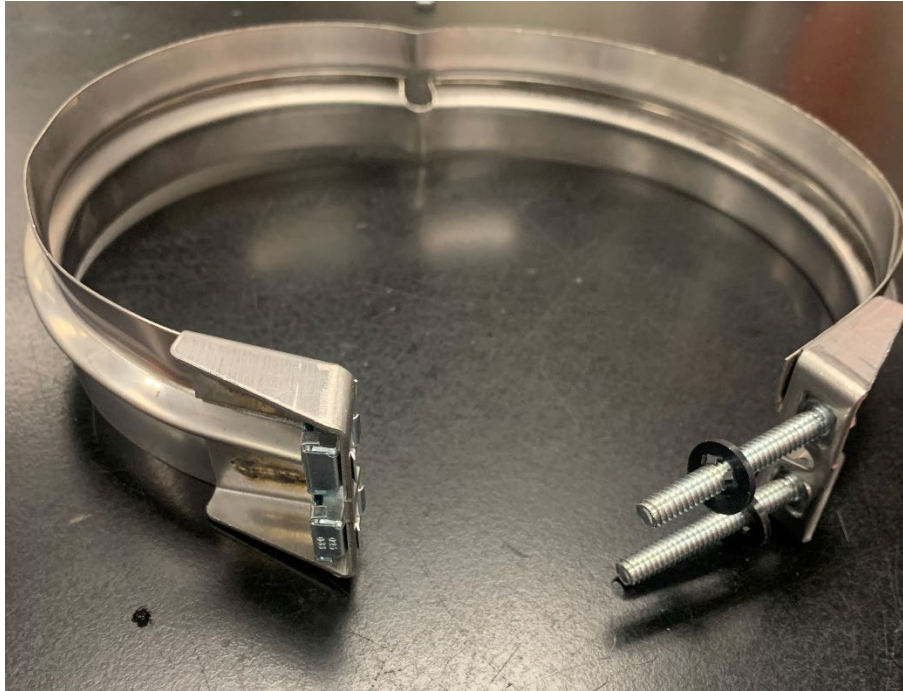


Figure 2-5. Picture of V-clamps for connecting FPA duct sections.

Another deviation from the standard is that the duct sections were not coated internally with FEP resin. This is because the pros of the FEP resin were not believed to outweigh the cost of labor and expense of the FEP. Stainless steel does not corrode easily, and if the inside of the duct does corrode exceptionally and needs to be replaced, the design of the exhaust system allows for a duct section to be replaced while still retaining all the testing instruments.

Because of the large length of the main exhaust duct, it was imperative to support the duct assembly and prevent it from swaying from its original position. To do this, the duct system was clamped tightly by two crescent moon steel plates in the middle of the mixing duct section, as seen in Figure 2-6 and 2-7. These crescent moon steel plates were

bolted and fixed onto two din rails running parallel from the ground and 0.457 m apart from each other. The din rails are held up by metal rods anchored to the ceiling.



Figure 2-6. Picture of steel plates clamping the duct fixture in place.



Figure 2-7. Picture of mixing section and test section installed.

2.2.2 Intake funnel

The biggest difference of the intake funnel design is that the bottom of the intake funnel is 305 mm instead of 610 mm. The reason for this change is that the duct manufacturers could not provide a stainless-steel tapered increaser with a diameter increase from 152 mm to 610 mm across a 260 mm length. Because the ceiling height was already a limiting factor, the reduction of diameter was chosen over lengthening the intake funnel length. The 305 mm diameter is still large enough to collect all the products of combustion, which is the main goal of the intake funnel.

As stated before, the intake funnel is flanged to the mixing duct using V-clamps. This eliminates the need of flanging the intake funnel to the mixing section from the inside as per the standard. At the transition point where the diameter of the duct becomes 152 mm, there are mounting openings on the inside to hold an orifice plate, as seen in Figure 2-8. The orifice plate is used to promote mixing within the exhaust flow. The standard calls for an orifice diameter of 89 mm, but for the University of Maryland laboratory setup, an orifice size this small increases the pressure significantly and triggers the duct system's pressure alarm. After testing many different orifice plates, the one chosen that provided the correct nominal flow and did not trigger the pressure alarm with the blast gate closed had a 140 mm internal diameter. This orifice size was chosen for the final design, but because of the modularity of the exhaust design, it is simple to uninstall the intake funnel and replace the orifice plate with whichever orifice size is desired. This is advantageous when very low flows or high flows are desired that are outside the range of flows that can be controlled with the blast gate for the designed orifice size.

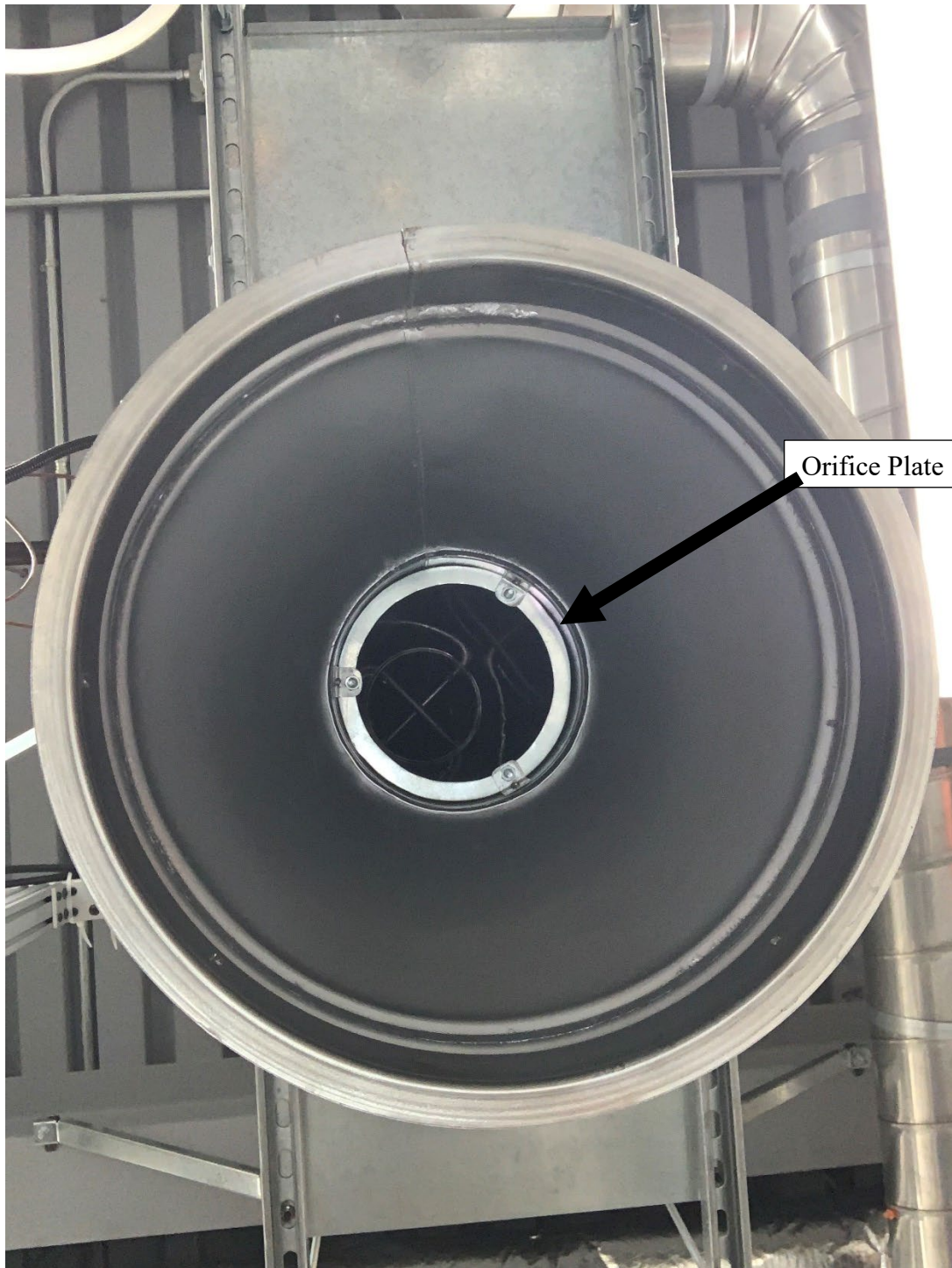


Figure 2-8. View looking up from the bottom of the duct system. At the transition of the intake funnel, an orifice plate with an internal diameter of 140 mm is mounted.

2.2.3 Testing section

In the standard, there is limited information on the design of the test section. The locations for the measurement ports are indicated, but there is confusion on which measurement port corresponds to which measurement device. For example, as seen from Figure 1-5, the thermocouple probe and product sampling probe are located on the same plane. However, the product sampling should be done on both ends of the probe, and thus two ports should be needed that are 180° apart from each other, which is not indicated on the diagram. Furthermore, there are ports on the diagram with no indication of what testing instrument the port is used for. Because of this, a redesign of the exhaust diagram and test section was created, as shown in Figure 2-9. This diagram provides further detail on the testing instruments and provides planar views of the testing instrument locations. A mechanical drawing of the test section can be found in Appendix B.1, with the drilled openings in the section where ports are located. As can be seen from Figure 2-9, the distance between the bottom of the intake funnel and the first port in the new exhaust design is the same as that of the standard exhaust design. This same distance was kept to provide sufficient mixing of the combustion products before reaching the testing instruments.

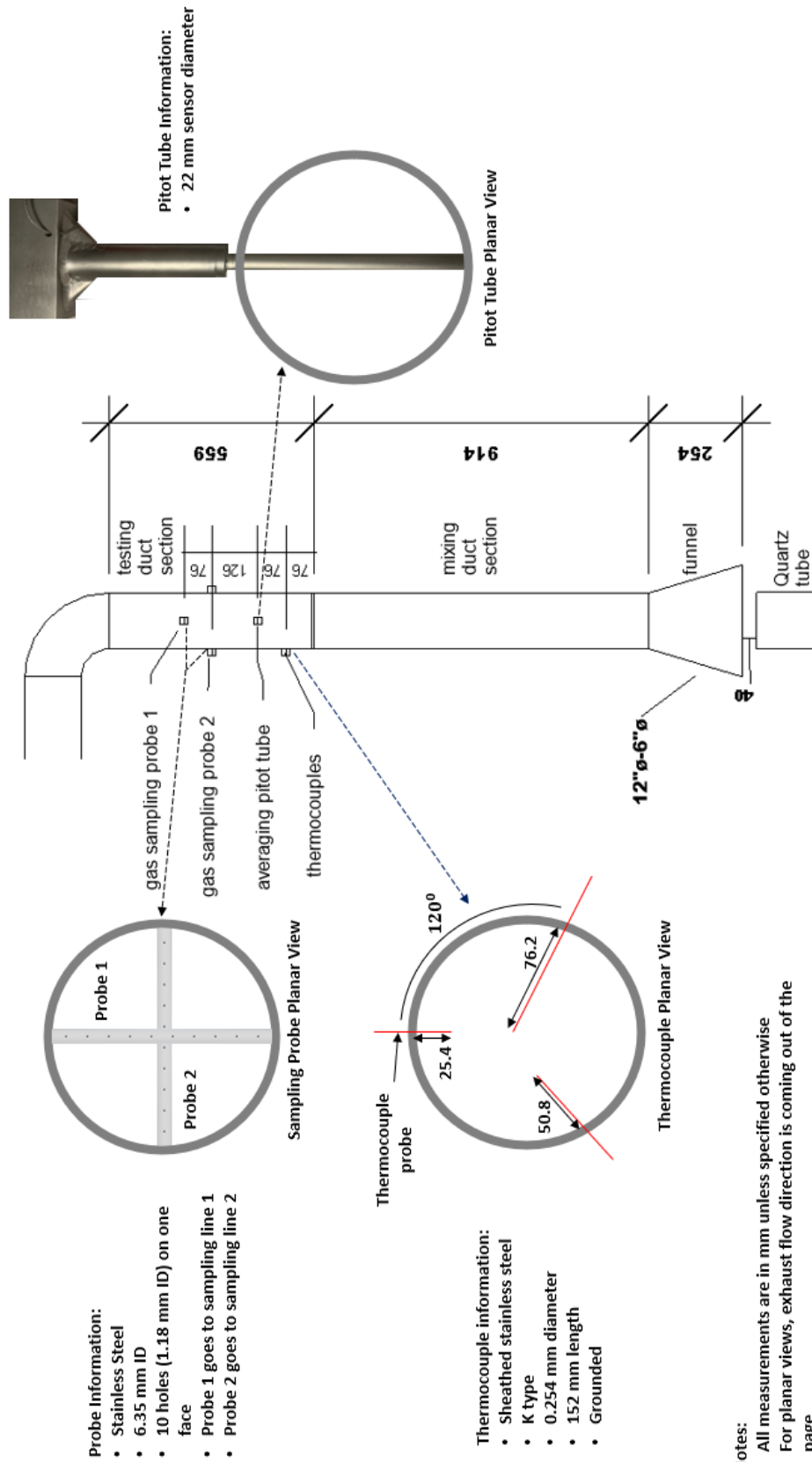


Figure 2-9. Diagram of testing section.

2.2.4 Thermocouples

The thermocouple ports are located 76 mm above the bottom of the test section, per the standard. Along with having a thermocouple with the temperature sensing bead located in the center of the duct, two more thermocouples were installed in the same plane with beads located 25.4 mm and 50.8 mm axially inward from the inside duct wall. The reasoning to use three thermocouples instead of one is because the gas is sampled along the diameter of the duct and not just the center, so using multiple thermocouples to measure the temperature at different radial locations in the duct and averaging the temperature was believed to provide a more accurate description of the temperature of the gas being sampled.

Each thermocouple was a sheathed stainless steel K type thermocouple with a 152.4 mm probe length and a probe diameter of 0.254 mm (model SCASS-010G-6 from Omega). Each thermocouple port was uniformly distributed along the circumference of the duct. The thermocouple ports were made using Swagelok SS-400-61 bulkheads with one end machined down to the nut so that the fitting does not protrude far inside the duct. The seal between the drilled opening in the duct and the fitting was made using a Buna-N U-Cup Seal. To close the gap inside the fitting, a Teflon ball with a drilled opening of 0.33 mm was used, which made the opening just large enough for the thermocouple to pass through inside the duct. High temperature gasket sealant was used to fix the thermocouple probe to the Teflon ball, as seen from Figure 2-10.



Figure 2-10, Picture of Thermocouple port

2.2.5 Pitot Tube

The Veris Verabar V100 averaging pitot tube used for mass flow measurements is located 76 mm above the thermocouple plane. The averaging pitot tube was fixated to the duct using a Swagelok SS-1610-61 bulkhead. The fitting was machined further, making the inside bored through so that the pitot tube can fit through it. One end was shaved off also so that the fitting on the inside did not cover any of the sensor orifices of the pitot tube, as seen from Figure 2-11. The seal between the drilled opening in the duct and the fitting was made using a Buna-N- U-Cup Seal.



Figure 2-11. Picture of inside of testing section with the pitot tube installed.

The pitot tube is connected to the Setra 264 pressure transducer to measure the differential pressure in the pitot tube. The pressure transducer calculates differential pressure with a range of 0 to 373 Pa with a full-scale accuracy of 0.25%. The pressure transducer requires a power supply of 9 to 30 VDC and provides a signal output of 0 to 5 VDC.

2.2.6 Gas sampling probe

The ASTM standard specifies that the “sampling probe, made of 6.35-mm O.D. stainless steel tubing inserted through a test section port, shall be positioned such that the open end of the tube is at the center of the test section.” [5]. However, the description is

somewhat vague as it does not indicate the number and size of the sampling orifices or the inside diameter, and there is no drawing provided of the sampling probe. ISO 12136 provides further detail by quantifying the number of orifices as 14 [13], but, again, does not provide the size of the orifices or the inside diameter of the probe.

A drawing of the gas sampling probe manufactured for the design of the UMD FPA can be found in the Appendix B.2. The gas sampling probe was made out of stainless steel, but the outside diameter is 9.53 mm and the inside diameter is 6.35 mm. The enlarged diameter for the probe was chosen to minimize pressure drop along the probe, which provides more uniform sampling of the duct flow. Furthermore, the sampling probe has 10 orifices with diameters of 1.18 mm each evenly distributed throughout the section of the probe that is inside the duct. The sampling orifices face upwards, away from the incoming flow in order to prevent soot from obstructing the probe's orifices. 1.18 mm was chosen for the diameter of the orifices as there was a worry that a smaller diameter drill bit would be too thin and break when drilling into stainless steel, damaging the probe. With this diameter, the number of orifices was decided by calculating the ratio of pressure drop across the entire sampling probe to the pressure drop across the orifice and confirming that this ratio was larger than 10 to 1 to ensure uniform flow velocity from each orifice [14]. The calculation for the pressure drop across the sampling probe was done by using the Poiseuille Equation,

$$\Delta P_{probe} = \frac{8\mu L \dot{V}_{probe}}{\pi R^4}, \quad (1)$$

where μ is the dynamic viscosity of air at 20 °C, L is the length from the center of the probe to the edge of the duct wall, \dot{V}_{probe} is the volumetric flowrate being drawn from one end of the sampling probe, R is the inside radius of the sampling probe, and ΔP_{probe} is the

resulting pressure drop. The calculation for the pressure drop across each orifice was done by using the equation for the pressure drop through an orifice,

$$\Delta P_{hole} = \left(\frac{\dot{V}_{hole}}{CA_{hole}} \right)^2 \frac{\rho}{2}, \quad (2)$$

where \dot{V}_{hole} is the volumetric flowrate being drawn from each orifice, C is the flow coefficient, 0.65, A_{hole} is the cross-sectional area of the orifice, ρ is the density of air at 1 atm and 20 °C, and ΔP_{hole} is the resulting pressure drop. With a 1.18 mm diameter orifice, 10 orifices is the maximum number that could be placed to keep the ratio of pressure greater than 10 to 1. If the sampling probe was designed with the proposed 14 orifices along its length, then the ratio of pressure would only be approximately 6 to 1, which would not ensure uniform sampling along the duct flow.

The sampling probe is attached to the duct by two ports that are 180° apart from each other. The ports were made using Swagelok SS-600-61BT bored through bulkheads with one end shaved off to the nut so that the fitting does not cover any of the probe orifices. The seal between the drilled opening in the duct and the fitting was made using a Buna-N U-Cup Seal. 63 mm of the sampling probe protrudes out from each end of the duct to allow elbow fittings to be connected to the ends of the sampling probes. Teflon PTFE tubing is then used to draw flow from each end of the probe, and a tee connection is used to combine the flows.

Sampling is done in two different locations in the testing section. The sampling probe closer to the bottom of the test section is located 126 mm above the pitot tube, and the sampling probe that is higher up on the test section is located 202 mm above the pitot tube. The two sampling probes and ports are identical, but the sampling probes run perpendicular to each other, as seen from the planar view in Figure 2-9. Two sampling

locations are used because one sampling line is used for the CO/CO₂ analysis per the standard and one sampling line is used for soot and additional gas analysis. The sampling line that is used for CO/CO₂ analysis will be focused on this paper. Its respective gas sampling probe is located 202 mm above the pitot tube. This sampling probe and sampling line will be called gas sampling probe 1 and sampling line 1 respectively.

2.3 Gas sampling system

A flow diagram for the Gas Sampling System is provided in the standard and is shown in Figure 1-7. A new flow diagram was made for the redesign of the FPA and is shown in Figure 2-12. This flow diagram has less items than the than the ASTM standard diagram because some features were able to be consolidated into one device (i.e. gas analyzer). The main features of the redesigned gas sampling system include a soot filter to remove soot particles from the sampling flow, a chiller to remove condensation from the sampling flow, a rotameter with valve to control the sample flow, a pump to draw in the sample flow, a tee fitting to split the flow, a Drierite tube to remove any other moisture, mass flow controllers to control the flow to its respective analyzers, a hydrocarbon analyzer, and a CO/CO₂/O₂ analyzer.

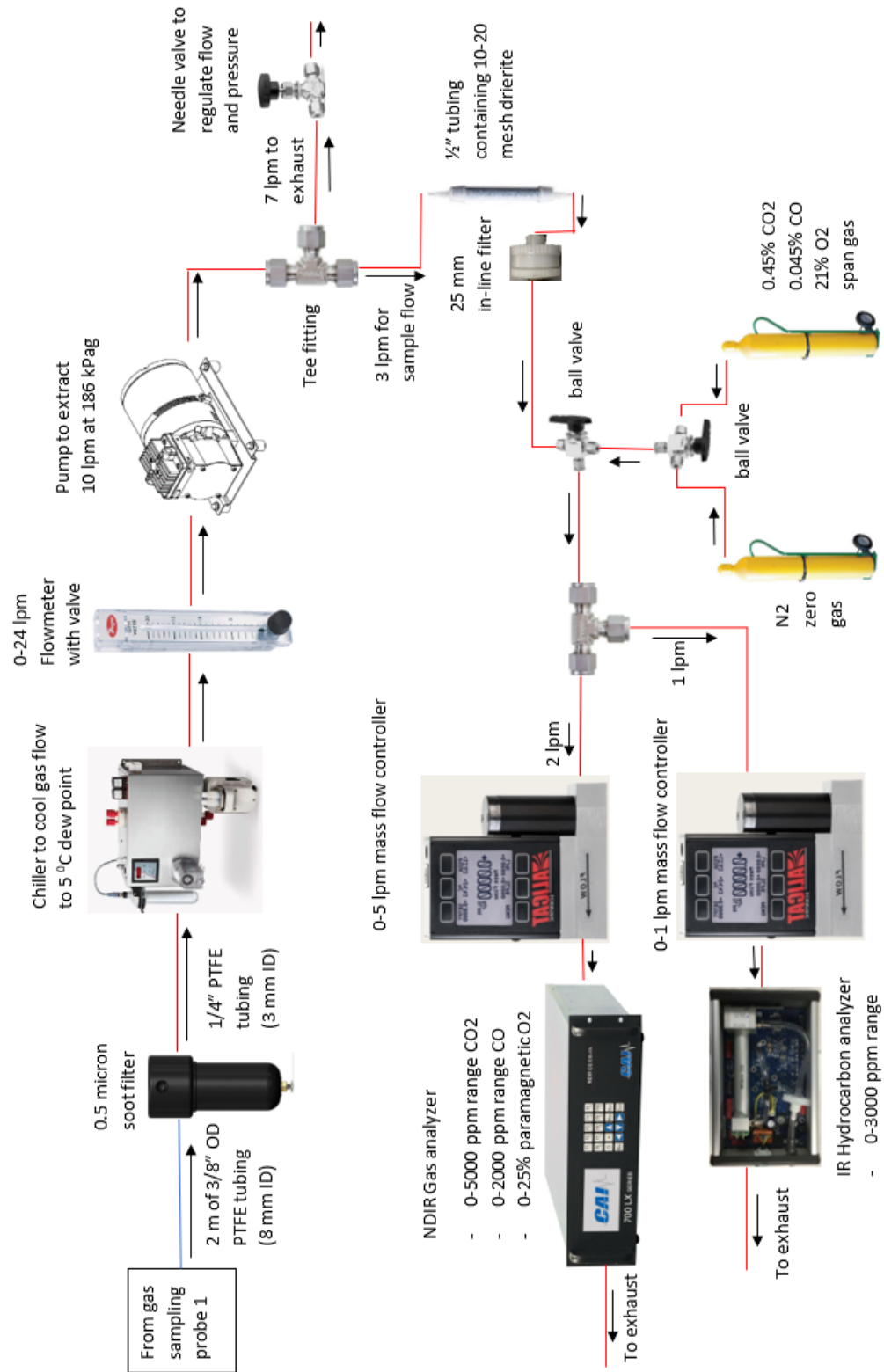


Figure 2-12. Diagram of FPA sampling flowchart.

2.3.1 Sampling System Shelf

All the gas sampling and analyzing equipment for sampling line 1 was mounted or placed on a shelf approximately 0.1 m from the Lamp Stand Frame. The frame is made from t slot aluminum profiles. The total height of the frame is 1.98 m tall and has a footprint of 0.91 m x 0.56 m. There is a separate t slot aluminum frame for the pump located within the bigger frame. The frame for the pump has dimensions of 0.36 m x 0.43 m with a height of 0.91 m. The reasoning for mounting the pump to its own frame is to ensure that the vibrations of the pump do not propagate to the analyzing equipment on the main shelf and affect measurements.

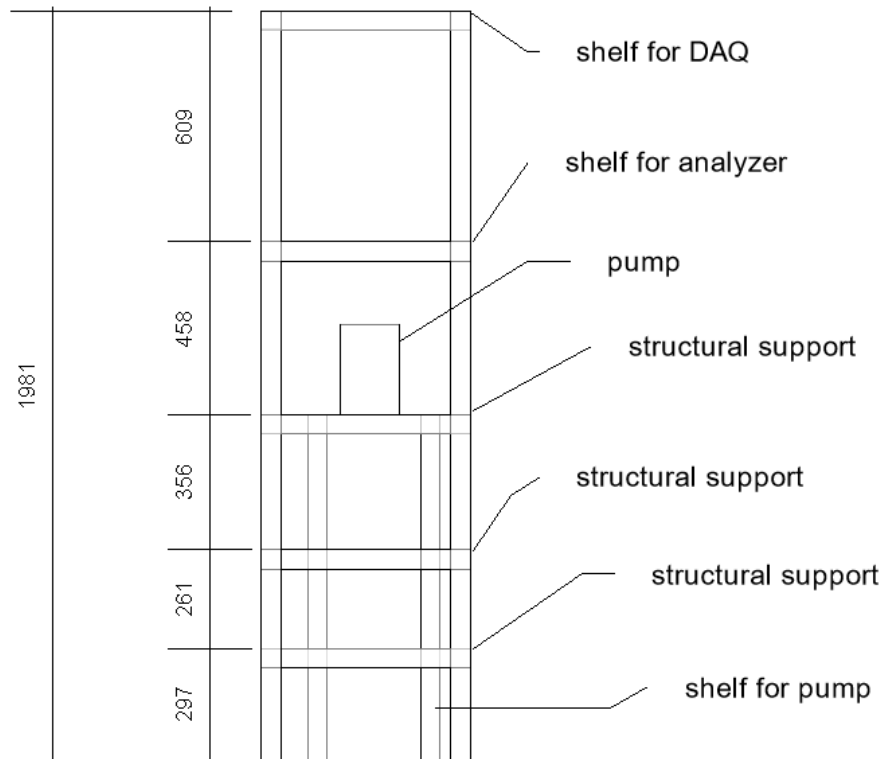


Figure 2-13. Dimensioned diagram of sampling system shelf.

2.3.2 Soot filter

8 mm ID Teflon PTFE tubing is used from the gas sampling probe to the soot filter. Following the soot filter, 3 mm ID Teflon PTFE tubing is used for the rest of the sampling line to reduce delay time. The larger sized tubing is used before the soot filter to help prevent soot clogging in the line. Teflon PTFE tubing is used for the sampling line for its chemical inertness from toxic gasses that may be present in the sample flow such as HCl, HF, and HBr [15].

The soot filter is mounted on an angle bracket mounted to the inside of the top horizontal t-slot aluminum profile, as seen in Figure 2-14. The soot filter housing is a cylindrical aluminum housing with an internal volume of 165 cc (Model 365A from United Filtration). The filter element is disposable borosilicate glass microfiber and has a mesh size of 0.5 microns (Model 25-64-70C from United Filtration). A finer filter element than was indicated in the standard was chosen because the particles of soot are known to be finer than the 5 micron size mesh that the standard suggests [16].



Figure 2-14. Picture of FPA soot filter.

2.3.3 Chiller

A chiller is used after the soot filter to cool the sample flow and remove moisture (Model TC-MIDI+ from Buhler Technologies). The chiller is mounted to the main frame structure at a height of 56 cm with the use of two vertical aluminum extrusions spaced 24 cm from each other, as seen in Figure 2-15. The Peltier cooler inside the instrument cools the flow to a dewpoint temperature of 2 °C. A peristaltic pump is attached to the chiller to discharge the moisture from the chiller. The power requirement for the chiller is 3.6 Amps at 115 VAC.



Figure 2-15. Picture of FPA chiller.

2.3.4 Pump

A diaphragm pump is used to draw in the sample flow from the exhaust duct (Model R221 from Air Dimensions). The pump has a designed flow range of 0-27 slpm of air and a zero flow pressure of 379 kPa. The power requirement for the pump is 3 Amps at 115 VAC. The pump is mounted to an expanded metal sheet on the pump stand frame using visco-elastic polymer bushings to dampen vibrations, as seen in Figure 2-16.



Figure 2-16. Picture of sample pump for FPA.

A rotameter with a valve (Model RMB-52D-SSV from Dwyer) is placed in the sampling line before the pump to control the sample flow to 10 lpm, as per the standard. After the pump, a tee connection is used to purge 7 lpm of the sample flow and retain 3 lpm to be further analyzed. A pressure gauge is placed right after the purge line to monitor the pressure in the line downstream of the pump. If the pressure is outside the range for the analyzing equipment, the pressure can be controlled by opening or closing the needle valve

on the purge line. The flowmeter, pressure gauge, and needle valve are mounted onto a PVC panel on the south side of the sampling shelf frame, as seen in Figure 2-17.



Figure 2-17. Front view of the FPA sampling system shelf.

2.3.5 Drierite

Any excess moisture in the sample flow is removed after the split flow by an 11 mm ID tubing filled with 10-20 mesh Drierite, as seen in Figure 2-17. An in-line paper filter is used after the Drierite to ensure that dust produced from the Drierite does not enter and damage the analyzer. The filter housing is an in-line Delrin plastic filter holder (PN 1109 from Pall). The filter element is a Glass Microfiber Filter disk with a diameter of 25 mm and a pore size of 1.6 microns (Grade GF/A from Whatman).

2.3.6 Mass flow controllers

After the in-line filter, there is a Swagelok SS-43GXS4 3-way ball valve which is used to either direct the sample flow or the calibration gas flow to the mass flow controllers. After the correct flow is directed, a tee is used to split the flow to two mass flow controllers (Model MC Series from Alicat). One controls the flow for the CO/CO₂/O₂ analyzer at 2 lpm and the other controls the flow to the hydrocarbon analyzer at 1 lpm. These mass flow controllers are mounted to the same PVC panel as the flowmeter, as seen from Figure 2-17.

2.4 Analyzing and Data Acquisition Equipment

The signals acquired from the exhaust and sampling system include duct flow temperature readings from the thermocouples, differential pressure readings in the duct flow from the pitot tube and pressure transducer, CO₂, CO, and O₂ concentration readings from the CO/CO₂/O₂ analyzer, and hydrocarbon concentration readings from the hydrocarbon analyzer. These signals are acquired through the use of various data

acquisition modules. These data acquisition modules are within a module chassis that is placed on the top shelf of the gas sampling shelf structure. The module chassis sends the signals to a laptop through a USB extension cord. The computer program LabView from National Instruments collects and logs these signals to be used in later calculations. The program LabView also has the ability to characterize signals, and it also allows users to input equations that relate one or more measurement signals.

Absolute temperature, relative humidity, and barometric pressure measurements are also acquired at the beginning of tests through the use of the Omega iBTHX-W probe and the Omega iConnect software on the laptop.

The main electrical signal connections for the standard FPA design are displayed in Figure 2-18. As can be seen from Figure 2-18, the signal outputs from the pressure transducer and the CO/CO₂/O₂ analyzer are acquired by a 16-bit differential voltage module (Model NI-9215 from National Instruments). The signal outputs from the thermocouples are acquired by a Temperature Input Module with a measurement accuracy of 0.77 °C (Model NI-9213 from National Instruments). All signal outputs are measured at a frequency of 5 Hz. Figure 2-18 also shows the power connections of large instruments and a description of the wattage requirement.

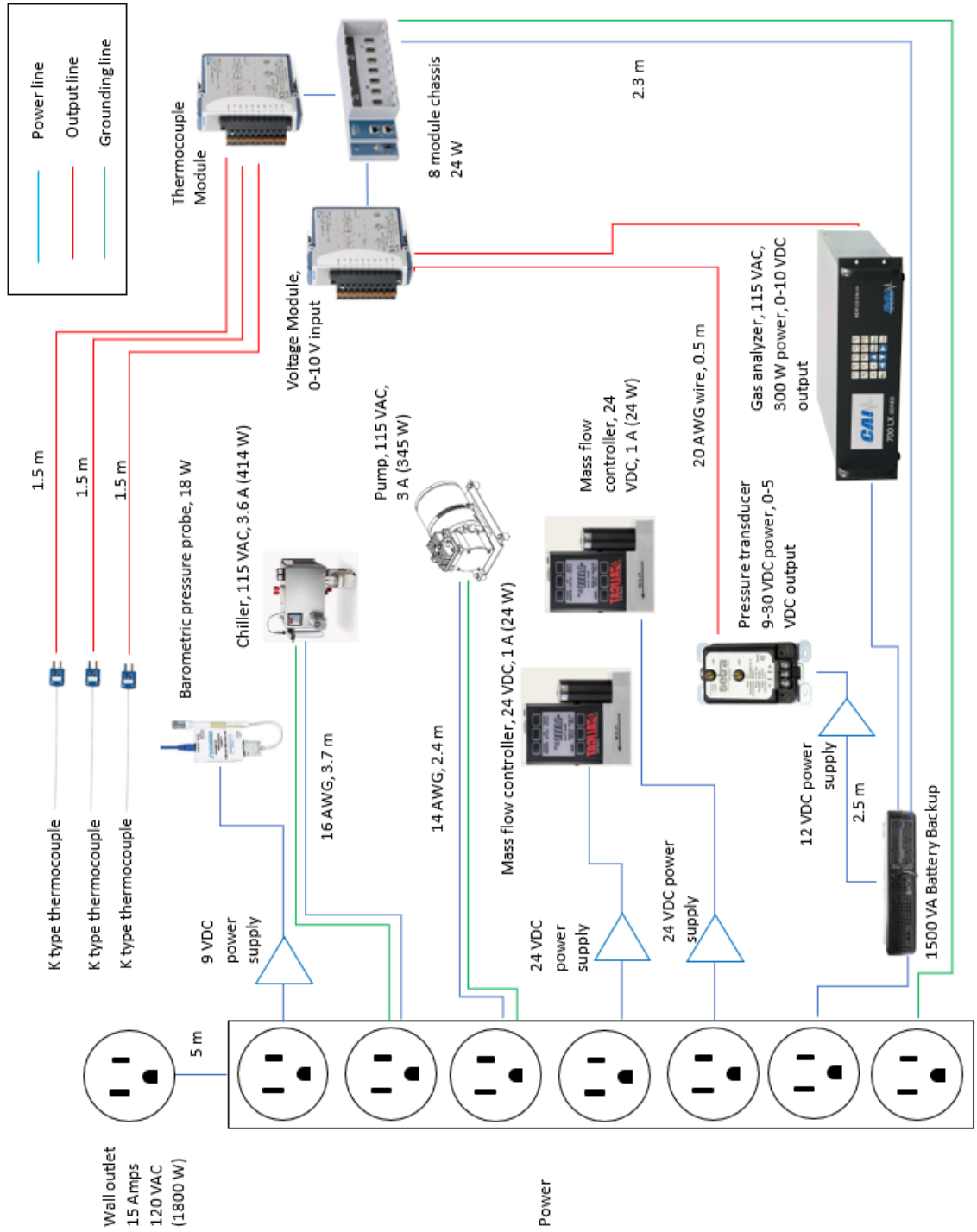


Figure 2-18. FPA electrical diagram.

2.4.1 CO/CO₂/O₂ analyzer

The 2 lpm flow is directed to an analyzer that measures CO, CO₂, and O₂ (Model 703LX Analyzer from California Analytical Instruments). The CO and CO₂ concentrations are measured using Non-dispersive IR (NDIR) technology, and the O₂ concentration is measured using paramagnetic technology. The analyzer ranges are: 0-5000 ppm for CO₂, 0-2000 ppm for CO, and 0-25% for O₂. The precision of these measurements is better than 1% full scale and the zero and span drift are less than 1% of full scale per 24 hrs.

The CO₂ range was chosen by calculating the theoretical concentration of CO₂ produced in the exhaust flow in a complete combustion scenario of polyethylene and multiplying that concentration by a factor of 2 [17]. This resulted in a range lower than the 15000 ppm per the standard, but, as the calculation confirmed that CO₂ concentration should not exceed 2532 ppm in the exhaust flow, a smaller full-scale range was selected in the hopes of getting more precise measurements. The calculation for the maximum CO₂ concentration can be found in Appendix C.1.

The CO range was chosen by looking at the CO yield for polyethylene in an under ventilated scenario, as the CO yield is greater when the equivalence ratio is greater than 1. As the FPA has the ability to change the gaseous environment to oxygen limited, the CO yield in this environment was considered to ensure that the range of CO concentration chosen for the analyzer is large enough for this condition. Using the data from the SFPE Handbook for the CO yield of polyethylene at a fuel to air equivalence ratio of 3 [9] and coupling that yield with the standard exhaust flowrate, the theoretical maximum CO concentration in the exhaust was found to be around 1450 ppm. This is an overestimation as the mass loss rate for polyethylene at an equivalence ratio of 3 would be less than the

mass loss rate at a well ventilated scenario, but a 2000 ppm range was chosen to ensure that the concentration will not exceed the analyzer range, especially for fuels that produce a larger CO yield. This calculation for the CO concentration is further explained in Appendix C.2.

The paramagnetic O₂ sensor is used if oxygen consumption calorimetry is desired to be used instead of carbon oxide generation calorimetry. This gives flexibility in choice of which method to use to calculate heat release rate depending on what burning scenario is used for the test and how well the composition of the fuel is known. The ability to use both methods is also useful in verifying one method or the other as the heat release rate calculated from carbon oxide generation should be close to the one calculated from oxygen consumption [12]. The range 0-25% was used as the concentration of ambient air is approximately 21%.

The CO/CO₂/O₂ analyzer runs continuously on 3 Amps and 115 VAC and is located on a shelf of expanded metal sheet 1.38 m above the ground. The analyzer provides a total of three output signals, one for CO, one for CO₂, and one for O₂, that range from 0-10 VDC.



Figure 2-19. Picture of CO/CO₂/O₂ analyzer.

2.4.2 Hydrocarbon Analyzer

1 lpm of the sample flow goes to an infrared hydrocarbon sensor (Boxed Gascard from Edinburgh Sensors) with a range of 0-3000 ppm. It is mounted between the analyzer and a PVC panel on the side of the shelf frame, with a flame retardant foam block cushioning the analyzer from the panel, as seen in Figure 2-20.



Figure 2-20. Picture of Hydrocarbon Analyzer.

The hydrocarbon analyzer is used in conjunction with the toxicity analysis measurements from gas sampling line 2 which is out of the scope of the standard apparatus and this project. However, as explained in Chapter 1.2.3, it is important to note that incorporating the hydrocarbon concentration to the heat release calculations can improve the accuracy of the heat release calculation for extreme under-ventilated fire scenarios.

2.4.3 Surge Protector

A 1500VA Smart UPS Battery back-up and surge protector is used to provide uninterrupted regulated power to all measuring and data acquisition devices. The specific devices connected to the surge protector can be seen in Figure 2-18.

2.4.4 Atmospheric Pressure/Humidity/Temperature Probe

The absolute pressure, temperature, and humidity of the laboratory is measured through the Omega i-BTHX-W probe, which is mounted on the top shelf of the sampling system shelf, as seen in Figure 2-21. The readings are acquired by the iConnect software on the laptop using a crossover ethernet cable. The absolute pressure, temperature, and humidity are used in the calculation for the heat release rate.



Figure 2-21. Picture of barometric pressure/absolute temperature/absolute humidity probe.

2.5 Calibration system

Before each day of experiment with the CO/CO₂/O₂ analyzer, the analyzer needs to be calibrated. The zero gas is delivered from a high purity N₂ gas cylinder through a 3mm semi-flexible tubing. The span gas is delivered through a 3 mm semi-flexible tubing from a gas mixture consisting of 0.045% CO, 0.45% CO₂, 20.95% O₂, with the rest of the mixture being N₂. A Swagelok SS-43GXS4 3-way ball valve is used to choose which gas to deliver to the gas analyzer, as shown in Figure 2-22. The calibration procedure is outlined in Appendix A.1.

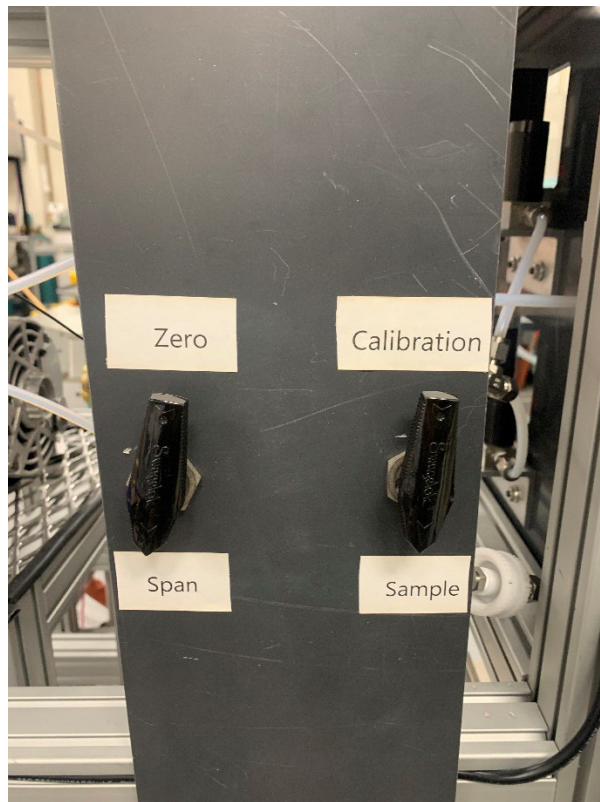


Figure 2-22. Picture of calibration panel.

Chapter 3: Apparatus Characterization

After construction of the FPA, the outputs for the sampling and analyzing system needed to be characterized and verified to ensure that the system works correctly and provides the desired outputs. This chapter characterizes the pressure transducer and CO/CO₂/O₂ analyzer outputs as well as verifies the measurements for the exhaust mass flow and analyzer gas concentrations.

3.1 Mass flow check

3.1.1 Pressure Transducer Calibration

The pressure transducer manufacturer provided a calibration sheet specific to the transducer used in the FPA that relates the voltage output to a differential pressure. The calibration points were plotted and a second-degree polynomial curve was fit through all the points to produce a plot that relates voltage output to differential pressure in Pascals. The curve, along with the equation for curve of best fit and its coefficient of determination, can be seen in Figure 3-1.

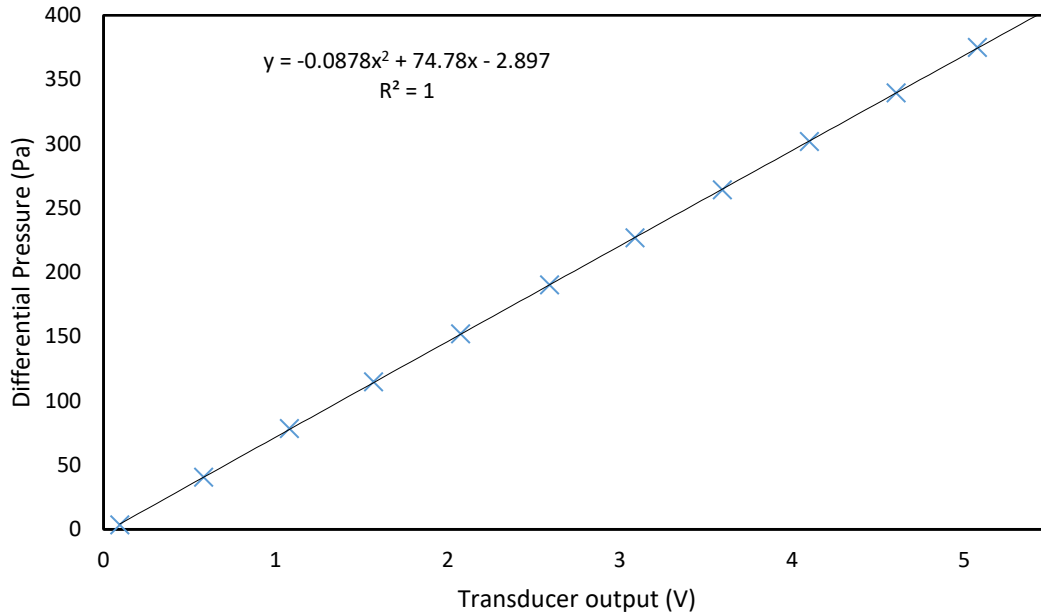


Figure 3-1. Calibration curve for FPA Pressure Transducer.

This calibration equation was inserted into LabView to produce an output of differential pressure in LabView instead of volts.

3.1.2 Pitot Tube Flow Calculation

The Bernoulli equation [18] was used to relate the differential pressure reading of the pitot tube to actual flowrate in the duct. The Bernoulli equation, as given by,

$$P_1 + \frac{1}{2}\rho u_1^2 + \gamma h_1 = P_2 + \frac{1}{2}\rho u_2^2 + \gamma h_2, \quad (3)$$

where P is pressure, ρ is density of the air, u is velocity, γ is specific weight, and h is height, can be simplified further by eliminating the hydrostatic pressure terms on both sides (γh), since the elevation gain within the pitot is zero, and eliminating the second dynamic pressure term ($\frac{1}{2}\rho u_2^2$), since the dynamic pressure is converted to added static pressure in the pitot tube. Simplifying and solving for velocity, the equation becomes,

$$u_1 = \sqrt{\frac{2(P_2 - P_1)}{\rho}}. \quad (4)$$

Since the desired value is volumetric flow, both sides are multiplied by the inside area of the duct to get the right side of the equation to be volumetric flow. Furthermore, the flow coefficient of the Veris Verabar V100 pitot tube, K , which is 0.7297, is added to the formula. This flow coefficient is calculated by the pitot tube manufacturer and is related to the flow resistance from the pitot tube. Lastly, density of the air is replaced using the ideal gas law,

$$\rho = \frac{P_a MW}{RT}, \quad (5)$$

where P_a is the static pressure at the point of measurement in Pa, MW is the molecular weight of air (0.02896 kg/mol), R is the universal gas constant (8.31451 J/(mol K)), and T is the temperature of the exhaust flow in Kelvin. The terms P_a and T are used instead of ρ as these terms are measured precisely unlike the density of the air. The temperature of the duct flow is calculated by averaging the three thermocouple measurements in the duct at the same time instant that the differential pressure is being measured by the pitot tube. Since the thermocouples read the temperature in Celsius, the thermocouple readings at each time step t are converted into Kelvin using the formula,

$$T^t = \left(\frac{T_1^t + T_2^t + T_3^t}{3} \right) + 273.15. \quad (6)$$

The pressure of the flow at the pitot tube (P_a) is calculated by taking the barometric pressure measurement from the Omega iBTHX-W probe at the beginning of the test and subtracting it by the differential pressure measured by the pressure transducer. Because the probe reads the pressure in bar, the pressure of the flow at the pitot tube is converted to units of pascals using the formula,

$$P_a^t = P_{room} * 1 \times 10^5 - \Delta P^t \quad (7)$$

where P_{room} is the barometric pressure in the room in bar and ΔP^t is the differential pressure outputted by the pressure transducer in units of Pascals at time step t . This leads to an equation for the volumetric flow at any time step t inside the duct,

$$\dot{V}^t = \frac{\pi}{4} D^2 K \sqrt{2(\Delta P^t) \left(\frac{RT^t}{P_a^t MW} \right)}, \quad (8)$$

where D is the inside diameter of the duct in meters, K is the flow coefficient (0.7297), R is the universal gas constant in units of J/K mol, and MW is the molecular weight of air in units of kg/mol.

The manufacturer of the pitot tube, Veris, provided an equation relating the differential pressure to volumetric flow,

$$\dot{V} = \frac{N * K * Y_v * F_a * D^2}{\sqrt{MW}} \sqrt{\frac{h_w T Z_f}{P_a}}, \quad (9)$$

where N is the numerical constant 103, K is the flow coefficient of the pitot tube with a value of 0.7292, Y_v is the expansion factor of the gas with a value of 0.9998, F_a is the thermal expansion factor of the gas with a value of 1, D is the diameter of the duct in inches, MW is the molecular weight of the gaseous flow in units of g/mol, h_w is the differential pressure read by the pressure transducer in units of inches of water column, T is the temperature of the flow in units of Rankine, Z_f is the flowing compressibility of the gas with a value of 0.999, and P_a is the pressure of the flowing gas at the pitot tube in units of inches of water column. The Veris flow equation calculates volumetric flow in units of cfm, but, converting it to m^3/s is necessary to compare it to the volumetric flow equation derived from Bernoulli's, so the Veris flow equation is multiplied by a factor of 0.000472 to convert the units to m^3/s .

The Veris flow equation was compared to the flow equation derived from Bernoulli's by calculating the volumetric flow for an array of voltage outputs from the range of 0.1 to 5 Volts for both flow equations and plotting them together in MATLAB. This was done for two different temperature and pressure scenarios. For the first plot, the temperature of the flow is given as 16 °C and the pressure is given as 101325 Pa. For the second plot, the temperature of the flow is given as 38 °C and 99000 Pa. As seen from Figures 3-2 and 3-3, for both cases, the two equations produce identical flows within the voltage range of the pressure transducer, showing that the two equations can be used interchangeably. As the equation derived from Bernoulli has less terms in general and all its terms are in SI units, this equation was chosen to be programmed into LabView to directly display volumetric flow to the user.

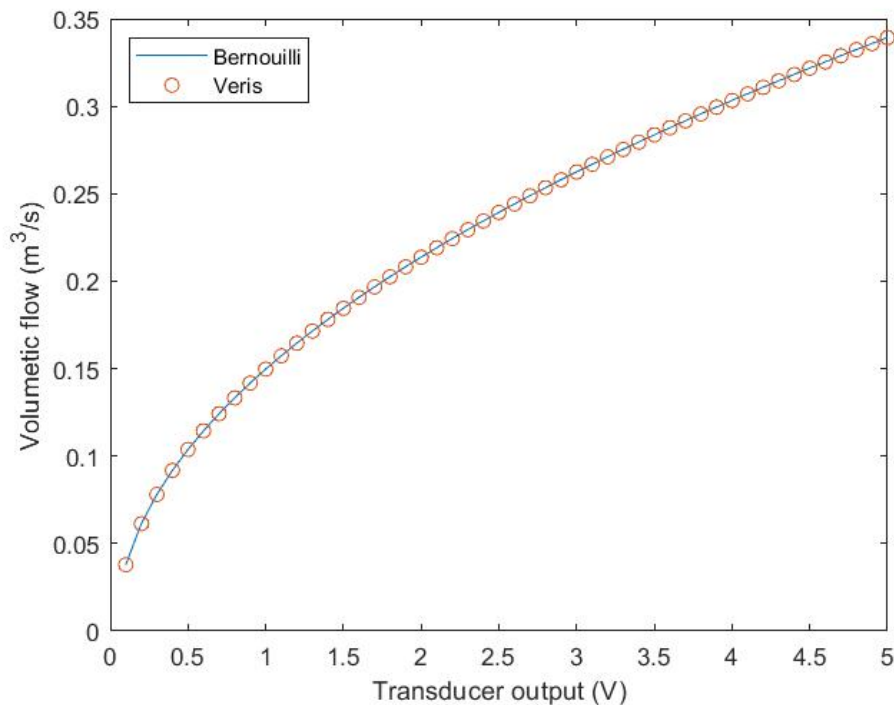


Figure 3-2. Comparison between Bernoulli flow calculations and Veris flow calculations for case with T = 16 °C and P_a = 101325 Pa.

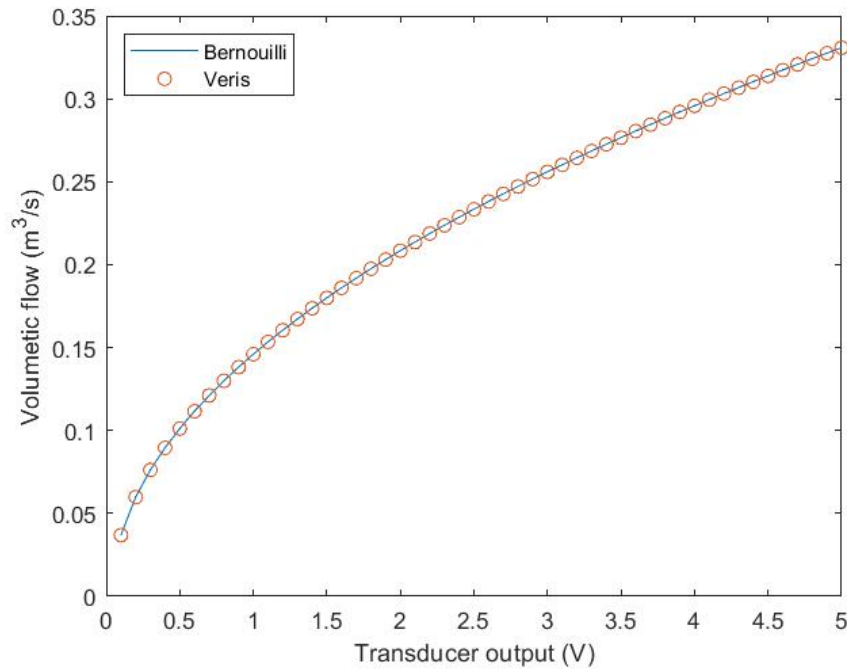


Figure 3-3. Comparison between Bernoulli flow calculations and Veris flow calculation for case with $T = 38\text{ }^{\circ}\text{C}$ and $P_a = 99000\text{ Pa}$.

3.1.3 Anemometer flow calculation

To verify the flow calculated from the pitot tube, the duct flow was also measured using an Omega HHF-SD1 Hot Wire Anemometer. The anemometer measured the flow by inserting it into a cardboard tube with a cross sectional area of 0.0182 m^2 that extended from the mixing duct. The anemometer probe was inserted through an opening 130 mm from the bottom of the tube extension in an orientation where the probe was perpendicular to the direction of the duct flow. A honeycomb and mesh were inserted in the bottom of the extension to make the flow laminar. The honeycomb has a diameter of 0.1524 m and a thickness of 18 mm. The width of the openings on the honeycomb is 7 mm. The mesh has a diameter of 0.1524 m and a thickness of 1 mm. The width of the openings on the mesh is 4 mm. Figure 3-4 shows this setup.

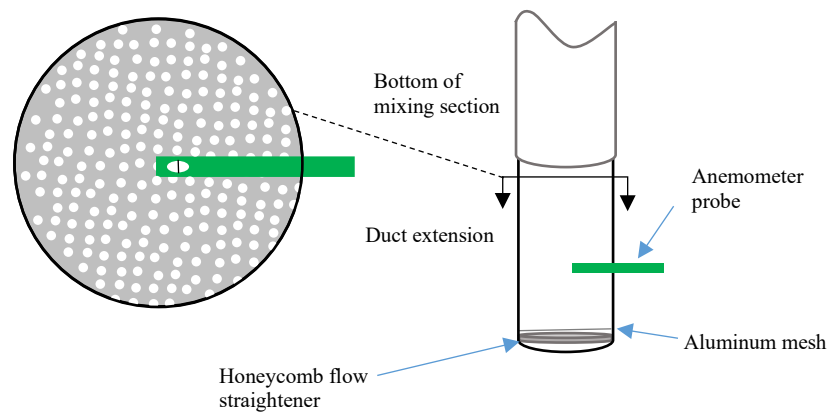


Figure 3-4. Setup for Anemometer flow calculations.

The anemometer was traversed in a straight line along the diameter of the duct extension, and measurements were taken at 7 locations along this line. Two measurements were taken at the center of the duct, and one measurement was taken on each side of the center at locations 25.4 mm, 50.8 mm, and 66.7 mm away from the center. Each point corresponded to a fraction of the cross-sectional area of the duct extension, as seen from Figure 3-5.

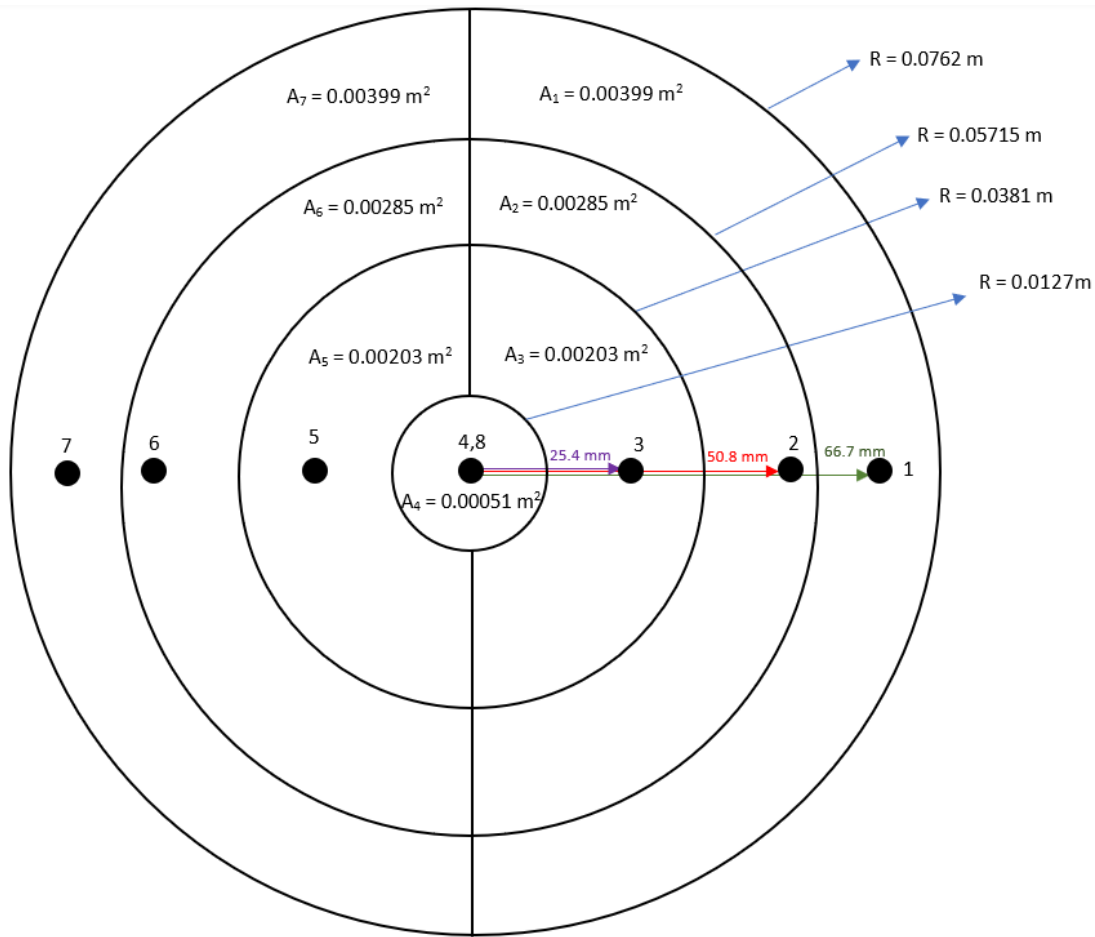


Figure 3-5. Diagram showing the anemometer probe locations and corresponding sectional areas. The circle is symmetric and the radial distance of the anemometer locations on the left side are equivalent to the radial distance of the anemometer locations on the right side.

The volumetric flow was computed by taking the area weighted average of the velocity readings and integrating it with the total cross-sectional area. Since the flow area in the duct decreases slightly from inserting the anemometer probe, which has a diameter of 0.01 m, into the duct extension, there is a coefficient in front of each term that considers that adjustment, assuming constant volumetric flow. The coefficient is calculated using the formulas,

$$\text{for } i = 1: 6, C_i = \frac{A_{\text{reduced}}}{A_{\text{original}}} = \frac{0.0182 - 0.01 * 0.025(i-1)}{0.0182}, \quad (10a)$$

$$\text{for } i = 7, C_i = \frac{A_{\text{reduced}}}{A_{\text{original}}} = \frac{0.0182 - 0.01 * 0.14}{0.0182} \quad (10b)$$

The reduced area was calculated by subtracting the original cross-sectional area of the duct extension by the area of the anemometer probe, estimating the anemometer probe as a rectangle with the probe diameter as the width and the amount of probe length inserted as the length. Adding this term, the volumetric flow equation becomes,

$$\dot{V}_a = C_1 u_1 A_1 + C_2 u_2 A_2 + C_3 u_3 A_3 + C_4 \frac{u_4 A_4}{2} + C_5 u_5 A_5 + C_6 u_6 A_6 + C_7 u_7 A_7 + C_4 \frac{u_8 A_4}{2} \quad (11)$$

The blast gate position was altered within a flow test to calculate multiple volumetric flow measurements for each test. The results of one of the volumetric flow calculations for a singular blast gate position within one of the flow tests are shown in Table 3-1.

Table 3-1. Example of Anemometer flow calculation at a single flow condition.

u ₁ (m/s)	u ₂ (m/s)	u ₃ (m/s)	u ₄ (m/s)	u ₅ (m/s)	u ₆ (m/s)	u ₇ (m/s)	u ₈ (m/s)	Q _{calc} (m ³ /s)
4.9	6.2	6.7	7.1	7.7	7.8	6.8	7.2	0.139

To verify the pitot tube readings, the flowrate measured by the pitot tube was acquired for the duration of the anemometer tests (approximately 5 minutes). Two tests were conducted, but, because the blast gate position was altered within each test, in total, seven flows were measured and compared with the pitot tube and the anemometer. Figure 3-6 shows the flow comparison between the anemometer calculations and the time averaged pitot tube readings for each blast gate position for the two tests. As seen from the graph, the pitot tube reading differs by an average of 2% of the volumetric flow calculated from the anemometer measurements, verifying the reading made by the pitot tube.

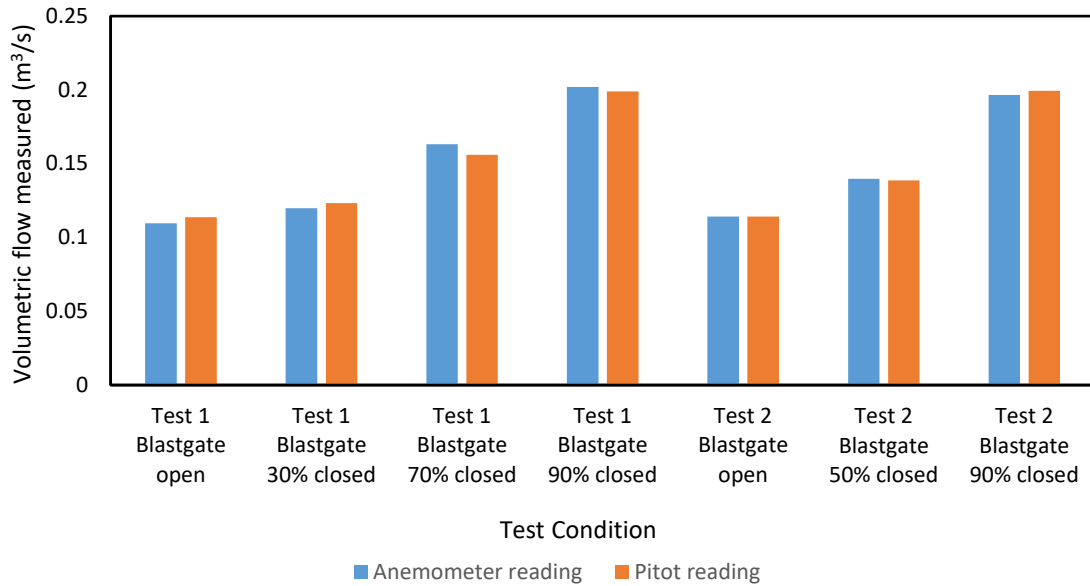


Figure 3-6. Comparison between Anemometer and Pitot readings for different flow scenarios.

The mass flow is calculated by multiplying the volumetric flowrate by the density of the exhaust flow, as shown in equation,

$$\dot{m}_{duct} = \rho \dot{V}. \quad (12)$$

The density of the exhaust air was calculated in equation 5. This mass flowrate is calculated in LabView and is used for the heat release calculations.

3.2 Sample Flow Concentration Check

To verify that the concentration of gas being sampled and measured by the analyzer is consistent with the gas concentration in the duct flow, an equation was derived to calculate the concentration of species in the duct flow when a known concentration of gas from a gas cylinder is introduced to the duct flow at a known standard flowrate. This

calculation is compared to the concentration of species measured by the CO/CO₂/O₂ analyzer.

3.2.1 Calculating concentration of species in the duct flow

The concentration of species in the sample flow to the analyzer is computed using the formula,

$$X_{i,calculated} = \frac{\dot{N}_i}{\dot{N}_{total,dry}}, \quad (13)$$

where X_i is the molar fraction of species i , \dot{N}_i is the molar flow of species i in the duct, and $\dot{N}_{total,dry}$ is the total molar flow of all species in the duct minus water vapor. Water vapor is taken out of this calculation as the sampling line removes moisture from the gas sample before it is sent to the gas analyzer.

To compute the total molar flow of all species in the duct minus the water vapor in the room air at a specific time step t , the following formula is used,

$$\dot{N}_{total,dry}^t = \dot{N}_{air}^t (1 - X_{H2O}^0) + \dot{N}_{bottle}, \quad (14)$$

where \dot{N}_{air}^t is the total molar flow of the room air entering the duct at time step t , X_{H2O}^0 is the moisture content in the room air, and \dot{N}_{bottle} is the molar flow of the gas being injected from the gas cylinder to the duct flow. The timestep t corresponds to the sampling rate of the output signals from the measurement devices.

The molar flow of gas injected from the gas cylinder is calculated using the ideal gas law, as shown below,

$$\dot{N}_{bottle} = \frac{\dot{V}_{bottle} * P_s}{R * T_s}, \quad (15)$$

where \dot{V}_{bottle} is the standard volumetric flow of the mixture controlled by the Alicat mass flow controller, P_s is standard pressure of 101325 Pa, R is the universal gas constant, and T_s is the standard temperature of 298 K.

X^0_{H2O} is found through the ratio of water vapor pressure and total ambient pressure in the room. The vapor pressure can be substituted with the saturation vapor pressure times the relative humidity in the room to give the equation of X^0_{H2O} as

$$X^0_{H2O} = \frac{\left(\frac{RH}{100} * P_{sat}\right)}{P_{room}}, \quad (16)$$

where RH is the relative humidity measured by the Omega iBTHX-W probe in percent, P_{sat} is the saturated vapor pressure at the room's temperature, and P_{room} is the ambient pressure in the room measured by the Omega iBTHX-W probe. The saturated vapor pressure in millibar is found through the Magnus-Tetens equation [19],

$$P_{sat} = (6.1078) * \exp\left(\frac{17.2694*(T_a-273.16)}{(T_a-35.86)}\right), \quad (17)$$

where T_a is the ambient temperature measured by the Omega iBTHX-W probe in Kelvin. This equation agrees with the water vapor pressure values reported in the NIST Webbook within a 1% error [20].

The total molar flow of the room air entering the duct at time step t is calculated using the formula,

$$\dot{N}^t_{air} = \dot{N}^t_{total} - \dot{N}^t_{bottle}, \quad (18)$$

where \dot{N}^t_{total} is the total molar flow entering the duct at time step t. The total molar flow can be calculated using the ideal gas law, as shown below,

$$\dot{N}^t_{total} = \frac{\dot{V}^t * P_a^t}{R * T^t}, \quad (19)$$

where \dot{V}^t is the volumetric flow inside the duct at time step t measured by the pitot tube, P_a^t is the pressure of the duct at the pitot tube location at time step t, R is the universal gas constant, and T^t is the average of the temperature readings of the three thermocouple probes at time step t.

Finding the total molar flow of each species entering the duct at time step t is calculated using the formula,

$$\dot{N}_i^t = X_{i,bottle} * \dot{N}_{bottle} + X_{i,dry\ air} * \dot{N}_{air} (1 - X_{H2O}), \quad (20)$$

where $X_{i,bottle}$ is the concentration of species i in the gas cylinder and $X_{i,dry\ air}$ is the concentration of species i in the room air without moisture. $X_{i,dry\ air}$ is found by sampling only the room air before injecting the gas from the cylinder and taking the average concentration measurement of species i from the analyzer during that time.

3.2.2 Characterizing CO/CO₂/O₂ analyzer outputs

Before verifying the CO/CO₂/O₂ gas analyzer measurements, the voltage output from the analyzer needed to be converted to concentration. Each voltage output for the analyzer has a range of 0-10 VDC. As the relationship between the voltage output and the concentration measured is linear, the concentration of each species can be found using the equation,

$$X_{i,measured} = \left(\frac{X_{max,analyzer,i}}{10} \right) * V_{output,i}, \quad (21)$$

where $X_{max,analyzer,i}$ is the maximum concentration that can be measured by the analyzer for species i, $V_{output,i}$ is the voltage output produced by the analyzer for species i, and $X_{i,measured}$ is the resultant concentration measured by the analyzer for species i. This

equation is incorporated in LabView so that the voltage output is displayed and logged as concentration measured for CO, CO₂, and O₂. To ensure that a voltage output of 0 corresponds to a concentration of 0, the analyzer is calibrated every day before experiments. When the zero calibration is performed, and only nitrogen is running through each sensor, the analyzer automatically changes the voltage output to zero. Similarly for the span calibration, the analyzer automatically changes the voltage output so that $V_{output,i}$ is the correct value that, when plugging into equation 21, gives an answer of $X_{i,measured}$ that matches the concentration of species i in the span gas. The procedure on doing the zero and span calibration is further explained in Appendix A.1.

3.2.3 CO₂ concentration check test

Experiments were conducted to verify that the concentration of species measured from the gas analyzer corresponded to the concentration calculated from equation 13. The first experiment introduced gas from a pure CO₂ gas cylinder at the location where the sample is placed during a burn test. The flowrate was controlled with an Alicat mass flow controller. The tubing connecting to the outlet of the mass flow controller was fed through the opening at the bottom of the air distribution chamber and affixed to the sample location height using the heat flux gauge mount, as seen in Figure 3-7. Before the test, the valve to the CO₂ gas cylinder is opened for a few seconds to allow the tubing to be filled with CO₂ gas. This way, during the test, CO₂ gas flows through the opening of the tube instantly after opening the valve to the gas cylinder. This is to simulate the gaseous mass flow during a burn test, so that an approximate delay time can be calculated as well.

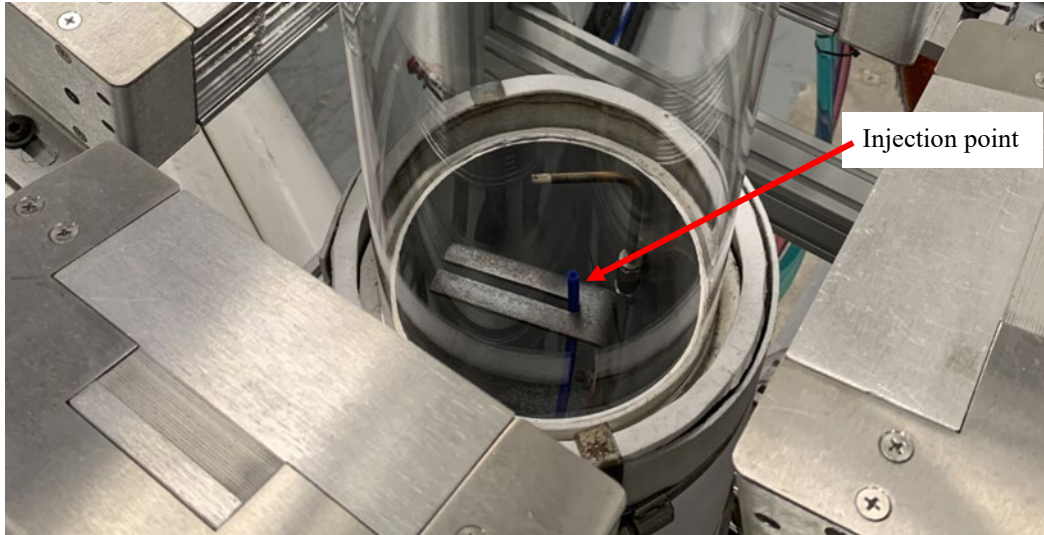


Figure 3-7. Setup for the CO₂ concentration check tests.

The test starts with the valve of the gas cylinder turned off to allow the analyzer to measure the sampled room air, which is used for $X_{i,dry\ air}$ in the duct flow concentration calculation. After approximately 30 seconds, the gas cylinder valve is turned on to discharge the cylinder gas flow. The time when the gas cylinder valve was opened is recorded. The gas travels upwards along the quartz tube with the help of the air flow from the FPA air distribution chamber and enters the duct. The new duct flow with the inclusion of the CO₂ gas is sampled and measured by the analyzer for approximately 90 seconds. Afterwards, the gas cylinder valve is turned off and room air is sampled for another 30 seconds for the conclusion of the test. The time when the gas cylinder valve is closed is recorded.

After calculating the molar fraction of each species from equations 13 through 20, this molar fraction is compared to the concentration read by the analyzer.

This test was conducted numerous times for two different blast gate positions and two different mass flowrates of CO₂ injected. The positioning of the blast gate position

affected the volumetric flowrate within the duct. With the blast gate fully closed, there is an average volumetric flowrate of 0.253 m³/s in the main exhaust duct, and, with the blast gate fully open, there is an average volumetric flowrate of 0.137 m³/s in the main exhaust duct. The two different mass flowrates chosen for the CO₂ gas were 10.20 slpm and 6.17 slpm. In total, seven different tests were conducted. The results of these tests, as well as test conditions, can be seen in Table 3-2. For each test, the calculated CO₂ concentration was averaged over a 50 second duration while the CO₂ gas was flowing into the duct system. The upper and lower bounds for the average concentration calculated represent two standard deviations of the mean from the average concentration value. The average measured concentration from the CO₂/CO/O₂ gas analyzer for the same 50 second duration is also recorded in Table 3-2. The error between the two values is calculated from the formula,

$$error_{CO_2} (\%) = \frac{X_{CO_2,measured} - X_{CO_2,calculated}}{X_{CO_2,calculated}} * 100. \quad (22)$$

As can be seen from Table 3-2, the concentration of CO₂ measured by the analyzer is within 2.2 % of the CO₂ concentration calculated through molar flowrates for all tests.

Table 3-2. Comparison between concentration of CO₂ being sampled to the analyzer and the concentration of CO₂ measured by the analyzer.

Test	Flowrate of CO ₂ (slpm)	Duct flowrate (m ³ /s)	Calculated CO ₂ concentration (ppm)	Measured CO ₂ concentration (ppm)	Error (%)
1	6.17	0.252 ± 0.012	939 ± 21	939 ± 23	0.0
2	6.17	0.253 ± 0.012	924 ± 18	944 ± 33	2.2
3	6.17	0.137 ± 0.010	1248 ± 55	1236 ± 62	-1.0
4	10.20	0.252 ± 0.014	1217 ± 36	1211 ± 26	-0.5
5	10.20	0.254 ± 0.012	1220 ± 29	1211 ± 34	-0.7
6	10.20	0.137 ± 0.009	1762 ± 82	1734 ± 63	-1.6
7	10.20	0.137 ± 0.010	1721 ± 75	1690 ± 58	-1.8

3.2.4 O₂ concentration check test

A similar experiment was conducted to verify the concentration of O₂ measured by the gas analyzer. This experiment was conducted by flowing pure N₂ from a gas cylinder through the tubing that is regularly used for the inlet airflow for the FPA. So, instead of air flowing through the air distribution chamber at a flow rate of 200 slpm, pure N₂ was flowing through, with the volumetric flow set to 125 slpm. This larger flow of N₂, compared to the flow of CO₂ for the previous mentioned experiments, allowed for a more noticeable dip in the O₂ measurement from the analyzer.

The experiment starts with the nitrogen gas cylinder valve closed to sample only room air to the gas analyzer. After approximately 30 seconds, the valve to the nitrogen gas cylinder is opened and the time is simultaneously recorded. The time when the mass flow controller stabilizes to a flowrate of 125 slpm is also recorded. After approximately 90 seconds of stable mass flow, the cylinder valve is closed and the room air is sampled for another 30 seconds for the conclusion of the test.

The concentration of O₂ calculated using equation 13 for each test was compared to the concentration of O₂ measured by the O₂ sensor. Four tests were taken, two with the blast gate fully closed and two with the blast gate fully open. The average measured and calculated concentration of O₂ for each test is shown in Table 3-3, along with the upper and lower bounds, which corresponds to two standard deviations of the mean. The average concentration was taken during a 50 second period where there was steady flow of N₂ gas flowing from the air distribution chamber. The error between the measured and calculated concentration was calculated using the equation,

$$error_{O_2}(\%) = \frac{X_{O_2,calculated} - X_{O_2,measured}}{X_{O_2,dryair} - X_{O_2,measured}} * 100, \quad (23)$$

where $X_{O_2,dryair}$ is the concentration of O₂ measured from the analyzer in the beginning of the test when only room air is sampled ($X_{O_2,dryair} \approx 20.97\%$). Unlike the case for CO₂, the denominator represents the change in O₂ concentration when the nitrogen gas is introduced. As the change in O₂ is small compared to the ambient O₂ present in the room, comparing the difference of the calculated and measured O₂ concentrations to the change in O₂ concentration gives a more accurate error representation.

Table 3-3. Comparison between concentration of O₂ being sampled to the analyzer and the concentration of O₂ measured by the analyzer.

Test	Duct Flowrate (m ³ /s)	Calculated O ₂ concentration (%)	Measured O ₂ concentration (%)	Error (%)
1	0.253 ± 0.012	20.803 ± 0.008	20.801 ± 0.023	-1.2
2	0.253 ± 0.012	20.808 ± 0.008	20.811 ± 0.020	1.8
3	0.136 ± 0.010	20.655 ± 0.023	20.663 ± 0.030	2.6
4	0.136 ± 0.010	20.657 ± 0.022	20.663 ± 0.021	2.0

As can be seen from Table 3-3, the average measured concentration of O₂ is within the upper and lower bounds of the average calculated O₂ concentration for all tests and is within 2.6% error for all tests. From the results of these tests, it was concluded that the sampling line provided the correct concentration of species in the duct to the CO/CO₂/O₂ analyzer.

3.2.5 Delay and Response time calculations

The concentration check tests were also used to determine the delay times for measurement signals and the response time for the CO/CO₂/O₂ gas analyzer.

Analyzer delay time is defined as the time it takes for a sample of the CO₂ gas ejected from the tubing shown in Figure 3-7 to reach the gas analyzer. This delay time is used to shift the gas analyzer measurements, so that they match to the time the gas was produced. The delay time was calculated by finding the time difference between the moment the valve was opened from the gas cylinder to the moment there was a noticeable increase in the CO₂ concentration. This noticeable increase was defined as 10% of the total increase in CO₂ concentration for the test.

Response time is defined as the time it takes for an instrument, in this case the CO/CO₂/O₂ analyzer, to reach 63% of a step change in physical property. The 63% comes from the time constant in the formula,

$$X_m = X_1 - (X_1 - X_0)e^{-t/\tau} \quad [21], \quad (24)$$

where X_m is the measurement value from the instrument, X_0 is the value of the property being measured before the step change, X_1 is the value of the property being measured after the step change, t is time, and τ is the time constant. When $t = \tau$, the measured value becomes equal to the base value plus 63% of the step change. To find the response time of the CO₂ analyzer, the time difference from the moment there was a noticeable increase in the CO₂ measurement, as defined in the calculation of the analyzer delay time, to the moment the analyzer measured 63% of the total increase in the CO₂ concentration for the test.

The CO₂ concentration as a function of time for test 5 is shown in Figure 3-8 with indicating lines to show when the CO₂ gas was introduced to the FPA system and when the CO₂ gas was removed from the FPA system, so that the delay time and response time can be calculated. This approach was taken for all seven CO₂ concentration tests and the average CO₂ sensor delay and response time for the system was calculated. The average delay time for the CO₂ sensor across the 7 tests was 8.11 ± 1.1 s, where the bounds are calculated as two standard deviations of the mean. The average response time for the sensor across these tests was calculated to be 3.37 ± 1.2 s, where the bounds are calculated as two standard deviations of the mean.

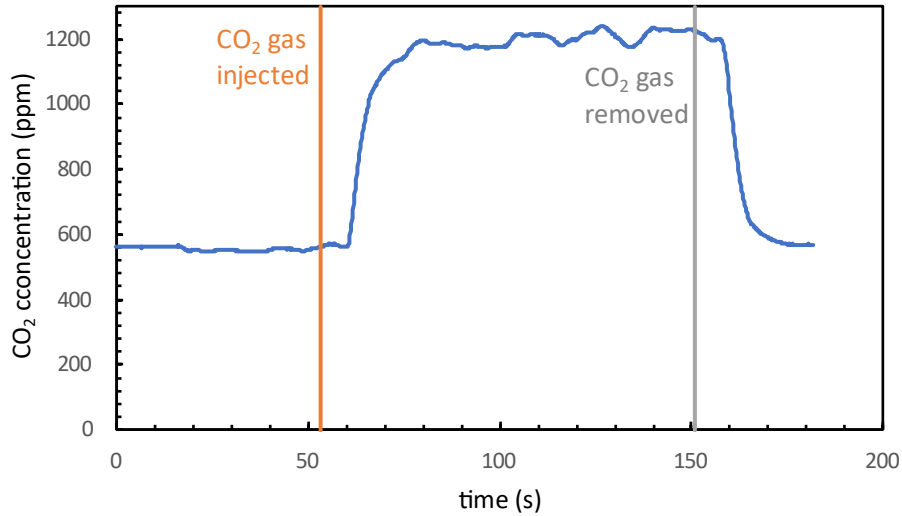


Figure 3-8. CO₂ concentration measured by gas analyzer over time for CO₂ gas flow test 5.

The O₂ sensor delay and response times were calculated similarly to the way the CO₂ sensor delay and response times were calculated. The delay time is determined as the time difference from when the N₂ gas bottle valve was opened to when 10% of the total decrease was observed in the O₂ measurements. The response time is determined as the time from when there was a 10% of the total decrease to 63% of the total decrease. The O₂ concentration as a function of time for test 3 is shown in Figure 3-9 with indicating lines to show when the N₂ gas was introduced to the FPA system and when the N₂ gas was removed from the FPA system, so that the delay time and response time can be calculated. The average sensor delay time for the O₂ sensor across all four O₂ concentration check tests was 12.48 ± 2.0 s, where the bounds are calculated as two standard deviations of the mean. The average response time for the sensor across these tests was calculated to be 4.1 ± 2.5 s, where the bounds are calculated as two standard deviations of the mean.

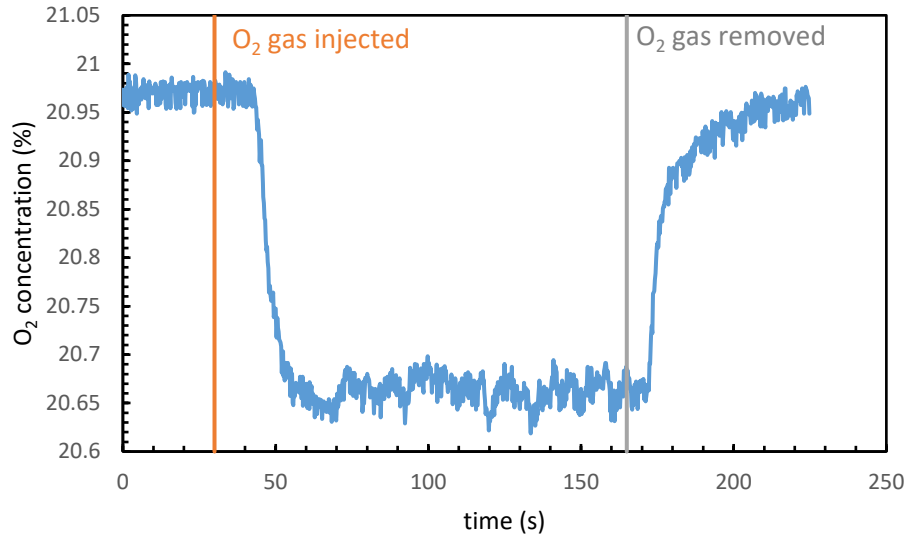


Figure 3-9. O₂ concentration measured by gas analyzer over time for N₂ gas flow test 3.

There is a discrepancy between the delay times for the CO₂ concentration tests and O₂ concentration tests, with the former having an average delay time that is 4.37 seconds shorter. It is important to note, however, that the flowrate in the quartz tube and the height of the gas injected is different for both tests, which affects the transport time for the gas in the quartz tube. From the thesis by Chaffer [8], it can be found that the airflow produced from the combustion air distribution chamber has a uniform upward velocity of 0.18 m/s when the flowrate is set to 200 slpm. The distance between the sample surface height and the bottom of the intake funnel is 0.701 m [5]. Using this distance and velocity, the time it takes for the CO₂ gas to travel to the bottom of the intake funnel for these tests was calculated to be 3.9 s. For the O₂ concentration tests, the nitrogen gas was introduced at the bottom of the air distribution chamber, which is 0.926 m from the bottom of the intake funnel. Furthermore, the N₂ gas flowing at 125 slpm replaced the usual 200 slpm of air supplied during the CO₂ concentration tests. Adjusting for this new flowrate, the upward velocity is calculated to be 0.11 m/s. Using this distance and velocity, the time it takes for

the N₂ gas to travel to the bottom of the intake funnel for these tests was calculated to be 8.2 s. This transport time to the duct system is 4.3 seconds longer than the transport time to the duct system for the CO₂ concentration tests. This matches almost identically to the 4.37 second difference in the delay time between the CO₂ concentration tests and the O₂ concentration tests, suggesting that the average time for the sample gas to travel from the duct system to the sensors was identical for both test scenarios. This verifies that for the standard flowrate of inlet airflow (200 slpm), the average delay time to the CO/CO₂/O₂ analyzer for a burn test is 8.1 s.

The delay time to the thermocouples and pitot tube were estimated as the transport time from the location of the sample surface during a typical burn test to the bottom of the intake funnel. The transport time from the bottom of the intake funnel to the thermocouple location was calculated to be 0.1 seconds when the blast gate is fully closed and 0.2 seconds when the blast gate is fully open. Since the temperature and differential pressure measurements are sampled at a rate of 5 Hz, this transport time within the duct was deemed small enough to ignore. Earlier, it was found that the transport time from the height of the sample surface to the bottom of the intake funnel for an inlet air flowrate of 200 slpm is 3.9 s. The relationship between this delay time and the flowrate of the inlet airflow can be calculated using the equation,

$$t_{delay,T} = t_{delay,dp} = 3.9 \frac{\dot{V}_{inlet}}{200}, \quad (25)$$

where \dot{V}_{inlet} is the volumetric flowrate of the inlet flow in slpm and $t_{delay,T}$ is the delay time for the thermocouple measurements, which is the same as the delay time for the pitot tube measurements, $t_{delay,dp}$. The delay time to the CO/CO₂/O₂ analyzer is calculated as

$$t_{delay,Xi} = t_{delay,T} + t_{sampling}, \quad (26)$$

where $t_{sampling}$ is the time it takes for the sample gas to travel from the sampling probe to the analyzer. This time is constant and is found by subtracting the delay time found in the CO₂ concentration check tests, 8.1 s, by the transport time from the injection point to the bottom of the intake funnel, 3.9 s. This gives a value of $t_{sampling}$ of 4.2 s. The delay times for each signal output for a standard inlet air flowrate is summarized in Table 3-4.

Table 3-4. Delay times for standard signal outputs for an inlet air flowrate of 200 slpm

$t_{delay,T}$	3.9 s
$t_{delay,dp}$	3.9 s
$t_{delay,XCO}$	8.1 s
$t_{delay,XCO2}$	8.1 s
$t_{delay,XO2}$	8.1 s

Chapter 4: Heat Release Rate Measurement Methodology

4.1 Carbon Oxide Generation Heat Release Rate Calculation

The outputs from the CO/CO₂/O₂ analyzer, thermocouples, and pressure transducer are taken to find the heat release rate of a combustion event in the FPA setup. The heat release rate equation using carbon oxide generation calorimetry can be characterized as

$$\dot{Q} = \dot{m}_{CO_2,generated} \Delta H_{CO_2} + \dot{m}_{CO,generated} \Delta H_{CO}, \quad (27)$$

where $\dot{m}_{CO_2,generated}$ and $\dot{m}_{CO,generated}$ are the mass generation rates of CO₂ and CO in the combustion process, respectively. ΔH_{CO_2} and ΔH_{CO} are the net heats of combustion per unit mass of CO₂ and CO generated, respectively [22]. These values, are on average, 13,300 kJ/kg for CO₂ and 11,100 kJ/kg for CO, according to Table A.38 of the SFPE Handbook [9].

The generation rate of CO₂ in the combustion process at time t is given as

$$\dot{m}^t_{CO_2,generated} = \dot{m}^t_{duct} (Y^t_{CO_2} - Y^0_{CO_2}), \quad (28)$$

where \dot{m}^t_{duct} is the mass flowrate of the duct flow at time t, $Y^t_{CO_2}$ is the mass fraction of CO₂ in the duct flow at time t, and $Y^0_{CO_2}$ is the mass fraction of CO₂ in the duct before the ignition of the sample. The mass fractions can be described in molar fractions through the equation,

$$Y^t_{CO_2} - Y^0_{CO_2} = MW_{CO_2} \left(\frac{X^t_{CO_2}}{MW^t_{duct}} - \frac{X^0_{CO_2}}{MW^0_{duct}} \right), \quad (29)$$

where MW_{CO_2} is the molecular weight of CO_2 , $X_{CO_2}^t$ is the molar fraction of CO_2 in the duct at time t, MW_{duct}^t is the molecular weight of the gaseous mixture in the duct flow at time t, $X_{CO_2}^0$ is the average molar fraction of CO_2 in the duct before ignition, and MW_{duct}^0 is the average molecular weight of the gaseous mixture in the duct before ignition.

The molar fraction of CO_2 in the duct at time t can be expressed as the number of moles of CO_2 in the duct divided by the number of moles in the duct, such as

$$X_{CO_2}^t = \frac{n_{CO_2}^t}{n_{total}^t}. \quad (30)$$

With some algebraic manipulation, this term can be expressed as

$$X_{CO_2}^t = \left(\frac{n_{total-H_2O}^t}{n_{CO_2}^t} + \frac{n_{H_2O}^t}{n_{CO_2}^t} \right)^{-1}, \quad (31)$$

where $n_{total-H_2O}^t$ is the total number of moles in the duct minus the moles of water in the duct, $n_{CO_2}^t$ is the total number of moles of CO_2 in the duct, and $n_{H_2O}^t$ is the total number of moles of water in the duct. The reciprocal of the term $\frac{n_{total-H_2O}^t}{n_{CO_2}^t}$ is the measured concentration of CO_2 from the gas analyzer at time t, $X_{CO_2,measured}^t$. The second term in the equation can be characterized further as

$$\frac{n_{H_2O}^t}{n_{CO_2}^t} = \frac{n_{H_2O}^0 + n_{H_2O,comb}^t}{n_{CO_2}^0 + n_{CO_2,comb}^t}, \quad (32a)$$

where $n_{H_2O}^0$ is the number of moles of water entering the duct from the ambient air, $n_{CO_2}^0$ is the number of moles of CO_2 entering the duct from the ambient air, $n_{H_2O,comb}^t$ is the number of moles of water being produced in the combustion process at time t, and $n_{CO_2,comb}^t$ is the number of moles of CO_2 being produced in the combustion process at time t. All the terms on the right-hand side can be divided by $n_{CO_2,comb}^t$ to modify the equation to

$$\frac{n_{H_2O}^t}{n_{CO_2}^t} = \frac{\frac{n_{H_2O}^0}{n_{CO_2,comb}^t} + \frac{n_{H_2O,comb}^t}{n_{CO_2,comb}^t}}{\frac{n_{CO_2}^0}{n_{CO_2,comb}^t} + 1} \quad (32b)$$

To define the ratios on the right-hand side of the equation, an assumption is made that the concentration of CO₂ in the duct flow is equal to the concentration measured by the analyzer. This is not entirely true as the concentration measured by the analyzer does not take into account the number of moles of water in the duct flow. This correction is made in equation 31 as the molar flow of water can constitute to a few percent of the total molar flow [23]. This is large enough to correct for. However, since the terms on the right-hand side of equation 32b correspond to a second order error, the error is only by a few percent of an already small error. Because correcting for the number of moles of water for this equation will constitute to a negligible change, the approximation of $n_{total-H_2O}^t = n_{total}^t$ is made for the following equations. Another approximation made is that the molar rate of flow through the duct is not affected significantly by combustion. This approximation is made because the maximum mass loss rate of PMMA in tests run by Chaffer [8] accounts for only 0.15% of the standard mass flow in the duct.

The ratio of the number of moles of water from ambient air to the number of moles of CO₂ generated from the combustion process at time t can be approximated as

$$\frac{n_{H_2O}^0}{n_{CO_2,comb}^t} \approx \frac{X_{H_2O}^0}{X_{CO_2,measured}^t - X_{CO_2,measured}^0}, \quad (33)$$

where $X_{H_2O}^0$ is the concentration of water vapor in the air derived in equation 16 and $X_{CO_2,measured}^0$ is the average concentration of CO₂ measured by the analyzer before ignition. The ratio of the number of moles of CO₂ in ambient air to the number of moles of CO₂ generated in the combustion process at time t can be approximated as

$$\frac{n_{CO_2}^0}{n_{CO_2,comb}^t} \approx \frac{X^0_{CO_2,measured}}{X^t_{CO_2,measured} - X^0_{CO_2,measured}}. \quad (34)$$

The ratio of the number of moles of water generated from the combustion process to the number of moles of CO₂ generated from the combustion process can be approximated as

$$\frac{n_{H_2O,comb}^t}{n_{CO_2,comb}^t} \approx \frac{\frac{1}{2} \left(\frac{H_{atoms}}{C_{atoms}} \right)}{\left(\frac{X^t_{CO_2,measured} - X^0_{CO_2,measured}}{(X^t_{CO_2,measured} - X^0_{CO_2,measured}) + (X^t_{CO,measured} - X^0_{CO,measured})} \right)}, \quad (35)$$

where $\frac{H_{atoms}}{C_{atoms}}$ is the ratio of hydrogen atoms to carbon atoms of the gaseous fuel, $X^t_{CO,measured}$ is the concentration of CO measured by the analyzer at time t, and $X^0_{CO,measured}$ is the average concentration of CO measured by the analyzer before ignition. This approximation assumes that all the carbon in the fuel is converted to CO₂ and CO, as these two are the dominant carbon-based products in combustion.

The average molar fraction of CO₂ in the duct before ignition, $X^0_{CO_2}$, can be expressed similarly to equation 31 as

$$X^0_{CO_2} = \left(\frac{n^0_{total-H_2O}}{n^0_{CO_2}} + \frac{n^0_{H_2O}}{n^0_{CO_2}} \right)^{-1}, \quad (36)$$

where $\frac{n^0_{total-H_2O}}{n^0_{CO_2}}$ is the reciprocal of the average measured concentration of CO₂ from the gas analyzer before ignition and $\frac{n^0_{H_2O}}{n^0_{CO_2}}$ is the ratio of the number of moles of water to the

number of moles of CO₂ before ignition. $\frac{n^0_{H_2O}}{n^0_{CO_2}}$ can be expressed as

$$\frac{n^0_{H_2O}}{n^0_{CO_2}} \approx \frac{X^0_{H_2O}}{X^0_{CO_2,measured}}. \quad (37)$$

The molecular weight of the gaseous mixture in the duct flow at time t, MW^t_{duct} , can be expressed as the summation of the molar fraction of each species in the duct multiplied by their respective molecular weight, such as

$$MW_{duct}^t = \left(\sum_{i=O_2,CO_2,CO} (MW_i X_{measured,i}^t) + MW_{N_2} (1 - \sum_{i=O_2,CO_2,CO} (X_{measured,i}^t)) \right) (1 - X_{H_2O}^t) + MW_{H_2O} X_{H_2O}^t \quad (38)$$

where MW_i is the molecular weight of species i and $X_{measured,i}^t$ is the concentration measured by the analyzer at time t for species i . $X_{H_2O}^t$ is the molar fraction of water in the duct and can be expressed as

$$X_{H_2O}^t \approx \frac{n_{H_2O}^t}{n_{CO_2}^t} * X_{CO_2}^t. \quad (39)$$

MW_{duct}^0 is the average molecular weight in the duct before ignition. This can be expressed as

$$MW_{duct}^0 = \left(\sum_{i=O_2,CO_2,CO} (MW_i X_{i,measured}^0) + MW_{N_2} (1 - \sum_{i=O_2,CO_2,CO} (X_{i,measured}^0)) \right) (1 - X_{H_2O}^0) + MW_{H_2O} X_{H_2O}^0, \quad (40)$$

where $X_{i,measured}^0$ is the average concentration measured by the analyzer for species i before ignition.

\dot{m}_{duct}^t is solved for already in equations 8 and 12. One key distinction is that, for heat release rate calculations, MW , instead of being the molecular weight of air, is the molecular weight of the gaseous flow in the duct, MW_{duct}^t , calculated in equation 38.

Equations 27 through 40 can be used in a similar fashion to calculate $\dot{m}_{CO,generated}^t$, but the values that are representative for CO_2 need to be changed to those representative of CO and vice versa.

With the generation rate of CO and generation rate of CO_2 solved, the heat release at any given time t can be solved for. However, since there is a delay between the combustion process and the signal outputs for temperature, differential pressure, and

species concentrations, these delay times need to be incorporated to sync up the output signals with the time when the products of combustion are generated at the sample surface. The calculation for the delay time for each signal output can be found in Chapter 3.2.5, and the delay time for all signals at the standard combustion inlet air flowrate can be found in Table 3-4. These delay times were averages calculated during standard cold flow tests but adjusting them for different burn scenarios can be easily done by the user after experiments. The device measurements can be processed after each experiment, and the amount of time it takes for a device to react after ignition can be used as the delay time for that specific experiment. This ability is useful especially for different inlet air flowrates, which alter the transport time.

A heat release rate equation is provided in the ASTM standard as

$$\dot{Q}_{standard} = 13300(\dot{G}_{CO_2} - \dot{G}_{CO_2}^0) + 11100(\dot{G}_{CO} - \dot{G}_{CO}^0), \quad (41)$$

where \dot{G}_{CO_2} and \dot{G}_{CO} are the generation rates in kg/s of CO₂ and CO respectively and \dot{G}_{CO}^0 and $\dot{G}_{CO_2}^0$ are the corresponding measurements before ignition of the specimen [5]. The generation rates of CO₂ and CO are given as

$$\dot{G}_{CO_2} = A * K \left(\frac{P_{room}}{101000} \right)^{\frac{1}{2}} \left(2 * \frac{353\Delta P}{T} \right)^{1/2} * 1.52X_{CO_2} \quad (42)$$

and

$$\dot{G}_{CO} = A * K \left(\frac{P_{room}}{101000} \right)^{\frac{1}{2}} \left(2 * \frac{353\Delta P}{T} \right)^{1/2} * 0.966X_{CO}, \quad (43)$$

where A is the cross-sectional area of the duct in m², K is the flow coefficient of the averaging pitot tube, P_{room} is the actual atmospheric pressure in Pascals outside the duct, ΔP is the pressure differential across the averaging Pitot tube in Pascals, T is the gas

temperature in the test section duct in Kelvin, and X_{CO_2} and X_{CO} are the measured volume ratio of CO₂ and CO respectively [5].

There are two key differences in calculation methodology between the derived and standard carbon oxide generation formulas. First, the standard heat release rate equation does not consider the concentration of water, artificially increasing the CO₂ concentration. Second, $\dot{G}_{CO_2}^0$ is a constant depending on the mass flow before ignition in the standard form of the heat release rate equation, but $\dot{m}^t_{duct} Y_{CO_2}^0$, the equivalent term in the derived equation, is a vector which changes its value based on the mass flow of the duct at that time, which is believed to grant a more accurate representation of the mass of CO₂ entering the duct from the room air at any given time.

4.2 Oxygen Consumption Heat Release Rate Calculations

A derivation of the heat release rate equation through oxygen consumption calorimetry was also made. The heat release rate equation using oxygen consumption calorimetry can be expressed as

$$\dot{Q}_{O_2} = \dot{m}_{O_2,consumed} \Delta H_{O_2}, \quad (44)$$

where $\dot{m}_{O_2,consumed}$ is the mass consumption rate of O₂ during the combustion process and ΔH_{O_2} is the heat of combustion per unit mass of oxygen consumed, which is, on average, 13,100 kJ/kg [9].

The mass consumption rate of O₂ after ignition can be expressed as

$$\dot{m}^t_{O_2,consumed} = \dot{m}^t_{duct} (Y_{O_2}^0 - Y_{O_2}^t), \quad (45)$$

where \dot{m}^t_{duct} is the same value used in the derived carbon oxide generation heat release rate equation, $Y_{O_2}^0$ is the average mass fraction of oxygen in the duct flow before ignition, and $Y_{O_2}^t$ is the mass fraction of oxygen in the duct flow at time t. The mass fractions can be described in molar fractions through the equation,

$$Y_{O_2}^0 - Y_{O_2}^t = MW_{O_2} \left(\frac{X_{O_2}^0}{MW_{duct}^0} - \frac{X_{O_2}^t}{MW_{duct}^t} \right), \quad (46)$$

where $X_{O_2}^t$ is the molar fraction of O_2 in the duct at time t and $X_{O_2}^0$ is the average molar fraction of O_2 in the duct before ignition.

Similarly to equation 31, $X_{O_2}^t$ can be expressed as

$$X_{O_2}^t = \left(\frac{n^t_{total-H_2O}}{n^t_{O_2}} + \frac{n^t_{H_2O}}{n^t_{O_2}} \right)^{-1}, \quad (47)$$

where the reciprocal of the term $\frac{n^t_{total-H_2O}}{n^t_{O_2}}$ is the measured concentration of O_2 from the gas analyzer at time t, $X^t_{O_2,measured}$, and $n^t_{O_2}$ is the total number of moles of O_2 in the duct at time t. The second term in the equation can be characterized further as

$$\frac{n^t_{H_2O}}{n^t_{O_2}} = \frac{n^0_{H_2O} + n^t_{H_2O,comb}}{n^t_{O_2}}. \quad (48a)$$

Similar to the derivation in the carbon oxide generation calorimetry heat release rate equation, all the terms on the right hand side are divided by $n^t_{CO_2,comb}$ to modify the equation to

$$\frac{n^t_{H_2O}}{n^t_{O_2}} = \frac{\frac{n^0_{H_2O}}{n^t_{CO_2,comb}} + \frac{n^t_{H_2O,comb}}{n^t_{CO_2,comb}}}{\frac{n^t_{O_2}}{n^t_{CO_2,comb}}}. \quad (48b)$$

$\frac{n_{H_2O}^0}{n_{CO_2,comb}^t}$ and $\frac{n_{H_2O,comb}^t}{n_{CO_2,comb}^t}$ are already defined in equations 33 and 35. The ratio of the number of moles of O₂ in the duct at time t to the number of moles of CO₂ generated at time t can be estimated as

$$\frac{n_{O_2}^t}{n_{CO_2,comb}^t} \approx \frac{X_{O_2,measured}^t}{X_{CO_2,measured}^t - X_{CO_2,measured}^0}. \quad (49)$$

The average molar fraction of O₂ in the duct before ignition, $X_{O_2}^0$, can be expressed similarly to equation 48 as

$$X_{O_2}^0 = \left(\frac{n_{total-H_2O}^0}{n_{O_2}^0} + \frac{n_{H_2O}^0}{n_{O_2}^0} \right)^{-1}, \quad (50)$$

where $\frac{n_{total-H_2O}^0}{n_{O_2}^0}$ is the reciprocal of the average measured concentration of O₂ from the gas analyzer before ignition and $\frac{n_{H_2O}^0}{n_{O_2}^0}$ is the ratio of the number of moles of water to the number of moles of O₂ before ignition. $\frac{n_{H_2O}^0}{n_{O_2}^0}$ can be expressed as

$$\frac{n_{H_2O}^0}{n_{O_2}^0} \approx \frac{X_{H_2O}^0}{X_{O_2,measured}^0}. \quad (51)$$

MW_{duct}^t and MW_{duct}^0 have already been defined in the derivation of the carbon oxide generation heat release rate equation. The same delay times between the combustion process and the signal outputs stated in Chapter 4.1 are used.

The ASTM standard provides a heat release formula using oxygen consumption calorimetry principles. However, in the standard, 12.8 kJ/g is used instead of the widely recognized 13.1 kJ/g for the heat of combustion per mass of O₂ consumed. For this work, this formula was altered to have the heat of combustion term to be 13.1 kJ/g in order to be consistent with the formula derived earlier for oxygen consumption calorimetry. This formula is given as

$$\dot{Q}_{standard_{O_2}} = 13100\dot{D}_{O_2}, \quad (52)$$

where \dot{D}_{O_2} is the consumption rate of O_2 in kg/s [5]. \dot{D}_{O_2} is expressed as

$$\dot{D}_{O_2} = A * K \left(\frac{P_{room}}{101000} \right)^{\frac{1}{2}} \left(2 * \frac{353\Delta P}{T} \right)^{1/2} * 1.1(X^0_{O_2} - X^t_{O_2}) \quad [5]. \quad (53)$$

The coefficient of 1.1 for equation 53 is derived from the ratio of the molecular weight of O_2 to that of air. Equation 53 does not consider the molar flow of water in the duct flow, while equation 45 does.

4.3 PMMA burn tests for heat release rate formula comparisons

The four heat release rate formulas discussed earlier were compared with each other by using them to calculate the heat release rates from measurements obtained through four PMMA burn tests. The PMMA samples were cut into circular disks with a diameter of 96 mm and thickness of 6 mm. The average weight of all the samples was 51.7 ± 0.6 g, with the bounds being the standard deviation of the mean for the four samples. The back surface and sides of the PMMA sample were wrapped in aluminum foil, and an insulation ring surrounded the sample before it was placed in the horizontal sample dish, as shown in Figure 4.1.



Figure 4-1. Picture of PMMA sample used in FPA burn test.

The tests were conducted with the lamps set to a power setting that provides a heat flux of 50 kW/m^2 to the sample surface. The concentrations for O_2 , CO_2 , and CO measured by the analyzer throughout one of the burn tests are shown in Figure 4-2. Furthermore, the average temperature measured by the thermocouples and the differential pressure measured by the pitot tube for the same test are shown in Figure 4-3.

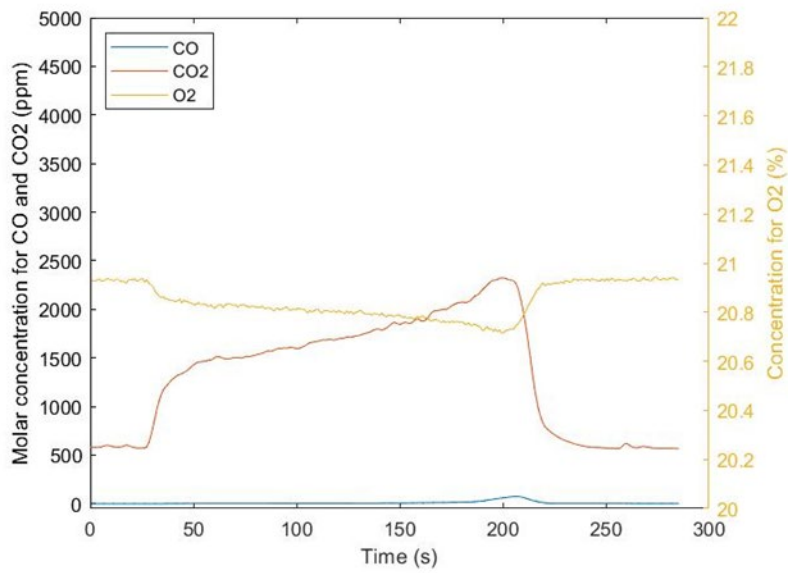


Figure 4-2. Concentrations measured by the analyzer for one of PMMA burn tests. Zero seconds indicates the time the heat flux first penetrates the sample surface.

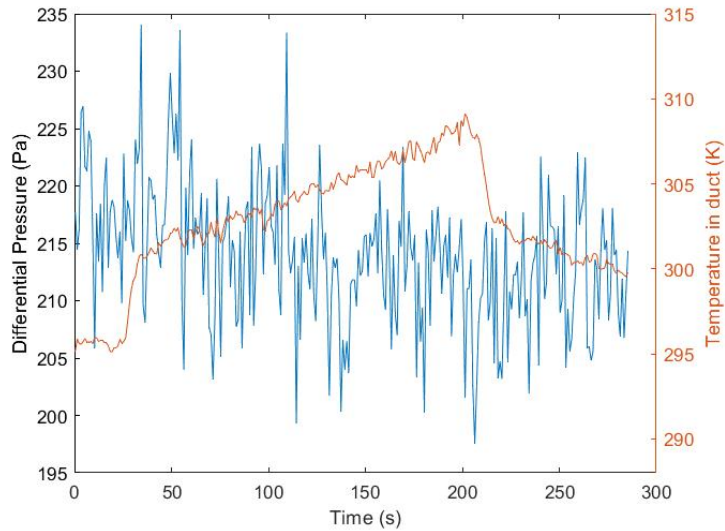


Figure 4-3. Temperature and differential pressure measured for one of PMMA burn tests. Zero seconds indicates the time the heat flux first penetrates the sample surface.

The resultant heat release rate curve obtained from the measurement signals obtained from one burn test is shown in Figure 4-4. The heat release rate was calculated

four times, one for each heat release rate formula discussed in this chapter. This results in four heat release rate plots for the same burn test.

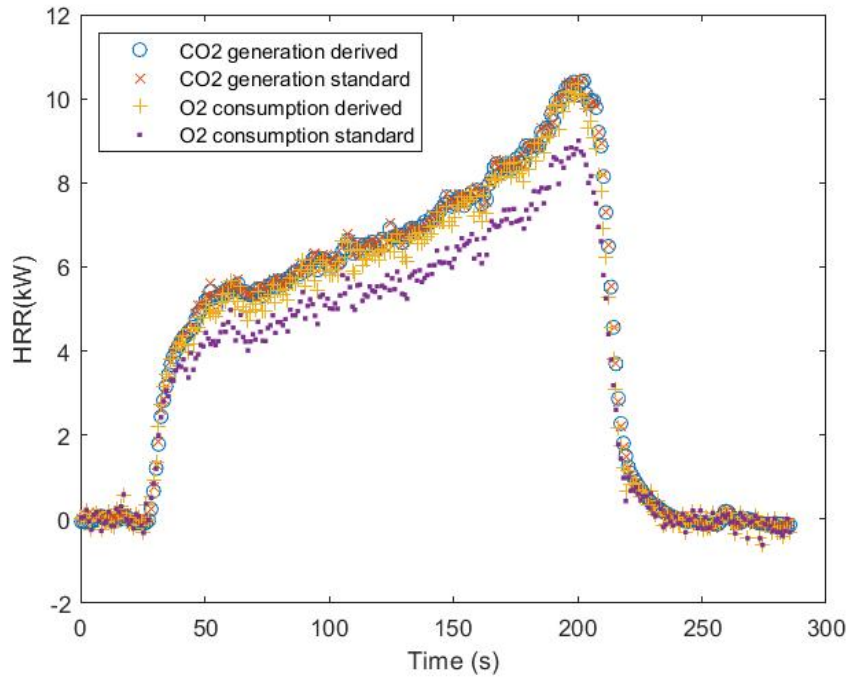
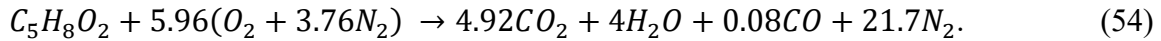


Figure 4-4. Heat release rates calculated using measurements from one FPA burn test.

As shown from the curves, the heat release rate found from the derived carbon oxide generation formula matches well with the heat release rate found from the carbon oxide generation formula provided in the standard. The heat release rate found from the derived oxygen consumption formula is also in close agreement to those found from carbon oxide generation formulas. The O₂ consumption formula provided by the standard calculated heat release rate significantly lower than the other three formulas.

The experimental heat of combustion for PMMA for each burn test can be obtained by integrating the heat release rate curve to obtain the total heat released and dividing by

the total mass of PMMA burned. This can be done for each of the four heat release rate curves generated for a burn test to obtain the heat of combustion of PMMA measured for each heat release rate calculation method. This heat of combustion can be compared to the theoretical heat of combustion of PMMA using the stoichiometric equation for the combustion of PMMA in air, described as



The coefficients for CO₂ and CO are implemented based on the average CO₂ and CO ratio produced during the burn tests. This was calculated by taking the ratio of the total mass generated of CO to CO₂ during the combustion process. The masses were then multiplied by the ratio of molecular weight of CO₂ to CO to get the molar ratio of CO to CO₂ used in the stoichiometric formula. Using this formula, the theoretical heat of combustion of PMMA can be calculated by either oxygen consumption principles or carbon oxide generation principles. The theoretical heat of combustion for PMMA, as well as the average measured heat of combustion for PMMA throughout all four tests for each heat release rate method is shown in Table 4-1, with the bounds for the measured heat of combustions being two standard deviations of the mean.

Table 4-1. Heat of combustion of PMMA calculated from experimental measurements and calculated from the stoichiometric equation.

Heat Release Formula used	$\Delta H_{PMMA, exp}$ (kJ/g)	$\Delta H_{PMMA, theo}$ (kJ/g)
Derived Carbon Oxide Generation Calorimetry	25.6 ± 0.58	29.0
ASTM Carbon Oxide Generation Calorimetry	25.6 ± 0.42	29.0
Derived O ₂ Consumption Calorimetry	24.6 ± 0.68	24.8
ASTM O ₂ Consumption Calorimetry	21.2 ± 0.64	24.8

The difference in the theoretical heat of combustion for PMMA calculated from oxygen consumption compared to carbon oxide generation is due to the difference in the heat of combustion terms for O₂ consumed and CO₂ and CO generated. The experimental heat of combustions calculated using carbon oxide generation calorimetry formulas are in good agreement with each other. The experimental heat of combustions calculated using O₂ consumption calorimetry formulas are not. This can be explained due to the derived O₂ consumption formula considering the moles of water generated during the consumption process while the standard formula does not. Since the concentration of O₂ is very sensitive in these calculations, even a small change in the O₂ concentration in the duct flow compared to the concentration in the sample flow makes a significant difference in the heat release rate calculations. As seen from the table, the average heat of combustion of PMMA calculated using the derived O₂ consumption formula is in good agreement with the theoretical heat of combustion using oxygen consumption calorimetry principles. However, the average heat of combustion calculated using the carbon oxide generation

calorimetry formulas are 11% lower than the theoretical heat of combustion using carbon oxide generation calorimetry principles.

To better understand why the heat of combustion calculated is lower than the theoretical heat of combustion for carbon oxide generation calorimetry, the mass generation rates for CO and CO₂ were examined for each combustion test. The total mass generated for CO and CO₂ were found for each combustion test by integrating the generation rate curves. The theoretical masses of CO and CO₂ generated can be expressed as the CO and CO₂ mass yields calculated from the stoichiometric formula provided in Equation 54 multiplied by the mass of the PMMA sample for each combustion test. Table 4-2 shows these calculations for each burn test.

Table 4-2. Mass of carbon products generated for each combustion test.

Test	Mass of PMMA lost (g)	$m_{CO/CO_2,theoretical}$ (g)	$m_{CO/CO_2,generated}$ (g)	G_{CO/CO_2} (g)
1	50.6	110.7	96.4	96.8
2	51.7	113.1	100.8	99.7
3	51.5	112.6	99.1	99.0
4	52.4	114.2	101.4	102.2

$m_{CO/CO_2,theoretical}$ is the total theoretical mass generated of carbon products according to the stoichiometric equation, $m_{CO/CO_2,generated}$ is the total mass generated of carbon products in the derived calculation of the carbon oxide generation calorimetry formula, and G_{CO/CO_2} is the total mass generated of carbon products in the calculation using the ASTM standard formula for carbon oxide generation calorimetry. On average, the mass generated of carbon products measured during the experiments is 12% lower than the mass expected to be generated based on the stoichiometric equation, which corresponds to an

average of 6 g of carbon from the sample not accounted for during the combustion process. Some explanations can be made for a part of this difference. First, the stoichiometric equation does not consider soot production, which would explain some of the carbon that is lost in the combustion measurements. An accurate measurement of soot cannot be made for the FPA currently, but the typical soot yield for the combustion of PMMA is stated in literature to be 0.022 g/g [17], which would not account for the whole 12% difference observed. Another reason that explains for part of the difference is the pyrolysis of the sample material before ignition, where some of the carbon gasifies and is unburned. As the mass lost before ignition is minimal, this explanation does not account for the whole 12% difference either. It is important to note that soot production and unburned hydrocarbon production does also lower the theoretical oxygen consumption during combustion.

The error propagation for the signal measurements was also considered to determine if the uncertainty in the mass generation rate calculated is large enough to account for the difference. The uncertainty of the thermocouple is estimated to be 1 °C. The accuracy of the pressure transducer is given as 0.25% by the manufacturer. The uncertainty for the CO₂ and O₂ sensors were calculated as the difference between the concentration measurements from each signal before and after the combustion process. This difference was determined to be, at most, 2% for the CO₂ sensor and 0.006% for the O₂ sensor. The uncertainty for the CO₂ sensor was applied to the average concentration measured by the sensor before ignition, while the uncertainty for the temperature and differential pressure were applied to the duration of the whole combustion tests. These uncertainties shift the calculation for the mass generated by 1.5% at most, which is lower

than the 12% difference observed between the mass generated of carbon products in the experiments and the expected mass generated of carbon products.

A theory for the remainder difference seen by the experimental and expected mass of CO₂ and CO generated is that, because the concentration of CO is at its lower limit for the duration of the experiment, it does not accurately represent the concentration of CO in the sample flow. This is due to non-linearities of these sensors at its concentration limits. In order to verify this, a span gas at the CO limit needs to be implemented in calibration to verify the linearity of the voltage output to concentration for the CO sensor at its lower limit.

The delay times were also calculated for the combustion experiments using the same methodology for calculating the delay times for the cold flow tests in Chapter 3. Ignition is characterized as the moment a visual flame was observed anywhere on the sample surface. The average delay time between all four tests to the thermocouple was 1.75 seconds, and the average delay time to the analyzer was 8.85 seconds.

Chapter 5: Summary and Future Work

This study presented the redesign and the construction of the FPA exhaust and gas sampling systems for the purposes of the Koffel Associates Fire Standards Laboratory for the University of Maryland Department of Fire Protection Engineering.

For the exhaust system, the location of the blast gate was moved in order to satisfy the height requirement of the entire exhaust system and to help with end user operability. The shape of the intake funnel was altered for ease of manufacturability. All the duct sections were connected in a simplistic manner for a more modular design. The instrument ports were made from mass-produced fittings and require no welding, making replacement of these ports and instruments manageable without replacing the duct.

For the gas sampling and analyzing system, all the standard instruments are located on a singular aluminum profile shelf next to the exhaust system to make the sampling line as compact as possible. A finer soot filter element was used to more effectively remove soot particles from the sampling line. A gas analyzer was chosen that has the ability to measure CO₂ and CO for carbon oxide generation calorimetry as well as O₂ for oxygen consumption calorimetry. The ranges for these sensors are chosen based on the concentrations that can be viably obtained in a burn test. Design diagrams and pictures were added to this work so that the locations of important instruments are clear.

The outputs for the pressure transducer and CO/CO₂/O₂ gas analyzer were characterized and verified through a series of tests. After the characterization of all outputs, a heat release rate formula for carbon oxide generation and oxygen consumption were

derived and compared with the heat release rate formulas provided in the ASTM standard through the use of combustion experiments of PMMA. The combustion test results showed that, although the derived O₂ consumption calorimetry formula measured the heat released that was expected, the carbon oxide generation formula measured heat release that was lower than expected. This could be because of the combination of the inability to accurately measure soot and unburned hydrocarbon production, uncertainty in measurement signals, and non-linearity of the CO sensor at its lower limit.

The future work includes determining the reason for the lower mass of carbon products generated from what is expected. This can be done by accurately measuring the unburned hydrocarbons and soot during the experiments through the use of the second gas sampling line and the hydrocarbon analyzer that needs to be implemented and incorporated. The CO and CO₂ sensors also need to have multiple span points, especially at the sensor limits, to better represent the concentrations of CO and CO₂.

Appendices

A : Standard Procedures

A.1 CO/CO₂/O₂ analyzer calibration procedure

Step 1: Open and run LabView file FPA_gas_analyzing.vi. The LabView file will be used to monitor the output signals from the analyzer during the calibration procedure.

Step 2: Ensure that the mass flow controller for the CO/CO₂/O₂ analyzer is set to 2 lpm. No flow should be measured from the mass flow controller at the moment.

Step 3: Ensure that the 3 way ball valves on the calibration panel are pointing at Zero and Calibration, as shown in Figure A-1.



Figure A-1. Ball valves on calibration panel in correct orientation for zero calibration.

Step 4: Open the valve to the Nitrogen cylinder and check the pressures on the gauges on the regulator valve. Make sure that the outlet pressure does not exceed 50 psi. Check the mass flow controller to make sure 2 lpm is flowing to the gas analyzer.

Step 5: Go to the manual zero calibration on the gas analyzer menu by pressing the following buttons on the analyzer in order: Menu -> F3 -> F1 -> F1 -> F1. The screen shown in Figure A-2 should be displayed. Use the left and right arrow buttons to scroll through the different outputs. Ensure that the CO, CO₂, and O₂ have stabilized and are close to 0.

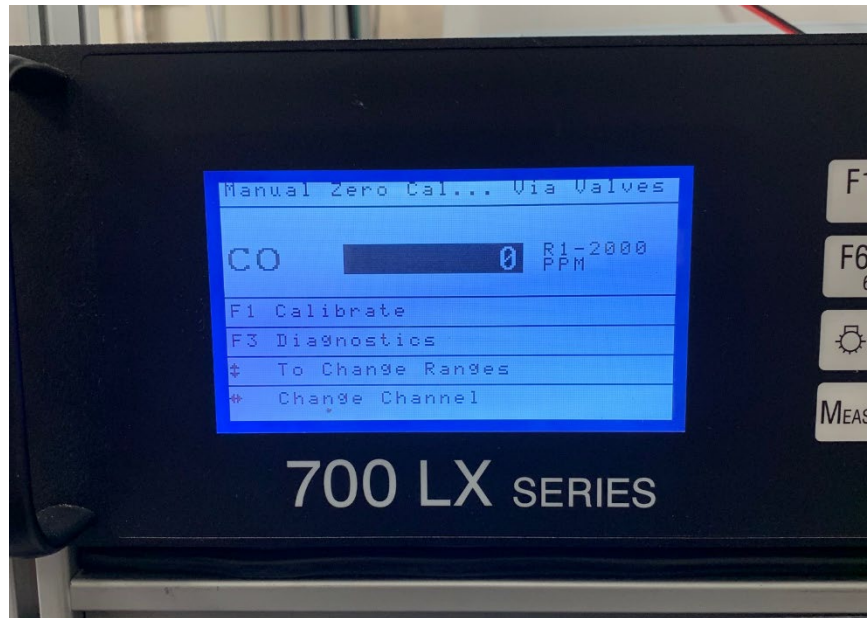


Figure A-2. Picture of analyzer screen after Step 5.

Step 6: Press F1 to calibrate the analyzer for a specific species. If the calibration is successful, the screen should look like Figure A-3. The output from the analyzer for that species should also automatically change so that it is outputting zero volts. Check the LabView to ensure that this is the case.



Figure A-3. Picture of analyzer screen after Step 6.

Step 7: Repeat Step 6 for the other two species. Use the left and right arrows to change the screen to the specific species you want.

Step 8: After all sensors have been calibrated, press the back button on the analyzer and close the valve to the N₂ bottle.

Step 9: Turn the left 3-way ball valve on the calibration panel so that it is facing towards the span line, as shown in Figure A-4.

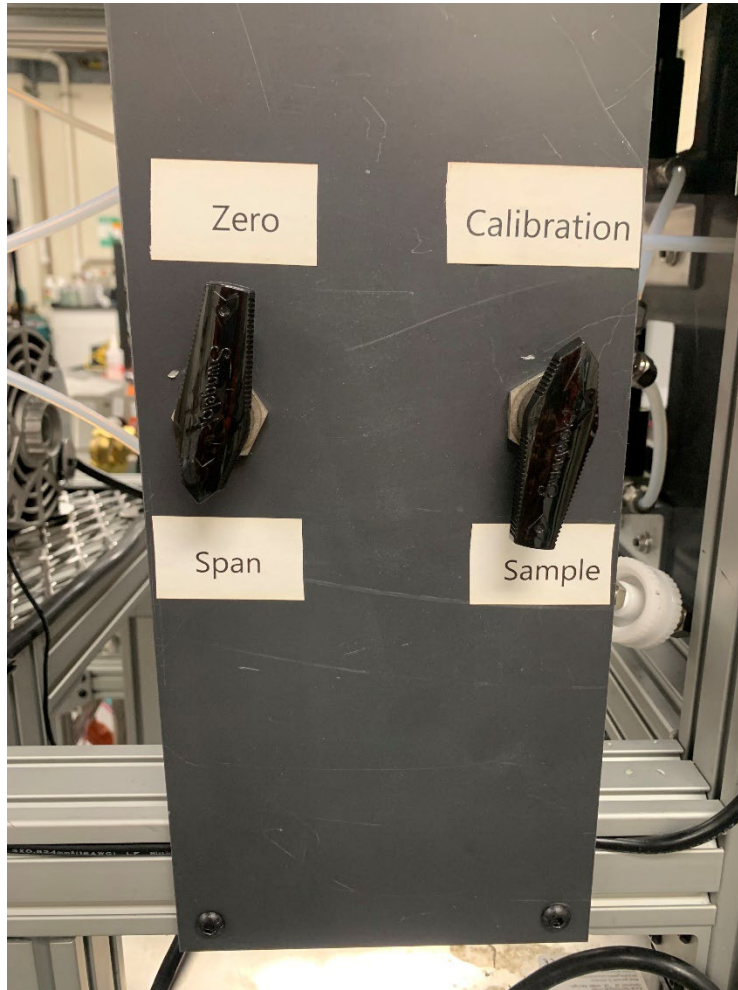


Figure A-4. Ball valves on calibration panel in correct orientation for span calibration.

Step 10: Open the valve to the mixed gas cylinder used for the span calibration of the CO/CO₂/O₂ analyzer and check the pressures on the gauges on the regulator valve. Make sure that the outlet pressure does not exceed 50 psi. Check the mass flow controller to make sure 2 lpm is flowing to the gas analyzer.

Step 11: Go to the manual zero calibration on the gas analyzer menu by pressing the following buttons on the analyzer in order – Menu -> F3 -> F1 -> F1 -> F2. The screen

shown in Figure A-5 should be displayed. Use the left and right arrow buttons to scroll through the different outputs. Ensure that, for each species, the number next to Span Gas matches the concentration for that species in the calibration bottle. Ensure that the range for each species is the maximum analyzer range for that species.



Figure A-5. Picture of analyzer screen after Step 11.

Step 12: Press F1 to calibrate the analyzer for a specific species. If the calibration is successful, the screen should look like Figure A-6. The output from the analyzer for that species should also automatically change so that its output voltage is the maximum voltage range of 10 V times the ratio of the span gas concentration to the maximum analyzer range concentration, which is 2000 ppm for CO, 5000 ppm for CO₂, and 25% for O₂. Check the

LabView to ensure that this is the case. The concentration reading in LabView should be the same as the concentration of the species in the span gas bottle.

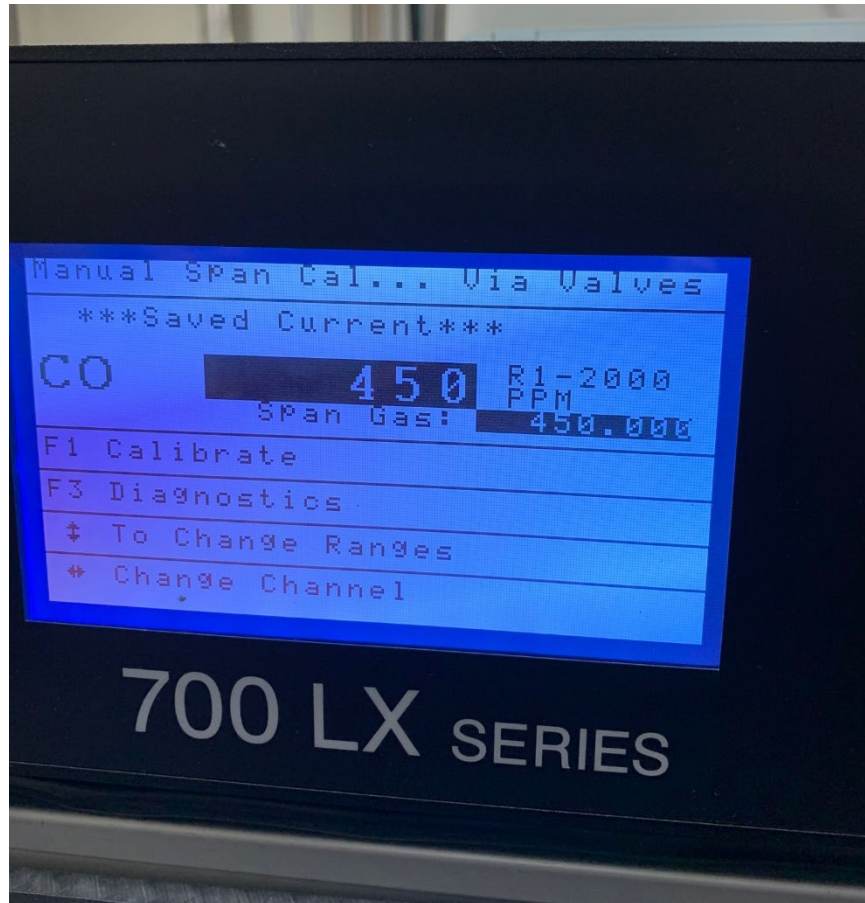


Figure A-6. Picture of analyzer screen after Step 12.

Step 13: Repeat Step 12 for the other two species. Use the left and right arrows to change the screen to the specific species you want.

Step 14: After all sensors have been calibrated, press the back button on the analyzer and close the valve to the span gas bottle.

Step 15: Stop the LabView. The analyzer should now be calibrated for the day's experiments.

C : CO₂ and CO calculations

C.1 Maximum CO₂ concentration calculation

Polyethylene (C₂H₄) is shown to have a maximum heat release rate per unit area of 1300 kW/m² [24]. This heat release rate was multiplied by a safety factor of 1.5 to assume a heat release rate per unit area of 1950 kW/m² for worst case scenario. The heat of combustion of polyethylene is 46.5 MJ/kg. [11] The mass loss rate of polyethylene at this heat release rate for the sample surface area is

$$MLR = (HRRPUA)(A)/(H_c) = 1950 \frac{kW}{m^2} * \frac{\pi}{4} * (0.1 m)^2 / 46.5 \frac{kJ}{g} = 0.331 \frac{g}{s}.$$

To convert this to molar flow, the mass flow of polyethylene needs to be divided by the molecular weight of polyethylene. This gives a molar flow of 0.012 mol/s. Since two moles of CO₂ are generated per one mol of polyethylene, assuming complete combustion, the molar flow of CO₂ for this case is 0.024 mol/s. To convert the standard volumetric flow of the duct (0.25 m³/s) to molar flow, the following calculation is made,

$$\dot{N} = \frac{\rho \dot{V}}{MW} = \frac{1.2 \frac{kg}{m^3} * 0.25 \frac{m^3}{s}}{28.9 \frac{g}{mol}} = 9.5 \frac{mol}{s}.$$

The volumetric flow is multiplied by the density of air at 50 °C (1.1 kg/m³) for a high temperature burning case and divided by the molecular weight of air (28.9 g/mol). This gives a total molar flow of 9.5 mol/s. To approximate the maximum concentration measured by the CO₂ sensor, the molar flow of CO₂ is divided by the total molar flow,

$$X_{CO_2,max} = \frac{\dot{N}_{CO_2}}{\dot{N}} = \frac{0.024 mol/s}{9.5 mol/s} = 2.526 * 10^{-3}.$$

This gives a maximum concentration of CO₂ as **2526 ppm** for this burning scenario.

C.2 Maximum CO concentration calculation

The CO yield for polyethylene for a fire with a global equivalence ratio of 3 is given as 0.580 [9]. This yield is multiplied by the maximum mass loss rate of 0.331 g/s, as calculated earlier, to calculate the mass flow of CO produced through combustion. This will be an overestimation as the mass loss rate should not be as high for such a fuel rich scenario, but, the same mass loss rate was kept as a safety measure. The mass flow of CO is calculated to be 0.192 g/s. This is converted to molar flow by dividing by the molecular weight of CO. The molar flow calculated is 0.0137 mol/s. This molar flow is then divided by the total molar flow in the duct calculated in the CO₂ calculation. This provides a maximum concentration of CO of **1442 ppm**.

D : MATLAB Script

```
1 %% FPA HRR Calculations
2 clear all
3 clc
4 %% Import data from Labview
5
6 timeduct = (1)/(0.253/(pi/4*0.1524^2)); %time for species to get through duct
7 timeintakefunnel = (1/3*pi*((0.3048/2)^2+(0.1524/2)^2+0.1524*0.1524/2))^0.26/0.253; %time for species to get through intake funnel
8 Qin = 200; %inlet air flowrate to the combustion air distribution system
9 timequartztube = 0.701/0.18*Qin/200; %time for species to get through quartz tubes
10 delay1 = round((timequartztube)*5); %delay time to thermocouple and pitot tube measurements
11 delay2 = delay1 + 21; % delay time for sample to analyzer. This is calculated from the thesis as transport
12 %time in the quartz tube plus 4.2 s. As signals are sampled at a rate
13 %of 5 Hz, this is multiplied by 5 and rounded to the nearest integer. This is affected by the transport time in the
14 %quartz tube.
15 Labview = lvm_import('C:\Users\shuva\Documents\real grad school\Research\Matlab\lvm files\9_28 test 16'); %lvm function that
16 %reads lvm file from select desktop location and puts it into a data structure
17 Vdot_predelay = Labview.Segment1.data(:,1); %imports all the volumetric flow measurement signals from Labview into Matlab
18 Vdot_pb = Vdot_predelay(1+delay1:end- delay2 + delay1);
19 CO_predelay = Labview.Segment1.data(:,2)/1e6; %imports all the CO measurement signals from Labview into Matlab
20 CO_pb = CO_predelay(1+delay1:end);
21 CO2_predelay = Labview.Segment1.data(:,3)/1e6; %imports all the CO2 measurement signals from Labview into Matlab
22 CO2_pb = CO2_predelay(1+delay1:end);
23 O2_predelay = Labview.Segment1.data(:,4)/100; %imports all the O2 measurement signals from Labview into Matlab
24 O2_pb = O2_predelay(1+delay1:end);
25 T_C_predelay = Labview.Segment1.data(:,5); %imports all the temperature measurement signals from Labview into Matlab
26 T_C = T_C_predelay(1+delay1:end- delay2 + delay1);
27 T_pb = T_C + 273.15;
28 dp_predelay = Labview.Segment1.data(:,6);
29 dp_pb = dp_predelay(1+delay1:end- delay2 + delay1); %imports all the differential pressure measurement signals from Labview into Matlab
30 mdot_lab_predelay = Labview.Segment1.data(:,7); %imports all the mass flow measurement signals from Labview into Matlab
31 mdot_lab_pb = mdot_lab_predelay(1+delay1:end- delay2 + delay1);
32 Time1 = linspace(0,0.2*length(Vdot_pb)-0.2,length(Vdot_pb));
33 Time_pb = transpose(Time1); % time vector with the same shape and length as the measurement vectors. Each time step is 0.2 seconds
34 %% Binning
35 %this is to bin the signals to 1 second intervals. It takes the average of
36 %each signal in a 1 second interval
37 index = 0;
38
39 for i = 3:5:size(Time_pb)
40     if i>size(Time_pb)-2
41         break
42     else
43         index = index + 1;
44         Vdot(index) = mean(Vdot_pb(i-2:i+2));
45         CO(index) = mean(CO_pb(i-2:i+2));
46         CO2(index) = mean(CO2_pb(i-2:i+2));
47         O2(index) = mean(O2_pb(i-2:i+2));
48         T(index) = mean(T_pb(i-2:i+2));
49         dp(index) = mean(dp_pb(i-2:i+2));
50         mdot_lab(index) = mean(mdot_lab_pb(i-2:i+2));
51         Time(index) = mean(Time_pb(i-2:i+2));
52     end
53 end
54 Vdot = transpose(Vdot);
55 CO = transpose(CO2).*0.1;%CO = transpose(CO);
56 CO2 = transpose(CO2);
57 O2 = transpose(O2);
58 T = transpose(T);
59 dp = transpose(dp);
60 mdot_lab = transpose(mdot_lab);
61 Time = transpose(Time);
62
63 %% Inputting variables
64 time0 = 1; %start of test
65 time1 = 30; % when shield lowers (s)
66 time2 = 500; % when sample ignites (s)
67 time3 = 750; % when burning stops (s)
68
69 Pb = 100000*Labview.Segment1.data(1,8); % insert pressure from iConnect in Pascals
```

```

70 - Pm = Pb*0.01; % barometric pressure in mbar
71 - P = Pb - dp; %pressure inside the duct in pascals
72 - Ta = mean(T_C(1:100))+273.15; % ambient temperature in kelvin
73 - RH = labview.Segment1.data(1,9); % relative humidity from iConnect
74 - satvp = (6.1078)*exp(17.2694*(Ta-273.16)/(Ta-35.86)); %saturated vapor pressure from Magnus-Tetens equation in millibar
75
76 - moisture = RH/100*satvp/Pm; % moisture content in molar fraction based on pressure, temperature, and relative humidity
77 - C_atoms = 2; %number of carbon atoms in fuel
78 - H_atoms =0; %number of hydrogen atoms in fuel
79 - CO_amb = mean(CO(1:time1)); %ambient CO concentration in the air before ignition
80 - CO2_amb = mean(CO2(1:time1)); %ambient CO2 concentration in the air before igtion
81 - %% Molecular weight of species in duct
82 - MW_h2o = 0.018; %molecular weight of water in kg/mol
83 - MW_o2 = 0.032; %molecular weight of o2 in kg/mol
84 - MW_co = 0.028; %molecular weight of co in kg/mol
85 - MW_co2 = 0.044; %molecular weight of co2 in kg/mol
86 - MW_n2 = 0.028; %molecular weight of n2 in kg/mol
87
88 - %% calculating mass fraction of CO2 generated
89 - ncombh2o_ncombco2 = 1/2.*(H_atoms./C_atoms.*((CO2-CO2_amb)/(CO2-CO2_amb + (CO-CO_amb)))); % ratio of moles of h2o from
90 - %combustion proess to moles of co2 from combustion process. Equation 32 in thesis
91 - nambco2_ncombco2 = CO2_amb./(CO2-CO2_amb); % ratio of moles of co2 in ambient air to moles of co2 from combustion
92 - % process. Equation 31 of thesis
93 - nambh2o_ncombco2 = moisture./(CO2-CO2_amb);% ratio of moles of h2o in ambient air to moles of co2 from combustion
94 - %process. Equation 30 of thesis
95 - nh2o_nco2 = (nambh2o_ncombco2 + ncombh2o_ncombco2)/(nambco2_ncombco2 + 1); % ratio of moles of h2o to moles of co2
96 - % during combustion. Equation 29b of thesis.
97 - nh2o_nco2_amb = moisture/CO2_amb; % ratio of moles of h2o to moles of co2 before combustion. Equation 34 of thesis
98 - X_co2 = 1./(1./CO2 + nh2o_nco2); %molar fraction of CO2 in duct at each time step. Equation 28 of thesis
99 - X_co2_amb = 1/(1/CO2_amb + nh2o_nco2_amb); %molar fraction of co2 in ambient air. Equation 33 of thesis
100 - X_h2o = nh2o_nco2.*X_co2; %molar fraction of h2o in duct during combustion. Equation 36 of thesis
101 - MW_duct = (MW_o2.*O2 + MW_co.*CO + MW_co2.*CO2).*(1-X_h2o) + MW_h2o.*X_h2o + MW_n2.*(1 - X_h2o - (1 - X_h2o).*(O2 + CO2 + CO));
102 - %molecular weight of duct at each time step. Equation 35 of thesis.
103 - MW_duct_amb = mean(MW_duct(1:100)); %average molecular weight of flow in duct before combustion process. Equation 37 of thesis
104 - Yco2 = MW_co2.*(X_co2./MW_duct - X_co2_amb./MW_duct_amb); % co2 mass fraction at each time step minus the ambient co2 mass
105 - %fraction. Equation 26 of thesis
106 - %% calculating mass fraction of CO generated
107 - ncombh2o_ncombco = (H_atoms./C_atoms.*((CO-CO_amb)/(CO2-CO2_amb + (CO-CO_amb)))); % ratio of moles of h2o from combustion
108 - %proess to moles of co from combustion process
109 - nambco_ncombco = CO_amb./(CO-CO_amb); % ratio of moles of co in ambient air to moles of co from combustion process
110 - nambh2o_ncombco = moisture./(CO-CO_amb);% ratio of moles of h2o in ambient air to moles of co from combustion process
111 - nh2o_nco = (nambh2o_ncombco + ncombh2o_ncombco)/(nambco_ncombco + 1); % ratio of moles of h2o to moles of co
112 - %during combustion
113 - nh2o_nco_amb = moisture/CO_amb; % ratio of moles of h2o to moles of co before combustion
114 - X_co = 1./(1./CO + nh2o_nco); %molar fraction of CO in duct at each time step
115 - X_co_amb = 1/(1/CO_amb + nh2o_nco_amb); %molar fraction of co in ambient air
116 - Yco = MW_co.*(X_co./MW_duct - X_co_amb./MW_duct_amb); % co mass fraction at each time step minus the ambient co
117 - %mass fraction
118
119
120 - %% calculating mass flow
121 - D = 0.1524; %diameter of duct in meters
122 - K = 0.7297; %K factor of pitot tube
123 - R = 8.3145; %universal gas constant
124 - Q = pi/4.*(D^2).*K.*(2.*dp.*(R.*T)./(P.*MW_duct)).^(1/2); % volumetric flow equation derived from
125 - %Bernoulli. Equation 8 of thesis
126 - mdot = (P.*MW_duct)./(R.*T).*Q; %mass flow equation. Equation 12 of thesis
127
128 - %% calculating mass flow of CO2 and CO products of combustion
129 - mdot_co2 = Yco2.*mdot; %mass generation of CO2
130 - mdot_co = Yco.*mdot;%mass generation of CO
131 - HRR = 13300.*mdot_co2 + 11100.*mdot_co; %heat release rate using carbon oxide generation
132
133 - %% comparison with ASTM standard
134 - G_co2 = pi/4.*(D^2).*K.*(Pb./101000).^(1/2).*(2.*353.*dp./T).^(1/2).*1.52.*CO2; %generation rate of CO2 from ASTM standard
135 - G_co2_amb = pi/4.*(D^2).*K.*(Pb./101000).^(1/2).*(2.*353.*mean(dp(1:time1))./mean(T(1:time1))).^(1/2).*1.52.*mean(CO2(1:time1));
136 - %ambient mass flow of CO2 above
137 - G_co = pi/4.*(D^2).*K.*(Pb./101000).^(1/2).*(2.*353.*dp./T).^(1/2).*0.996.*CO; %generation rate of CO from ASTM standard
138 - G_co_amb = pi/4.*(D^2).*K.*(Pb./101000).^(1/2).*(2.*353.*mean(dp(1:time1))./mean(T(1:time1))).^(1/2).*0.996.*mean(CO(1:time1));
139 - %ambient mass flow of CO above
140 - HRR_standard = 13300.*(G_co2 - G_co2_amb) + 11100.*(G_co - G_co_amb); %heat release rate of carbon oxide generation
141 - %from standard
142 - total heat = trapz(Time,HRR) %total heat released

```

```

143 - total_heat_standard = trapz(Time,HRR_standard) %total heat released using standard equation
144
145
146 %below are placeholders for vectors to be used in the following for
147 %statements. h is the time step
148 - sum5(1) = 0;
149 - sum6(1) = 0;
150 - sum4(1) = 0;
151 - sum3(1) = 0;
152 - sum(1)=0;
153 - sum2(1) = 0;
154 - time(1)=0;
155 - h = 1;
156 - mduct_standard = pi/4.*(D^2).*K.*(P./101000).^ (1/2).*(2.*353.*dp./T).^ (1/2); %the mass flow of the duct using the ASTM standard equation
157
158 %integrating heat release rate to give total heat released
159 - for i=2:size(HRR)
160     sum(i)=sum(i-1)+h*(HRR(i)+HRR(i-1))/2;
161 - end
162 %integrating heat release rate to give total heat released for ASTM
163 %standard equations
164 - for i=2:size(HRR)
165     sum2(i)=sum2(i-1)+h*(HRR_standard(i)+HRR_standard(i-1))/2;
166 - end
167
168 %error in CO2 measurements between derived and ASTM etandard equations
169 - for i=2:size(HRR)
170     sum3(i)= sum3(i-1) + abs((CO2(i)-X_co2(i)));
171 - end
172
173 - for i=2:size(HRR)
174     sum4(i)= sum4(i-1) + (mduct_standard(i)-mdot(i));
175 - end
176
177 CO2_diff = sum3(end)
178 mdot_diff = sum4(end)
179 figure; %plotting heat release rates
180 plot(Time,HRR, 'o')
181 hold on
182 plot(Time,HRR_standard)
183 legend('derived','standard', 'Location', 'northwest')
184 xlabel('Time (s)');
185 ylabel('HRR (kW)');
186 hold off
187 figure; %plotting total heat released
188 plot(Time(1:5:end),sum(1:5:end),'o')
189 hold on
190 plot(Time,sum2)
191 legend('derived','standard', 'Location', 'northwest')
192 xlabel('Time (s)');
193 ylabel('Total heat released(kJ)');
194 hold off
195
196 %% O2 consumption
197 O2_amb = mean(O2(1:time1));%0.2097; ambient oxygen concentration before ignition
198 no2_ncombco2 = O2./(CO2-CO2_amb); % ratio of moles of o2 in duct flow to moles of co2 from combustion process. Equation 45 in thesis.
199 nh2o_no2_amb = moisture/O2_amb; % ratio of moles of h2o to moles of o2 before combustion. Equation 47 in thesis.
200 nh2o_no2 = (nambh2o_ncombco2 + ncombh2o_ncombco2)./(no2_ncombco2); % ratio of moles of h2o to moles
201 %of o2 during combustion. Equation 44b in thesis.
202 X_o2 = 1./(1./O2 + nh2o_no2); %molar fraction of O2 in duct at each time step. Equation 43 in thesis.
203 X_o2_amb = 1/(1/O2_amb + nh2o_no2_amb); %molar fraction of o2 in ambient air. Equation 46 in thesis.
204 Yo2 = MW_o2.*(X_o2_amb/MW_duct_amb - X_o2./MW_duct ); % o2 mass fraction at each time step subtracting the
205 %ambient o2 mass fraction. Equation 42 in thesis.
206 mdot_o2 = Yo2.*mdot; %mass consumption of oxygen
207 HRR_o2 = 12800.*mdot_o2; % heat release rate based on oxygen consumption. Equation 40 of thesis
208
209
210
211 - D_o2 = pi/4.*(D^2).*K.*(Pb/101000).^ (1/2).*(2.*353.*dp./T).^ (1/2).*1.1.*(O2_amb-O2); %equation provided by ASTM E2058 Equation X1.7

```

```

213 %plotting HRR over time
214 HRR_standard_o2 = 12800.*(D_o2);
215 figure;
216 plot(Time,HRR_o2,'o')
217 hold on
218 plot(Time,HRR_standard_o2)
219 legend('derived','standard', 'Location', 'northwest')
220 xlabel('Time (s)');
221 ylabel('HRR(kW)');
222 hold off
223
224 %plotting total heat released
225 total_heat_o2 = trapz(Time,HRR_o2)
226 total_heat_standard_o2 = trapz(Time,HRR_standard_o2)
227
228 %for loop to iterate total heat released at each time step
229 for i=2:size(HRR)
230
231     sum5(i)=sum5(i-1)+h*(HRR_o2(i)+HRR_o2(i-1))/2;
232 end
233 for i=2:size(HRR)
234
235     sum6(i)=sum6(i-1)+h*(HRR_standard_o2(i)+HRR_standard_o2(i-1))/2;
236 end
237
238 %plotting total heat released using oxygen consumption
239 figure;
240 plot(Time(1:5:end),sum5(1:5:end),'o')
241 hold on
242 plot(Time,sum6)
243 legend('derived','standard', 'Location', 'northwest')
244 xlabel('Time (s)');
245 ylabel('Total heat released(kJ)');
246 hold off
247 %% plotting mass generated and consumed for each species
248 figure;
249 plot(Time,mdot_co)
250 hold on
251 plot(Time,mdot_co2)
252 plot(Time,mdot_o2)
253 legend('CO generated','CO2 generated', 'O2 consumed', 'Location', 'northwest')
254 xlabel('Time (s)');
255 ylabel('mass production or consumption rate (kg/s)');
256 hold off
257 total_co2gen = trapz(Time_burn,mdot_co2(time3:time4)) %total co2 generated
258 total_cogen = trapz(Time_burn,mdot_co(time3:time4)) %total co2 generated
259 total_o2con = trapz(Time_burn,mdot_o2(time3:time4)) %total o2 consumed
260 total_co2gen_standard = trapz(Time_burn,ASTM_co2(time3:time4)) %total co2 generated
261 total_cogen_standard = trapz(Time_burn,ASTM_co(time3:time4)) %total co2 generated
262 total_o2con_standard = trapz(Time_burn,D_o2(time3:time4)) %total o2 consumed
263 mo2_error = trapz(Time(time4:end),mdot_o2(time4:end))
264 CO_CO2 = total_cogen/total_co2gen*44/28
265 CO_CO2_standad = total_cogen_standard/total_co2gen_standard*44/28
266
267 %% Measurement Signal Curves curves
268 figure;
269 plot(Time_test,1e6.*CO(time2:end))
270 hold on
271 plot(Time_test,1e6.*CO2(time2:end))
272 xlabel('Time (s)');
273 ylabel('Molar concentration for CO and CO2 (ppm)');
274 ylim([-50,5000])
275 yyaxis right;
276 ylabel ('Concentration for O2 (%)');
277 ylim([20,22]);
278 % plot(Time_test,T(time2:end))
279 plot(Time_test,1e2.*O2(time2:end))
280 legend('CO','CO2', 'O2', 'Location', 'northwest')
281 hold off
282
283 figure;
284 plot(Time_test,dp(time2:end))
285 hold on
286 xlabel('Time (s)');
287 ylabel('Differential Pressure (Pa)');
288 yyaxis right;
289 ylabel('Temperature in duct (K)');
290 ylim([288,315]);
291 plot(Time test,T(time2:end))

```

E : Parts List

Part Description	Manufacturer/Distributor	Part number
Duct Sections		
Intake Funnel	MetalFab	Custom
Mixing Section	MetalFab	Custom
Test Section	MetalFab	Custom
Thermocouple items		
Thermocouple	Omega	SCASS-010G-6
Thermocouple Port	Swagelok	SS-400-61
Thermocouple Port Seal (0.33")	McMaster-Carr	9691K52
Teflon Balls	McMaster-Carr	9660K19
Pitot Tube Items		
Pitot Tube	Yokogawa	Veris Verabar V100
Pitot Tube Port	Swagelok	SS-1610-61
Pitot Tube Port Seal (1.201")	McMaster-Carr	9691K61
Pressure Transducer	Setra	264-1R5WD-2D-T1-F
Sampling Probe Items		
Sampling Probe	McMaster-Carr	89995K558
Sampling Probe Port	Swagelok	SS-600-61BT
Sampling Port Seal (0.455")	McMaster-Carr	9691K53
Instruments on Sampling Line		
Soot Filter Housing	United Filtration	365A
Soot Filter Element	United Filtration	25-64-70C
Chiller	Buhler	TC-MIDI+
Pump	Air Dimensions	R221
Flowmeter	Dwyer	RRMB-52D-SSV
Filter Housing after Drierite	Pall	1109
Filter element after Drierite	Cytiva	1820-025
Mass flow controller	Alicat	MC-5SLPM-D-PCV65/10M
CO/CO ₂ /O ₂ Analyzer	California Analytical Instruments	703LX
Hydrocarbon Analyzer	Edinburgh Sensors	BOXED GASCARD
Surge Protector	TrippLite	SMART1500LCD
Barometric pressure probe	Omega	iBTHX-W
Data Acquisition		
Data Acquisition Module Chassis	National Instruments	cDAQ-9178
Voltage Input Module	National Instruments	NI-9215
Thermocouple Module	National Instruments	NI-9213

Sample Shelf		
Frame	80/20	2020-S
Connector Brackets	80/20	4114
Mounting Feet	80/20	2416
Shelf Plate	80/20	2480
Tubing		
Sample line ¼" tubing	McMaster-Carr	5033K31
Sample line 3/8" tubing	McMaster-Carr	5239K14
Tubing for Drierite	McMaster-Carr	5239K16
Tubing for Calibration Gasses	McMaster-Carr	5648K31
Tubing for Sample Flow Exhausted	McMaster-Carr	50375K53

Bibliography

- [1] “Global Building And Construction Plastics Market Trends Report, 2025,” GVR-2-68038-729-2. Accessed: Jul. 13, 2022. [Online]. Available: <https://www.grandviewresearch.com/industry-analysis/building-construction-plastics-market>
- [2] S. T. McKenna *et al.*, “Fire behaviour of modern façade materials – Understanding the Grenfell Tower fire,” *J. Hazard. Mater.*, vol. 368, pp. 115–123, Apr. 2019, doi: 10.1016/j.jhazmat.2018.12.077.
- [3] ASTM E1354-17, “Standard Test Method for Heat and Visible Smoke Release Rates for Materials and Products Using an Oxygen Consumption Calorimeter, ASTM International, West Conshohocken,” 2017.
- [4] J. D. Swann, Y. Ding, M. B. McKinnon, and S. I. Stoliarov, “Controlled atmosphere pyrolysis apparatus II (CAPA II): A new tool for analysis of pyrolysis of charring and intumescent polymers,” *Fire Saf. J.*, vol. 91, pp. 130–139, Jul. 2017, doi: 10.1016/j.firesaf.2017.03.038.
- [5] ASTM E2058-19, “Standard Test Methods for Measurement of Material Flammability Using a Fire Propagation Apparatus (FPA), ASTM International, West Conshohocken”.
- [6] C. Dewaghe and P. Dubois, “Cone Calorimetry - an overview | ScienceDirect Topics.” <https://www.sciencedirect.com/topics/chemistry/cone-calorimetry> (accessed Sep. 06, 2022).
- [7] V. Babrauskas, W. H. Twilley, M. Janssens, and S. Yusa, “A cone calorimeter for controlled-atmosphere studies,” *Fire Mater.*, vol. 16, no. 1, pp. 37–43, 1992, doi: 10.1002/fam.810160106.
- [8] R. T. Chaffer, “A REDESIGN OF THE FIRE PROPAGATION APPARATUS TO SIMPLIFY MANUFACTURING AND IMPROVE MEASURING CAPABILITIES,” p. 202.
- [9] M. M. Khan, A. Tewarson, and M. Chaos, “Combustion Characteristics of Materials and Generation of Fire Products,” in *SFPE Handbook of Fire Protection Engineering*, M. J. Hurley, D. Gottuk, J. R. Hall, K. Harada, E. Kuligowski, M. Puchovsky, J. Torero, J. M. Watts, and C. Wieczorek, Eds. New York, NY: Springer, 2016, pp. 1143–1232. doi: 10.1007/978-1-4939-2565-0_36.
- [10] C. Huggett, “Estimation of rate of heat release by means of oxygen consumption measurements,” *Fire Mater.*, vol. 4, no. 2, pp. 61–65, 1980, doi: 10.1002/fam.810040202.
- [11] M. J. Hurley *et al.*, Eds., *SFPE Handbook of Fire Protection Engineering*. New York, NY: Springer, 2016. doi: 10.1007/978-1-4939-2565-0.
- [12] M. Janssens, “Calorimetry,” in *SFPE Handbook of Fire Protection Engineering*, M. J. Hurley, D. Gottuk, J. R. Hall, K. Harada, E. Kuligowski, M. Puchovsky, J. Torero, J. M. Watts, and C. Wieczorek, Eds. New York, NY: Springer, 2016, pp. 905–951. doi: 10.1007/978-1-4939-2565-0_27.
- [13] ISO 12136, “Reaction to fire tests- Measurement of material properties using a fire propagation apparatus, Geneva: International Organization for Standardization,” 2011.

- [14] D. M. Chaudhari, “EXPERIMENTS AND SEMI-EMPIRICAL MODELING OF BUOYANCY-DRIVEN, TURBULENT FLAME SPREAD OVER COMBUSTIBLE SOLIDS IN A CORNER CONFIGURATION,” 2021, doi: 10.13016/yt2m-qgq2.
- [15] ASTM E800-07, “Standard Guide for Measurement of Gases Present or Generated During Fires ASTM International, West Conshohocken”.
- [16] D. Bolstad-Johnson, “The Hidden Hazards of Fire Soot,” *AIC News*, p. 3, Sep. 2010.
- [17] V. Babrauskas, ” *Fire Protection Handbook*, 17th ed. Quincy, MA: National Fire Protection Association, 1991.
- [18] “Munson, Young and Okiishi’s Fundamentals of Fluid Mechanics, 9th Edition | Wiley,” *Wiley.com*. <https://www.wiley.com/en-us/Munson%2C+Young+and+Okiishi%27s+Fundamentals+of+Fluid+Mechanics%2C+9th+Edition-p-9781119598114> (accessed Oct. 16, 2022).
- [19] N. Persaud, J. Lehr, E. Keeley, J. Wiley, and Sons, “Vapor Pressure. Water Encyclopedia (2005),” *Water Encycl.*, Jan. 2005.
- [20] W. Wagner and A. Pruss, “The IAPWS Formulation 1995 for the Thermodynamic Properties of Ordinary Water Substance for General and Scientific Use,” *J. Phys. Chem. Ref. Data*, vol. 31, no. 2, pp. 387–535, 2002, doi: 10.1063/1.1461829.
- [21] J. Thornton and R. Wood, “Time Response.” <https://atmos.washington.edu/~robwood/teaching/451/labs/timeresponse.html> (accessed Oct. 02, 2022).
- [22] S. Brohez and C. Delvosalle, “Carbon dioxide generation calorimetry—Errors induced by the simplifying assumptions in the standard test methods,” *Fire Mater.*, vol. 33, no. 2, pp. 89–97, 2009, doi: 10.1002/fam.988.
- [23] The Editors of Encyclopaedia Britannica, “humidity | atmosphere | Britannica.” <https://www.britannica.com/science/humidity> (accessed Oct. 08, 2022).
- [24] S.-K. Hahn, M. Rost, and U. Krause, “Quantifying The Combustion Behavior of Polymers by the Combustion Efficiency with Regard to the Weighting of Fire Loads,” *Trans. VŠB – Tech. Univ. Ostrava Saf. Eng. Ser.*, vol. 9, Jan. 2014, doi: 10.2478/tvsbses-2014-0002.

